Earth-Science Reviews 208 (2020) 103258

Contents lists available at ScienceDirect

Earth-Science Reviews

journal homepage: www.elsevier.com/locate/earscirev

Invited Review

Geochemical characterization of ophiolites in the Alpine-Himalayan Orogenic Belt: Magmatically and tectonically diverse evolution of the Mesozoic Neotethyan oceanic crust

Harald Furnes[a,*], Yildirim Dilek[b], Guochun Zhao[c], Inna Safonova[d,e], M. Santosh[f,g]

[a] Department of Earth Science, University of Bergen, Allegt. 41, 5007 Bergen, Norway
[b] Department of Geology & Env. Earth Science, Miami University, Oxford, OH 45056, USA
[c] Department of Earth Sciences, University of Hong Kong, Pokfulam Road, Hong Kong
[d] Sobolev Institute of Geology and Mineralogy, 3 Koptyuga ave., Novosibirsk 630090, Russia
[e] Novosibirsk State University, 1 Pirogova St., Novosibirsk 630090, Russia
[f] School of Earth Science and Resources, China University of Geosciences Beijing, 29 Xueyuan Road, Beijing 100083, China
[g] Department of Earth Science, University of Adelaide, Adelaide, SA 5005, Australia

ARTICLE INFO

Keywords:
Mesozoic Neotethyan ophiolites
Alpine-Himalayan orogenic belt
Suprasubduction zone magmatism
Geochemical discrimination of oceanic lavas
Mid-ocean ridges
Mantle melt source

ABSTRACT

Ophiolites are important archives of oceanic crust development and preservation in the rock record, and the Alpine-Himalayan Orogenic Belt (AHOB) is one of the most comprehensive ophiolite depositories in earth's history. We have compiled published data on the field occurrences and geochemistry from 137 AHOB ophiolites, ranging in age from Triassic through Cretaceous, in order to characterize the nature of the Mesozoic Neotethyan oceanic crust. We have used in this synthesis our recent ophiolite classification approach and applied the most effective geochemical discrimination diagrams to categorize the Neotethyan ophiolites within the AHOB. The subduction-related, *Backarc* (BA), *Forearc* (FA), *Backarc to Forearc* (BA-FA) and *Volcanic Arc* (VA) ophiolites exhibit different geochemical features, with the BA and FA types defining the end-members with low-high and high subduction influence, respectively. The subduction-related ophiolites constitute 76% of the ophiolite record in the AHOB, with the BA type ophiolites being the most dominant group (43%), followed by the BA-FA (19%) and with FA and VA types as subordinate groups (8% and 6%, respectively). The subduction-unrelated ophiolites, making up 24% of the AHOB ophiolite archive, include *Mid-Ocean Ridge* (MOR), *Continental Margin*, and *Plume type* ophiolites. The MOR type comprises 19% of this total and is the dominant type in the western part of the AHOB. Both major ophiolite categories are commonly associated with tholeiitic to alkaline ocean island basalt (OIB) associations, which represent the remnants of plume-proximal magmatism in different Neotethyan seaways. Subduction-unrelated ophiolites in the westernmost end of the Neotethyan realm were derived from downgoing oceanic plates, and were involved in high-pressure, subduction zone metamorphism prior to their exhumation along the suture zones. Subduction-related ophiolites, derived from the upper plates at Neotethyan convergent margins, escaped such high-pressure metamorphism and extreme fragmentation during their emplacement. Therefore, their complete Penrose ophiolite stratigraphy with greenschist facies metamorphic overprint is commonly well preserved in the collision zones of the AHOB. Different subduction contributions (from zero to 100% in the MOR and FA, respectively) may attest to variable slab dip angles and fluctuations in slab-induced elements and sediments into the mantle melt source of ophiolite–forming magmas.

1. Introduction

Fragments of ancient oceanic lithosphere preserved in orogenic belts constitute ophiolite complexes, which provide 3-D archives to examine the products of geochemical, magmatic, metasomatic and tectonic processes that operated at seafloor spreading centers and in subduction zone environments in the earth's past (e.g., Moores, 1982; Abbate et al., 1985; Ishiwatari, 1994; Maruyama et al., 1996; Dilek and Moores, 1990; Dilek, 2006; Furnes et al., 2015; Dilek and Yang, 2018). Early studies considered ophiolites as on-land fragments of fossil mid-ocean ridge crust (e.g., Gass, 1968; Moores and Vine, 1971; Anonymous, 1972; Coleman, 1977), a conclusion based particularly on

* Corresponding author.
E-mail address: harald.furnes@uib.no (H. Furnes).

https://doi.org/10.1016/j.earscirev.2020.103258
Received 16 January 2020; Received in revised form 3 June 2020; Accepted 8 June 2020
Available online 29 June 2020

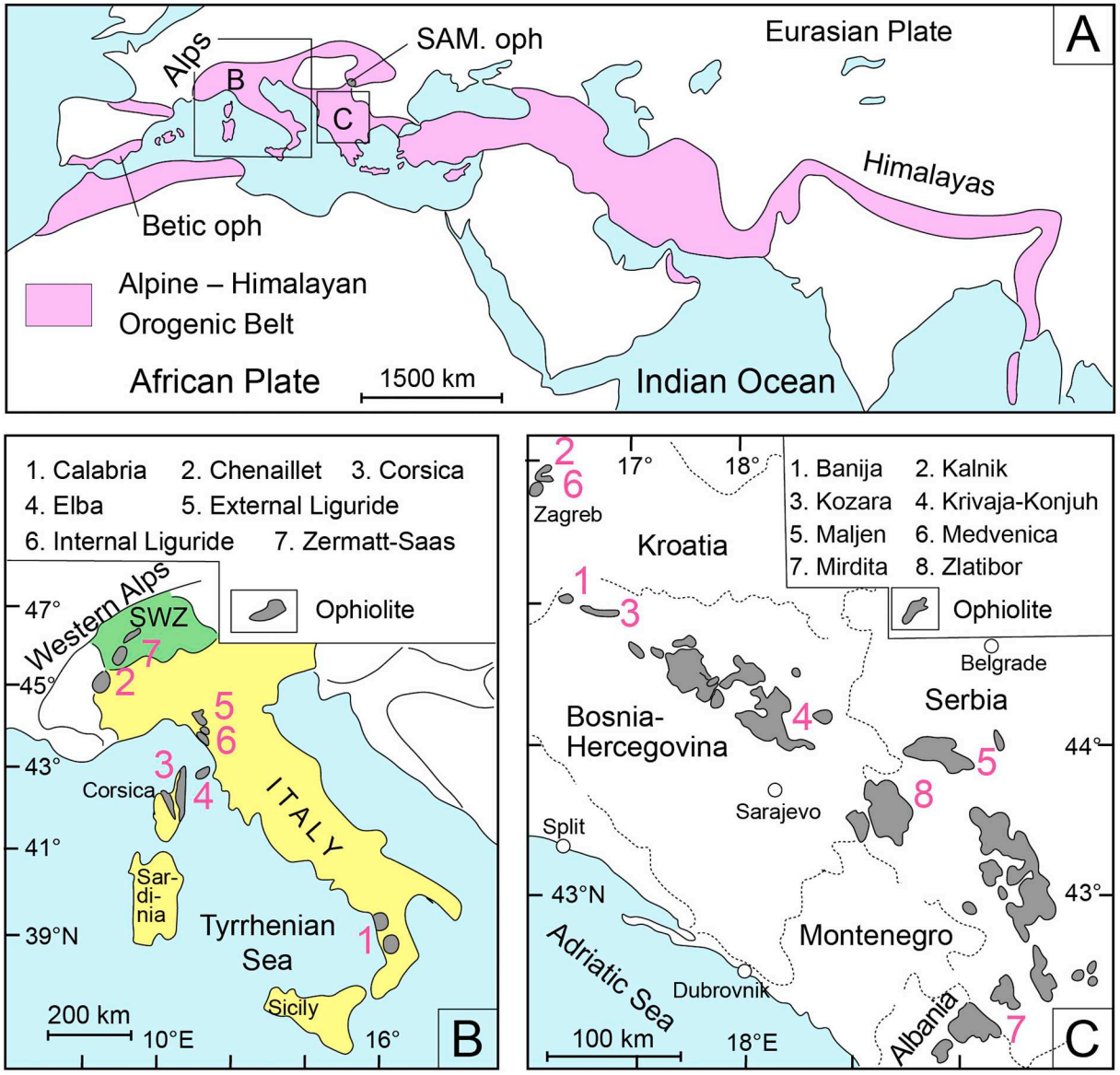

Fig. 1. A. Tectonic map showing the geographical extent of the Alpine-Himalayan Orogenic Belt (AHOB). Several published papers, as well as unspecified internet sources, have been used for the construction of the map, and the main sources are: Lister et al. (2001); Dilek et al. (2008); Dilek and Furnes (2009); Furnes et al. (2014); Chen et al. (2017); Liu et al. (2017). On this map the location of two of the ophiolite complexes included in the paper, i.e. the Betic ophiolite in SE Spain (Puga et al., 2011), and the South Apuseni Mountains (SAM) ophiolite in Romania (Gallhofer et al., 2016), are indicated. The location of the maps B and C is shown. In the upper right corner the ophiolite types are indicated. The subduction-unrelated are: MOR = mid-ocean ridge type; Pl/R/CM = plume/rift/continental margin type. The subduction-related are: BA = backarc type; FA = forearc tyoe; BA-FA = backarc to forearc type; VA = volcanic arc type.
B. Map showing the location of the seven ophiolite complexes of Italy and Switzerland (SWZ), arranged in alphabetical order. References to the relevant sources are shown in Table 1.
C. Map showing the location of the eight ophiolites complexes of Kroatia, Serbia, Bosnia-Hercegovina and Albania, arranged in alphabetical order. References to the relevant sources are shown in Table 1.

the previous interpretations of the Troodos (Cyprus) and Semail-Oman ophiolites. However, subsequent work on the Troodos ophiolite revealed geochemical characteristics of its lava sequences that hint subduction influence on its melt evolution and possible island arc origin (Miyashiro, 1973). This revolutionary proposal subsequently led to the concept of supra-subduction zone ophiolites (Pearce et al., 1984) that in turn played a major role in changing the paradigm of ophiolite–oceanic crust analogy (Dilek, 2003a).

Further geological and geochemical studies on ophiolites have shown a wide variety with respect to their lithological makeup and geochemical characteristics (e.g., Dilek and Thy, 1998; Searle and Cox, 1999; Dilek and Flower, 2003; Dilek and Furnes, 2009, 2011, 2014; Hébert et al., 2012; Pearce, 2014; Saccani, 2015). Hence, it has become clear that not all ophiolites are the melt products of conventional mid-ocean ridge processes, as once presumed in the 1972 Penrose definition of ophiolites (Anonymous, 1972). Furthermore, contrary to many recent models on the origin of ophiolites in different orogenic belts, ophiolites are not invariably associated with subduction zone processes during their magmatic construction within different subduction tectonic settings (i.e., arc, forearc, backarc), either. Globally, ophiolites are highly diverse and include subduction-related and subduction-unrelated types in regard to their primary igneous development prior to becoming incorporated into continental margins (Dilek and Furnes, 2011, 2014). Following the development of new concepts on the application of geochemical discriminant trace element ratios and abundances (Furnes et al., 2014, 2015; Furnes and Dilek, 2017) and careful

Table 1
Summary of location, age, and lithology of the investigated AHOB ophiolite complexes.

Complex/location	Age (in Ma or Period)	General geological framework	Lithology		Metamorhic grade	Main reference(s)
			Crustal rocks	Mantle rocks		
Spain						
Betic	Initiation 185 Spreading 165–140	Tectonic slices	Gabbro and pillow basalt	Peridotite	Eclogite	Puga et al. (2011)
France-Italy						
Chenaillet	165–153		Gabbro, diorite, dolerite dikes, pillowed and massive flows	Lherzolite, harzburgite, wehrlite, dunite, pyroxenite	Low grade/hydrothermal alteration	Charlot-Prat, (2005), Manatschal et al. (2011)
Switzerland-Italy						
Zermatt-Saas	164	Dismembered oph.	Gabbro, basalt pillow lava	Serpentinites	Blueschist to eclogite	Kramer et al. (2003), Bucher et al. (2005), Bucher and Grapes (2009)
Italy						
Calabrian	150 - 140	Separate outcrops	Massive and pillow basalt flows	Serpentinized harzburgite	Greenschist to blueschist	Liberi et al. (2006)Liberi and Piluso (2009), Tortorici et al. (2009)
Corsica	159	Schistes Lustres Balange Nappe	Gabbro, pl.granite, pillow lava	Serpentinized peridotite	Blueschist Unmetamorphosed	Saccani et al. (2008a), Li et al. (2015
Elba	Middle Jurasic	Two oph. Units	Gabbro, sheeted dike complex, basalt pillow, limestone and shale	Serpentinite	Ocean-floor metamorphism	Saccani and Principi (2016)
External Ligurides	180–170	Ophiolitic melange	Gabbro, pillow basalt	Lherzolite	Ocean-floor hydrothermal alteration	Montanini et al. (2008)
Internal Ligurides	c. 170		Gabbro, plagio-granite, basalt dikes, basaltic pillow lava	Serpentinized peridotites	Greenschist to amphibolite	Ottonello et al. (1984), Rampone et al. (1998)
Croatia						
Banija	170–160	Ophiolitic melange	Gabbro, pl.granit, keratophyre, dolerite, diabase	lherzolite, garnet-pyroxenite	Prehnite -pumpellyite	Lugović et al. (1991), Garašič et al. (2004)
Kalnik	Upper Jurassic -Lw. Cretaceous	Ophiolitic melange	Isotropic gabbro and basalt	Lherzolite, harzurgite	Prehnite	Lugović et al. (2015), Šegvić et al. (2016), Slovenec and Šegvić (2018)
Medvednica	Middle to Late Jurassic	Ophiolitic melange	Gabbro and basalt (boninitic)	Peridotite	Greenschist to pumpellyite/prehnite	Slovenec and Šegvić (2018)
Bosnia						
Kozara	81	Overlain by ophiolitic melange	Isotropic gabbro, dolerite dikes, basaltic pillow lava, rhyolite.Pelagic sediments intercalated with the pillow lavas	Not reported	Low-temperaturemetamorphism	Ustaszewski et al. (2009), Cvetković et al. (2014)
Krivaja-Konjuh	Jurassic	Oph. overlain by Jurassic sediments	Ultramafic - mafic cumulates, gabbro,diabase and basalt lava	Lherzolie, harzburgite	Prehnite/laumonite	Trubelja et al. (1995)
Serbia						
Maljen Massif	Early Jurassic	In Wardar zone	Gabbro, basalt dikes and pillows	Serpt. Lherz. and harz.	Low grade	Chiari et al. (2011)
Zlatibor Massif	Early Jurassic	In Dinaric oph. Belt	Gabbro, basalt dikes and pillows	Serpt. Lherz. and harz.	Low grade	Chiari et al. (2011)
Romania						
SAM (South Apsueni Mountains)	168	Dismemberedophiolite	Gabbro, Q-diorite, sheeted dike complex, pillowed and massive flows	Not reported	Ocean floormetamorphism	Saccani et al. (2001)
Bulgaria						
Satovcha	160	Ass. with marbleand mica schist	Gabbro and plagiogranite	Serpentinite	Amphibolite	Froitzheim et al. (2014)
W. Rhodope massif	Permian (310–253)		Amphibolite (meta-gabbro)	Not reported	Amphibolite (relict eclogite)	Bonev and Dilek (2010)
Armenia						
Sevan	165		Gabbro, pl.granite, massive and pillowed basalt lava	Peridotites	Hydrothermal alreration	Galoyan et al. (2009)

(*continued on next page*)

Table 1 (*continued*)

Complex/location	Age (in Ma or Period)	General geological framework	Lithology		Metamorhic grade	Main reference(s)
			Crustal rocks	Mantle rocks		
Albania						
Mirdita (North)	165	Complete oph.	Layered and isotropic gabbro, pl.gr.,Q.di., sheeted dikes, basalt and bas. andesite pillows, andesite and dacite	Lherzolite, harzburgite, dunite	low greenschist	Dilek et al. (2008), Bortolotti et al. (2006, 2013), Saccani et al. (2018)
Mirdita (South)	Middle to Late Triassic	Four tectonic units	Basalt, bas. and., andesite, dacite and rhyolite	Lherzolite, harzburgite	Ocean-floor to low-grade gr.sch.	Bortolotti et al. (2006)
Greece (mainland)						
Almopias	Mid-Late Jurassic	Ophiolitic melange	Massive and pillow basalt flows, red radiolarian cherts on top	Harzburgite	Greenschist to amphibolite	Saccani et al. (2015)
Argolis	Triassic	Several tectonic units	Massive and pillowed basalt flows	Serpentinite	Low-grade greenschist	Saccani et al. (2003)
Evros	168		Cum. and isotr. gb, pl.gr., basalt dikes and lavas (massiv and pillows)	Harzburgite, dunite	Low-grade	Koglin (2008)
Guevgueli	c. 165	W & E unita	Layered ultramafic-mafic and isotro-pic gabbro, basalt dikes and pillows	Not reported	Low-grade prehnite to low gr.schist	Saccani et al. (2008b), Zachariadis (2007)
Kassandra-Sithonia	165		Basalt and bas.and., dikes and lava	Not reported	Greenschist	Zachariadis (2007)
Koziakas	Mid-Late Jurassic	Fout tectonic units	Massive and pillowed basalt, capped by siltstone, shale and chert	peridotites	Pumpellyite to low greenschist	Pomonis et al. (2004), Chiari et al. (2012)
Oraeokastron	Mid Jurassic	In tectonic contact with Triassic limsst	Gabbro, pl.gr. as lenses in gabbro, dikes (single and swarms),pillow lava	Harzburgite	Pumpellyite to lowgreenschist	Zachariadis (2007)
Othris	169	Several imbricated thrust sheets	Ultramafic and mafic cumulates, sheeted dikes, pillow lava	Lherzolite, harzburgite	Low-greenschist	Barth et al. (2003), Koutsovitis and Magganas (2010), Bröcker et al. (2014), Kapsiotis et al. (2016)
Pindos	165	Composed of three main thrust sheets	Ultram. cum., gabbro, sheeted dikes, basalt pillow lava, felsic and boni-nite lavas on top of sequenc	Harzburgite and Dunite, minor lherzolite	Upper zeolite to gr.sch., amph. In meamorphic. sole	Pe-Piper et al. (2004), Dilek and Furnes (2009), Bröcker et al. (2014)
Rhodiani	Jurassic	Two tectonic ophiolitic units	Sheeted dikes, pillow lava, capped by calcareous sediments	Harzburgite, dunite and chromite pods	Low-grade greenschist	Saccani et al. (2008c)
Thessaloniki	169		Gabbro and diorite, sheeted dikes, massive and pillowed basalt flows	Ultramafic rocks	Greenschist	Zachariadis (2007)
Greek Islands						
Andros	Cretaceous	Oph. Melange	Gabbro and acidic rocks	Ultramafic rocks	Blueschist	Bulle et al. (2010)
Crete oph.	160	Oph. melange	Gabbro dikes and pl.granite Intruding mantle lherzoliteIntruding mantle lherzolite	Lherzolite	Amphibolite	Langosch et al. (2000), Koepke et al. (2002)
Evia	Cretaceous	Oph. Melange	Gabbro	Serpentinite lenses	Blueschist	Bröcker et al. (2014)
Ikaria	Cretaceous	Oph. Melange	Gabbro, diorite, volcanic rocks, red mudstone	Not reported	Greenschist to amphibolite	Pe-Piper and Photiades (2006)
Lesvos	253 (Permian)	Tectonic melange	Gabbro and basalt	Lherzolite, harzburgite	Pump.-prehnite to greenschist	Koglin et al. (2009a)
Naxos	Jur. or Cret.?	Dismembered oph.	Gabbro and basalt	Serpentinite, dunite	Amphibolite	Stouraiti et al. (2017)
Paros	Jur. or Cret.?	Dismembered oph.	Gabbro	Harz. (serpentinized)	?	Stouraiti et al. (2017)
Samos	Jur. or Cret.?	Tectonic melange	Gabbro and mafic volcanic	Harz. (serpentinized)	Ocean-floor metamorphism	Bröcker et al. (2014), Stouraiti et al. (2017)
Samothraki	160		Cum. and isotr. gb, diorite, basalt dikes and lavas (massiv and pillows)	Not reported	Hydrothermal alteration	Koglin et al. (2009b)
Serifos	Triassic?	Oph.melange	Gabbro, basalt, basaltic andesite	Not reported	Bluesch./amph., retrogr. to gr.sch.	Stouraiti (2010)
Siphnos	?		Blueschist, eclogite, chlorite-actiolite rocks	Not reported	gr.sch.-bluesch.-eclogite	Mocek (2001)
Skyros	125	Oph. melange	Gabbro, dolerite dikes, massive basalt and bas.andesite lava	Harzburgite (serpentinized)	Low to moderate meamorphim	Karkalis et al. (2016), Stouraiti et al. (2017)
Syros	80	Oph. melange	Gabbro, eclogite, glaucophanites	Ultram. rocks, jadeite	Blusch.-eclogite	Seck et al. (1996), Bulle et al. (2010)
Tinos	162	Oph.melange	Gabbro	Serpentinite	Blusch.-eclogite	Katzir et al. (1996), Bulle et al. (2010), Lamont et al. (2019)
Cyprus						

(*continued on next page*)

Table 1 (*continued*)

Complex/location	Age (in Ma or Period)	General geological framework	Lithology		Metamorhic grade	Main reference(s)
			Crustal rocks	Mantle rocks		
Troodos	92	Complete ophiolite	Gabbro, sheeted dikes, massive and pillow basalt	Lherzolite, harzburgite, dunite	Unmetamorphosed	Rautenschlein et al. (1985), Dilek and Furnes (2009), Pearce and Robinson (2010), Osozawa et al. (2012), Woelki et al. (2019)
Turkey						
Anatolian	Late Cretaceous	Oph. melange Mehmetan, Mollatopuz and Alabayir oph.	Gabbro and diabase dikes	Harzburgite, dunite	Low-grade metamorphism	Colakuglo et al. (2012)
Ankara	Late Jurassic to Early Cretaceous	Oph. melange	Massive and pillow basalt, radiolarian chert	Serpentinite	Low-grade metamorphism	Bortolotti et al. (2013, 2018)
Antalya	Upper Cretaceous	Complete oph.	Ultramafic - gabbroic cumulates, isotropic gabbro, sheeted dikes, volcanics and intercalated seds.	Harzburgite with dunite, chromitite	Low-temperature alteration	Bağci et al. (2006)
Beysehir-Hoyran	Late Jurassic to Early Cretaceous	Oph. melange	Gabbro and basalt dikes	Harzburgite, dunite	?	Elitok and Drüppel (2008)
Çiçekdağ	Upper Cretaceous	Complete crustal sequence	Layered and isotropic gabbro, pl.gr., dolerite dike complex, massive and pillow basalt, limestone and chert	Not reported	Hydrothermal alteration	Yaliniz et al. (2000)
Eldivan	105	Dismembered oph. in Ankara Melange	Gabbro, massive and pillow basalt, andesite, dacite and rhyolite volc.	Serpentinized peridotite	Sea-floor metamorphism	Dangerfield et al. (2011), Çelik et al. (2013)
Göksun	Late Cretaceous	Complete ophiolite	Ultramafic-mafic cum., isotr. gabbro, sheeted dikes, pl.gr., basalt pillows, bas. andesite, andecite, dacite, rhy.	Mantle tectonite	Some alteration	Rizaoğlu (2017), Parlak et al. (2020)
Guleman	Late Cretaceous		Layered and isotropic gabbro, sheeted dikes, basalt, bas. andesite, and andesite volcanics	Serpentinized Harz-burgite, dumite with chromitite pods	?	Beyarslan and Bingöl (2014), Özek et al. (2017)
Ispendere	Late Cretaceous	Complete ophiolite	Ultramaf.-mafic cum., isotr. gabbro, sheeted dikes, pl.gr., volcanic rocks	Mantle tectonite	Unmrtamorphised	Parlak et al. (2012)
Kahramanmaras	Upper Cretaceous	Dismembered ophiolite	Ultramafic-mafic cumulates, isotropic gabbro, diorite	Harzburgite	Hydrothermal alteration	Bağci (2013), Parlak et al. (2020)
Karadağ	Late Cretaceous	Complete ophiolite	Cumulate-isotropic gabbro, plagio- granite, sheeted dikes, pillow lava	Serpt. harzburgite and dunite. Podiform chromite	Blueschist	Parlak et al. (2013)
Kizildag	92–90	Complete ophiolite	Ultramafic cumulates, gabbro, sheeted dike complex, basaltic pillow lava	Harzburgite and dunite	Ocean-floor altera- tion to greenschist	Dilek and Thy (2009), Karaoğlan et al. (2013)
Kömürhan	Upper Cretaceous	Complete ophiolite	Gabbro, diabase dikes, wehrl. Intr., granite Intr., sheeted dikes, basalt to andesitic massive and pillowed lava	Serpentinite, pyroxenite	Greenschist to amphibolite	Beyarslan and Bingöl (2000)
Konya	c.86	Oph. melange	Amphibolite (metamorphic sole)	Sheared serpentinies and harzburgite	Amphibolite	Daşçi et al. (2015)
Küre	169	Complete ophiolite	Layered and isot. gabbro, sheeted dikes, massive and pillow lava, conformable sst.-siltst.-shale seq.	Serpentinized harz., dunite lenses with chromite	Ocean-floor alteration/meta-morphism	Alparslan and Dilek (2018)
Lycian	93–91	Oph. melange	Gabbro, basalt, radiolarian chert, siliceous marble	Serpentinite	Hydrotherm.alt., amph. (met.sole)	Çelik and Chiaradia (2008)
Mersin	96–90	Complete ophiolite	Ultramaf.-mafic cum., isotr. gabbro, basalt volcanics cut by dolerite dikes. Top part associated with deep marine sediments	Harzburgite and dunite, cut by dolerite dikes	Hydrothermal alteration	Çelik (2008), Ishimaru et al. (2018), Saka et al. (2019)
Meydan	Late Cretaceous	Almost complete ophiolite	Cumulate and isotropic gabbro, sheeted dikes	Serpentinized peridotite	Unmetamorphosed	Yildirim (2015)
Pinarbaşi	Late Cretaceous	Oph. melange	Wehrlite, clinopyroxenite, troctolite, gabbro, diabase dikes	Harzburgite and dunite	Greenschist to amphibolite	Vergili and Parlak (2005)
Pozanti-Karzanti	87 Ma	Complete ophiolite	Ultramafic cum., gabbro, pl.gr., sheeted dike complex, pillow lava	Harzburgite and minor dunite	Low-temperature alteration	Parlak et al. (2002), Lian et al. (2017, 2019)
Refahiye	Late Cretaceous	Complete ophiolite	Cumulate and isotropic gabbro, plagiogranite, sheeted dikes	Harz., dunite, wehr., massive chromite	Blueschist	Parlak et al. (2013)

(*continued on next page*)

Table 1 (*continued*)

Complex/location	Age (in Ma or Period)	General geological framework	Lithology		Metamorhic grade	Main reference(s)
			Crustal rocks	Mantle rocks		
Şahvelet	Late Cretaceous	Oph. melange	Isolated dikes in mantle tectonite	Serpt. harz., chrom.- rich dunite	Blueschist	Parlak et al. (2013)
Sarikaraman	Late Cretaceous	Dismembered ophiolite	Isotropic gabbro, pl.granite, sheeted dikes, basalt pillow lava	Not reported	Greenschist	Yaliniz et al. (1996)
Sivas	c.90	Oph. melange	Gabbro and isolated dikes	Serpt. harz., dunite	?	Kavak et al. (2017)
Syria						
Baer-Bassit	Late Cretaceous	Complete ophiolite	Ultram. cumulates, gabbro, plagio- granite, sheeted dikes, pillow lava	Harzburgite, dunite	Weakly altered	Al-Riyami et al. (2002)
Iraq						
Bulfat	Cretaceous	Part of Zagros Thust Zone	Basalt and andesite	Serpentinite	Medium green- schist	Buda (1993), Ali (2015)
Mawat	Upper Cretaceous	Part of Zagros Thust Zone	Basalt, basaltic andesite, trachy- andesite	Harzburgite and dunite	Ocean-floor hydr. met.	Mirza and Ismail (2007), Mirz (2008), Azizi et al. (2013)
Penjween	Late Cretaceous	Part of Zagros Thust Zone	Amphibolites	Serpentinized peridotite	Amphibolite	Hadi et al. (2013)
Iran						
Band-e-Zeyarat/ Dar Anar	142–141	Oph. melange	Gabbro, tr.hjemite, sheeted dikes, pillow lava. Associated with carbon- aceous pel.sed. and radiolarian chert	Harzburgite	Ocean-floor hydrothermal alteration	Ghazi et al. (2004)
Birjand	113–107	Oph. melange	Troctolite, gabbro, massive and pillow basalt, limestone, shale and chert	Harzburgite, dunite	Alteration	Zarrinkoub et al. (2012)
Deshir	Late Cretaceous	Complete ophiolite	Gabbro, dikes, pl.granite, sheeted dikes, massive and pillow lava, pelagic limestone and chert	Harzburgite and dunite pods	Low greenschist	Moghadam et al. (2010, 2012)
Gogher-Baft	Late Cretaceous	Dismembered ophiolite	Isotropic gabbro, pl.granite, diabase dikes, massive and pillow lava, basalt-andesite-dacite sills, pelagic Limest. and radiolarite on top	Harzburgite, with chromite pods	Ocean-floor alteration	Moghadam et al. (2013a)
Haji-Abad	Late Cretaceous	Oph. melange	Ultramafic cumulates, pl.gr., tonalite, diabase dikes, massive and pillow lava, pel. limest. and turbidites on top	Lherzolite, harzburgite, dunite, chromite pods	Greenschist	Moghadam et al. (2013b)
Harsin-Sahneh	Late Cretaceous	Complete ophiolite	Isotropic and mylonitic gabbro, pl.- granite, dike complex, pillow lava	Lherzolite, harzburgite	Low-grade hydro- thermal alteration	Sahamich and Miradpour (2015)
Kermanshah	Mesozoic	Oph. melange	Gabbro, dike complex, massive and pillow lava	Lherzolite, harzburgite, dunite	Ocean-floor metamorphism	Saccani et al. (2013a)
Khoy	Late Cretaceous		Layered and isotropic gabbro, massive and pillow basalt	Lherzolite, harzburgite	Unmetamorphosed	Hassanipak and Ghazi (2000), Khalatbari-Jafari et al. (2006), Moghadam et al. (2019)
Misho	356 (E. Carb.)		Cumulate and isotropic gabbro, iso- lated dikes and sheeted dike complex	Not reported	Variably altered	Saccani et al. (2013b)
Nain	c. 100	Dismembered oph.	Gabbro, sheeted dike complex, massive and pillow lava, pelagic limestone Interbedded with lava	Harzburgite	Ocean-floor metamorphism	Moghadam et al. (2008, 2009)
Nehbandan	100–60	Oph. melange	Cumulate and high-level gabbro, massive and pillow lava	Harzburgite	Sea-floor alteration	Saccani et al. (2010)
Neyriz	Late Cretaceous	Complete ophiolite	Gabbro, isolated dikes, sheeted dike complex, pillow lava, associated pelagic limestone and radiolarite	Lherzolite, harzburgite, dunite	Sea-floor alteration	Babaie et al. (2006), Rajabzadeh et al. (2013), Moghadam et al. (2014a), Monsef et al. (2018)
Sabzevar	Mid Cretaceous	Tectonic melange	Layered ultram.-mafic cumulate and isotropic gabbro, pl.granite, sheeted dikes, pillow lava. Associated limest.	Lherzolite, harzburgite, dunite and chromitite	Low greenschist	Moghadam et al. (2014b)Shojaat et al. (2003)
Shahr-e-Babak	c-100	Dismembered ophiolite	Gabbro, sheeted dike complex, massive and pillow lava, pelagic limestone Interbedded with lava	Harzburgite	Ocean-floor metamorphism	Moghadam et al. (2008, 2009)

(*continued on next page*)

Table 1 (*continued*)

Complex/location	Age (in Ma or Period)	General geological framework	Lithology		Metamorhic grade	Main reference(s)
			Crustal rocks	Mantle rocks		
Oman						
Oman oph	98–83	Complete ophiolite	Layered and isotropic gabbro, tr.hjemite and tonalite, sheeted dike complex, pillow lava	Harzburgite, dunite, wehrlie	Ocean-floor metamorphism	Searle and Cox, 1999), Godard et al. (2003), Goodenough et al. (2010, 2014), Ambrose and Searle (2019)
Pakistan						
Bela	Late Cretaceous	Complete oph.	Layered and isotropic gabbro, sheeted dike complex, pillow lava	Serpentinized harzburgite	Greenschist	Sarwar (1992), Gnos et al. (1998), Zaigham and Mallick (2000), Bashir et al. (2012), Khan et al. (2018)
Muslim Bagh	80		Ultramafic-mafic cumulate gabbro, pl.granite, sheeted dike complex	lherzolite, harzburgite, dunite	Greenschist to amphibolite	Khan et al. (2007a), Kakar et al. (2012, 2014, 2015a, 2015b).
Waziristan	100	Dismemered	Sheeted dikes, basalt pillow lava	Harzburgite	Greenschist	Khan et al. (2007b)
Yarlung-Zangbo and Bangong Lake - Lijiang ophiolite belts Tibet & India (I)						
Amdo	184	Oph. overlain by late Cret. Rocks	Gabbro and basalt	Serpentinized peridotite	Low-grade metamorphism	Wang et al. (2016)
Asa	116	Oph. melange	Layered and isotropic gabbro, pillow baasalt	Metaperidotite	Ocean-floor metamorphism	Zeng et al. (2018a)
Bangong Lake	Jurassic	Oph. melange	Gabbro, mafic dikes and lava	Harzburgite	Varably altered	Shi et al. (2004, 2008)
Beimerang	125	Oph. melange	Gabbro, basalt dikes and pillows	Lherzolite, harzburgite, dunite	Ocean-floor metamorphism	Huot et al. (2002), Dubois-Côté et al. (2005)
Beinang	125		Gabbro, basalt dikes and sills, pillow lava	Lherzolite, harzburgite	Alteration/hydro metamorphism	Dubois-Côté et al. (2005)
Dazhuqu	126	Complete ophiolite	Gabbro and basalt (dikes, lava)	Lherzolite, harzburgite, dunite	Ocean-floor metamorphism	Hébert et al. (2003), Malpas et al. (2003), Dubois-Côté et al. (2005), Bao et al. (2013)
Dong Tso	177–171	Oph. melange	Layered and isotropic gabbro, sheeted dikes, basalt pillow lava	Harz.burgite, serpentinite	Amphibolite	Wang et al. (2008)
Dongco	167	Oph. Melange	Troctolite, gb, pl.gr., sheeted dike compl., pillow basalt	Metaperidotite (serpentinized)	Low-grade	Wang et al. (2016)
Dongbo & Purang	130–128		Gabbro and basalt lava	Lherz., harz., dunite	Unmetamorphosed	Liu et al. (2013, 2015)
Dongqiao	188–181	Complete ophiolite	Layered and isotropic gabbro, massive and pillowed basalt	Harzburgite, dunite	Low-grade metamorphism	Liu et al. (2016)
Dingqing	218	Oph. Intercalated with Jur. Flysch and melange	Gabbro and dolerite dikes	harzburgite, dunite	?	Liu et al. (2002), Xiong et al. (2018)
Dras (I)	110–70		Gabbro and basalt lava	Peridotite		Clift et al. (2002)
Eastern Syntaxis	200	Oph. melange	Basalt and basaltic andesite	Ultramafic rocks	Greenschist	Quanru et al. (2006), Saha et al. (2012)
Guomangco	Mid. Jurassic - Early Cret.	Oph. melange	Ultramafiic - mafic cumulate, basalt dikes, massive and pillow lava	Harzburgite	Low-grade metamorphism	Xu et al. (2014)
Jiding	128	Complete ophiolite	Gabbro and diabase dikes	Harzburgite	Variably altered	Hébert et al. (2003), Dubois-Côté et al. (2005)
Jinlu	128	Complete ophiolite	Ultramafic- mafic cumulate, dikes, basalt and basaltic andesite lava	Harzburgite, lherzzolite	Variably altered	Hébert et al. (2003), Dubois-Côté et al. (2005)
Julu	104	Several thrust slices	Gabbro, basalt dikes and lava	Ultramafic rocks	Low-grade met.	Liu et al. (2014)
Kangqiong	115	Oph. melange	Cumulate gabbro, dikes and pillow lava	Serpentinite	Low-grade metamorphism	Xu et al. (2015b)
Lagkor Tso	177–170	Oph. melange	Layered and isotropic gabbro, pillow lava	Serpentinized peridotite	Amphibolite	Wang et al. (2008)
Lanong	147	Oph. Melange	Gabbro, dolerite, basalt	Ultramafic rocks	Low-grade	Zhong et al. (2017)
Luobusa	163	Oph. melange	Gabbro and sheeted dikes	harzburgite, dunite	Variably altered	Zhang et al. (2016a, 2016b)
Nadong	Middle Jurasic		Basalt	Not reported	?	Fan et al. (2014)
Namco-Renco	178–150		Gabbro, basalt and diabase dikes	Lherzolite, harzburgite	Prehnite	Zhong et al. (2015)
Nidar (I)	140–110	Oph. melange	Gabbro, basalt and basaltic andesite lava	Serpentinized harz-burgite, lherzolite	Hydrotermal aleration	Mahéo et al. (2004), Ahmad et al. (2008)
Qunrang	126		Gabbro, diabase and basalt lava	Lherzolite, harzburgite, dunite	Low grade metamorphism	Dubois-Côté et al. (2005), Hébert et al. (2003)
Rebang Co	162	Oph. as several thrust slices	Isotropic gabbro, dike comples, pillow lava	Lherzolite, Harzburgite	Low-grade metamorphism	Liu et al. (2014)
Renbu	126	Oph. as big block	Cumulate gabbro, diabase dikes, basalt lava	Lherzolite, harzburgite, dunite	Low grade metamorphism	Xia et al. (2008)

(*continued on next page*)

Table 1 (*continued*)

Complex/location	Age (in Ma or Period)	General geological framework	Lithology		Metamorhic grade	Main reference(s)
			Crustal rocks	Mantle rocks		
Rutog	168	Oph. melange	Ultramafic and mafic rocks, gabbro, diabase, pillow lava	Harzburgite	Low-grade	Wang et al. (2016)
Saga	150–130	Oph. melange	Gabbro, diabase sills and dikes, massive and pillow lava flows	Lherzolite, harzburgite, dunite	Sea-floor metamorphism	Bédard et al. (2009), Guilmette et al. (2012)
SangSang	125	Oph. melange	Gabbro, diabase, basalt and basaltic andesite lava	Harzburgite	Sea-floor metamorphism	Bédard et al. (2009)
Spontang (I)	171	Complete ophiolite	Gabbro, sheeted dike complex, pillow lava	Harzburgite	Sea-floor metamorphism	Mahéo et al. (2004), Corfield et al. (2001), Pedersen et al. (2001)
Taoxinghu	Triassic	Oph. melange	Gabbro and basalt	Not reported	Greenschist	Wu et al. (2016)
Xigaze	126	Complete oph.	Ultramafic-mafic cumulate, gabbro, sheeted dike complex, pillow lava, overlain by chert	Lherzolite, harzburgite, dunite	Low-grade metamorphism	Chen and Xia (2008), Dai et al. (2013), Liu et al. (2018)
Xiugugabu	126–122	Tectonic melange	Microgabbro and diabase intrusions	Harzburgite	Greenschist	Xu et al. (2008), Bezard et al. (2011), Yang and Dilek (2015)
Yungbwa	147	Oph. thrust over Cret. melange	Gabbro and basalt dikes	Lherzolite, Harzburgite	Low-grade metamorphism	Miller et al. (2003)
Yunzhug	150	Oph. melange	Mafic cumulate, sheeted dikes, basalt pillow lava	Harzburite, lherzolite, dunite	Low-grade metamorphism	Zeng et al. (2018b)
Yushu	254	Oph. melange	Basalt	Not reported	Low-grade	Zhang et al. (2017)
Zedong	165–152		Gabbro, basalt dikes, basalt and andesite lava	Lherzolite, harzburgite, dunite	Pumpellyite- prehnite meta - morphic grade	Aitchison et al. (2000), Malpas et al. (2003), Zhang et al. (2014), Liu et al. (2019)
Zhongba	126	Oph. melange	Diabase dikes and basalt pillow lava	Harzburgite, dunite	Low-T alteration	Dai et al. (2012)
Zhongcang	163	Oph. melange	Cumulate-isotropic gabbro, pl.granite, massive and pillow basalt, chert	Serpentinized harzburgite	Greenschist	Tang et al. (2018)
India						
Andaman	92	Oph. overlain by deep-sea shales	Cumulate peridotite - gabbro, pl.- granite, dikes, basalt, andeste and dacite lava	Harzburgite, lherzolite, dunite with chromitite pods	Low-grade Ocean-floor metamorphism	Pedersen et al. (2010), Pal, (2011), Rasool et al. (2015)
Manipur	c. 70	Oph. melange	Gabbro, basalt dikes and volcanics	Peridotite, chromitite	Variably altered	Singh et al. (2012)
Naga Hills	119–116	Highly dismemered, imbricate sheets	Gabbro, pl.granite, diorite dikes, pillow lava	Lherzolite, harzburgite, websterite, clinopyroxenite	Greenschist to blueschist	Ao and Bhowmik (2014), Singh et al. (2017), Dey et al. (2018), Abdullah et al. (2018)
Myanmar						
Myitkyina	177–166	Dismembered ophiolie	Gabbro, pl.granite, basalt, andesite	Harzburgite, lherzolite, dunite	Amphibolite	Yang et al. (2012), Xu et al. (2017)

Abbreviations (alphabetically): Amph. = amphibolite; Ass. = associated; Bas.and. = basaltic andesite; Bluesch. = blueschist; Cret. = Cretaceous; Cum. = cumulate; Gr.schist = greenschist; Harz. = harzburgite; Hydr. = hydrothermal; Intr. = intrusion; Isot. = isotropic; Lherz. = lherzolite; Met. = metamorphism; Oph. = ophiolite; Pel.sed. = pelagic sediment; Pl.gr. = plagiogranite; Pump. = pumpellyite; Q-di. = quartz diorite; Retrogr. = retrograde; Serpt. = serpentinized; Ultram. = ultramafic; volc. = volcanic; Wehr. = wehrlite.

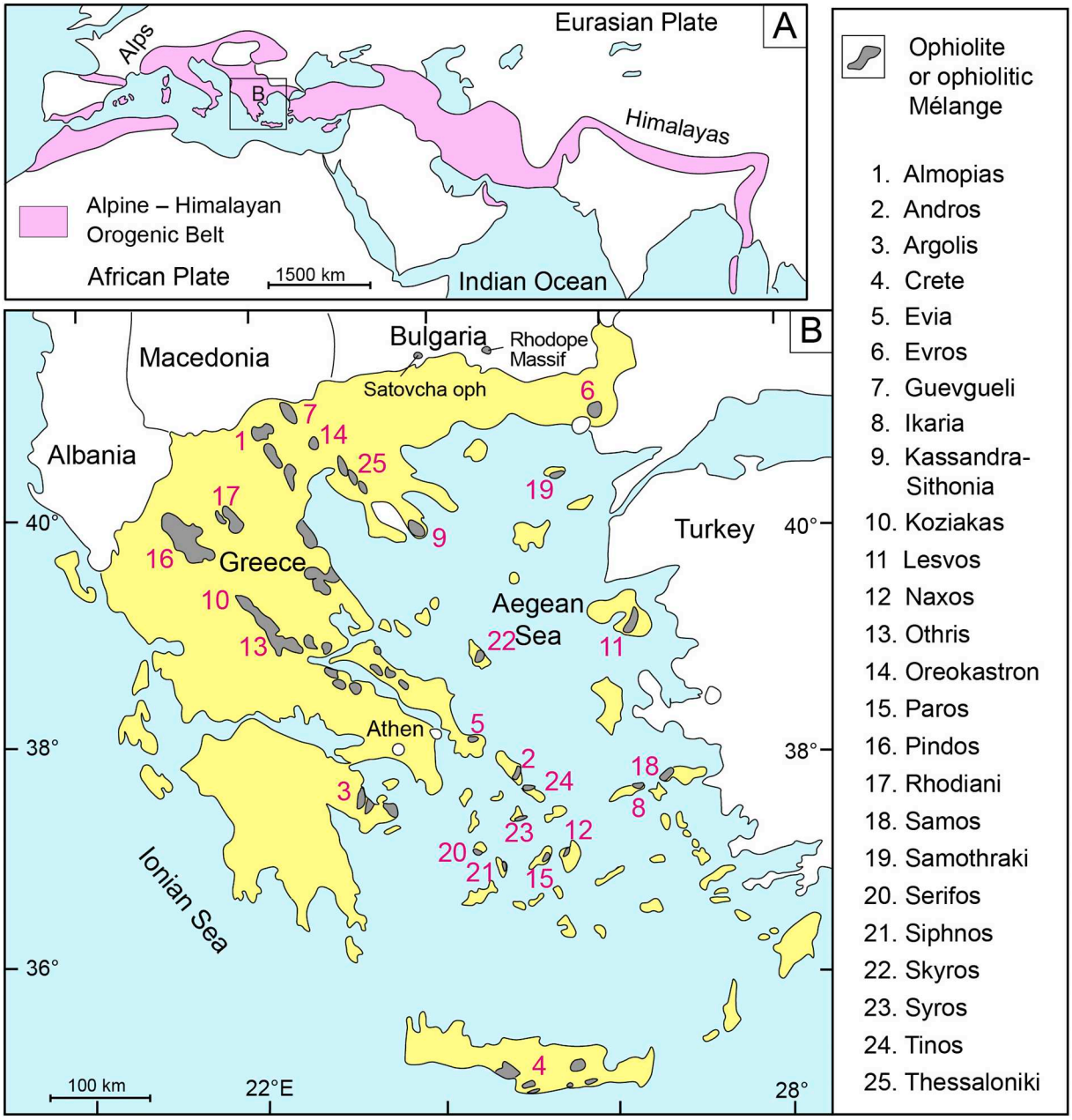

Fig. 2. A. Tectonic map showing the geographical extent of the Alpine-Himalayan Orogenic Belt (AHOB), and the location of map B.
B. Map of mainland Greece and the Greek islands showing the location of the twenty-five complexes of ophiolite or ophiolitic mélange, arranged in alphabetical order. All relevant references used in the compilation are shown in Table 1.

examination of their field occurrences and regional geology, ophiolites have been divided into several sub-categories with distinct lithological sequences, structural architecture and geochemical fingerprints (see fig. 2 of Dilek and Furnes, 2014, and fig. 1 of Furnes and Dilek, 2017).

In this paper, we present a comprehensive review of magmatic assemblages that have been interpreted as ophiolites within the Alpine-Himalayan Orogenic Belt (AHOB), which stretches from the Iberian Peninsula in the west to the Indochina Peninsula in the east. This vast orogenic belt formed during diachronous terminal closures of different Neotethyan seaways, which originally evolved between Eurasia in the north and the Gondwana–derived continental blocks in the south throughout the Mesozoic (Dilek and Moores, 1990; Dilek and Furnes, 2019, and references therein). We provide a systematic synthesis of field data and geochemistry of basalts (and also some isotropic gabbro samples), available from the published sources on these ophiolites. We further divide the data into Triassic (252–201), Jurassic (201–145 Ma) and Cretaceous (145–66 Ma) categories, based on the time of the formation of different seaways within Neotethys. A few examples, however, straddle the boundary between the Triassic and Permian, and hence we use the term Permo-Triassic for the oldest group. These older Permo-Triassic examples may be related to the initial continental rifting, and hence the beginning stage of Neothetys (Dilek and Furnes, 2019). We geochemically characterize and subdivide the ophiolite occurrences of this vast orogenic belt into various subtypes of the subduction-unrelated and subduction-related types, and quantify their relative abundances. We further compare the abundance of various ophiolite types of the collisional-type AHOB with those of the accretionary-type Central Asian Orogenic Belts. This synthesis has two major, overarching results: (1) Ophiolites in the AHOB archive are highly diverse in their geochemical makeup and hence in their mantle melt origins, and they display significant variations in their compositional and structural features along-strike within the same suture zones;

and (2) Subduction influence in the melt evolution of the Neotethyan ophiolites in the central and eastern domains of the AHOB was most dominant, and the Cretaceous SSZ ophiolites constitute the best preserved and complete Neotethyan oceanic crust within the AHOB.

2. The Alpine-Himalayan Orogenic Belt

The Alpine-Himalayan Orogenic Belt (AHOB) extends from the Maghrebides in NW Africa in the west, through the European Alps, Dinarides–Albanides–Hellenides in the Balkan Peninsula, Anatolides–Taurides in the eastern Mediterranean region, Makran and Oman in the west Indian Ocean, to the Tibetan–Himalaya in the east, and to the Indochina Peninsula in the southeast. It is a nearly 10,000 km–long mountain system with high elevation, young orogenic crust and widespread seismic activity (Fig. 1A; Dilek, 2006). The development of this orogenic belt occurred during the evolution of a broad Tethyan oceanic realm through prolonged and complex processes of the opening and closure of Paleotethyan and Neotethyan seaways, and the formation of multiple backarc basins that overlapped in time and space (Dilek and Moores, 1990; Dilek et al., 1990; Stampfli, 2000; Stampfli and Borel, 2002; Stampfli and Hochard, 2009; Metcalfe, 2013; Dilek and Yang, 2018; Dilek and Furnes, 2019). In this paper, we focus on those ophiolite complexes that represent various stages of oceanic crust development within the Neotethyan realm, mainly during the Jurassic and Cretaceous.

The pre-Neotethys plate tectonic history of the AHOB can be briefly summarized as follows. Silurian rifting of the northern Gondwana margin (Tasáryová et al., 2018) adjacent to the Prototethyan Ocean (Rheic and Asiatic oceans) produced the Hun Superterrane (Stampfli, 2000). Continued extension led to the opening and development of the Paleotethyan Ocean between the northern Gondwana margin and the Hun Superterrane, at the same time as the Rheic Ocean closed during Devonian time (Torsvik and Cocks, 2004; Stampfli et al., 2013). Localized intrusions of Permian gabbros into the continental crust of the Southern Alps attests to a period of lithospheric extension and attendant magmatism (Herrmann et al., 2001; Pohl et al., 2018; Dilek and Furnes, 2019) that caused rifting of the northern margin of Gondwana during the Middle Triassic (Mohn et al., 2012; Storck et al., 2018). Resulting detachment and drifting away of the Cimmerian continent led to the development of the Neotethyan Ocean in its wake and the coeval closure of Paleotethys in the late Triassic (for details, see Stampfli and Borel, 2002; Stampfli and Kozur, 2006). Around 220 Ma Neotethys opened, and Paleotethys closed as Gondwana-derived continental blocks became accreted to East Asia (Xu et al., 2015a; Zhao et al., 2018).

All the AHOB ophiolite complexes examined in this study developed during the rift–drift (MORB types) and subduction zone (SSZ types) tectonic evolution of Neotethys. They are principally of two age groups (Table 1): Jurassic group spanning in age from 170 Ma to 140 Ma, and a Cretaceous group with ophiolites having igneous ages between 125 Ma and 90 Ma. A minor Triassic group is also identified. The investigated ophiolite occurrences in these age groups are shown in Figs. 1 through 5. These figures only display the geographical location of the ophiolites. The geology, internal structure–stratigraphy, geochronology, petrogenesis, and emplacement tectonics of these ophiolites are discussed in a separate paper (Dilek et al., in preparation). The reader can find appropriate references about the individual ophiolite complexes in Table 1.

3. Classification of ophiolites

Ophiolites, as defined by Dilek and Furnes (2011), are “suites of temporally and spatially associated ultramafic to felsic rocks evolved from separate melting episodes and processes of magmatic differentiation in particular oceanic environments”. Characterization and classification of ophiolite complexes may be done on the basis of field examination, describing their rock components and structural anatomy. The tectonic environment of melt evolution, however, is best determined by the geochemical characteristics of the basaltic lavas and intrusive rocks, and thus ophiolites can be classified on a geochemical basis. This has been extensively described and explained in several recent publications (Dilek and Furnes, 2011, 2014; Furnes et al., 2014, 2015; Furnes and Dilek, 2017; Furnes and Safonova, 2019, and references therein). A brief summary of the ophiolite classification is given here. A general view of the tectonic settings in which subduction-unrelated and subduction-related oceanic crust undergoes its magmatic construction before emplacement into continental margins as ophiolites is shown in Fig. 6 (middle panel), and the lithological construction of the two main types is depicted in Fig. 6 (upper panel). The subduction-unrelated ophiolite types may be subdivided into Rift (R) and Continental Margin (CM) types, representing the embryonic stage in ocean crust formation. With the continental breakup and the onset of seafloor spreading, MOR–type oceanic crust develops as an end–member of subduction–unrelated ophiolite types. A special case is the Plume (Pl)-type ophiolites which may be part of oceanic plateaus or plume-proximal oceanic ridges (e.g., Iceland; Dilek, 2003b; Dilek and Furnes, 2014).

The subduction-related types, i.e. suprasubduction zone (SSZ) ophiolites, form as part of the upper plate of a subduction zone, and can be subdivided into four types. The Backarc (BA) and Forearc (FA) type ophiolites represent the trench–distal and trench–proximal end–-members of SSZ ophiolites, whereas the Backarc to Forearc (BA-FA) ophiolites constitute a hybrid type between the two former categories of SSZ oceanic crust. The Volcanic Arc (VA) oceanic crust represents a long-term magmatic construction in a suprasubduction zone setting (in the order of 20–30 million-years), and constitutes a rather thick accumulation of felsic to mafic intrusive and extrusive rock with a well–-developed middle crust (Dilek and Furnes, 2011; Fig. 6, upper panel).

In Fig. 6 (lower panel) we illustrate magma generation responsible for the subduction-related ophiolite types. The BA ophiolites are lithologically and structurally similar to MOR crust. Their magmatic construction was also related to decompression melting of the upwelling asthenosphere beneath backarc spreading centers. However, their geochemical character was influenced by variable but generally small amounts of slab dehydration originated fluid flux. The FA type, on the other hand, is characterized by large amounts of fluid-flux melt within the mantle wedge. The BA-FA types represent a combination of these two end-members.

The inference that we can draw from the above description and illustrations in Fig. 6 is that the evolution of ophiolites, both subduction-unrelated and subduction-related groups, was a time-dependent phenomenon. Each separate example presents a snapshot picture of time when crust-forming magmatic processes stopped operating. An ophiolite thus represents an ultramafic to mafic–felsic rock assemblage that is temporally associated with mantle melting and differentiation processes in a particular tectonic environment (Dilek and Furnes, 2014). As to the subduction-unrelated category, tectonic extension resulting in continental rifting and followed by rift-drift processes may ultimately lead to the onset of seafloor spreading, which in turn produces new, mid–ocean ridge (MOR)–type oceanic crust (Dilek and Furnes, 2011, 2014). MOR–type ophiolites display significant differences in their internal structure, igneous stratigraphy, and crustal thickness, depending on the spreading rate at which they were formed at the oceanic stage (Dilek and Furnes, 2011), much like the modern oceanic crust forming at mid-ocean ridges with different spreading rates and magma budgets (Dilek and Thy, 1998; Searle and Escartín, 2013). An example of in-situ, modern ocean – continent transition (OCT) zone is represented by the Early Cretaceous Iberian rifted margin (Seifert et al., 1997), which on land, would constitute a continental margin ophiolite as, for example, reported from the Western Alps (as discussed below) (Balestro et al., 2015; Festa et al., 2015).

Suprasubduction-zone (SSZ) ophiolites, orsubduction-related

Fig. 3. A. Tectonic map showing the geographical extent of the Alpine-Himalayan Orogenic Belt (AHOB), and the location of map B.
B. Map of Turkey showing the location of the twenty-five complexes of ophiolite or ophiolitic mélange, arranged in alphabetical order. All relevant references used in the compilation are shown in Table 1. The major tectonic belts as indicated are taken from Asparslan and Dilek (2018). Also shown are the Baer Bassit ophiolite in Syria (Al-Riyami et al., 2002), and the Bulfat (Ali, 2015), Mawat (Azizi et al., 2013) and Panjween (Hadi et al., 2013) ophiolite complexes in Iraq.

ophiolites, have four sub-types (as outlined above) and may develop in peri–continental marginal or back-arc basins, or entirely in intra-oceanic convergent margin settings (i.e., Izu–Bonin–Mariana, or Tonga–Kermadec arc–trench systems). Structural, lithological as well as magmatic development of SSZ ophiolites are in general more complex than that of subduction-unrelated ophiolites, because subduction – related parameters, such as subduction rate, slab rollback, slab flux, and dehydration melting, strongly control the mode of upper plate deformation, mantle heterogeneity and melting, and melt evolution of ophiolitic magmas. The increasing complexity in the lithological makeup of SSZ oceanic crust from BA to FA-BA, and further to FA and VA settings, and their increasing geochemical differences compared to subduction-unrelated ophiolites, are hence largely related to their proximity to subducting slabs. Ridge segmentation and ridge within backarc basins (e.g., Clark et al., 2008; Deschamps et al., 2008; Stern and Dickinson, 2010; Maldonado et al., 2014; Anderson et al., 2017; Magni, 2019) and the time spans for these processes to operate are also important factors in the development of different types of subduction-related ophiolites. The Semail–Oman ophiolite is one of the well-documented examples of an ophiolite, which underwent geochemical changes as it evolved from initially BA–type to a FA–type in later stages of its development (Dilek and Flower, 2003; Goodenough et al., 2014). We hence classify it as a BA-FA–type ophiolite. Most of the ophiolites reported in the literature do not have, however, detailed time constraints for their magmatic construction, like the Oman ophiolite. This is a critical impediment in better understanding and constraining the time–progressive melt evolution of ophiolitic magmas within different SSZ tectonic settings.

We have used a combination of four discrimination diagrams, applied mainly to basalts and some basaltic andesite in upper oceanic crust, as well as to subordinate isotropic gabbros, in our geochemical classification of the AHOB ophiolites. The three diagrams that we use first are Th/Yb vs Nb/Yb, V vs Ti/1000, and TiO_2/Yb vs Nb/Yb (Pearce, 2014). As an initial step, the Th/Yb – Nb/Yb diagram is employed to

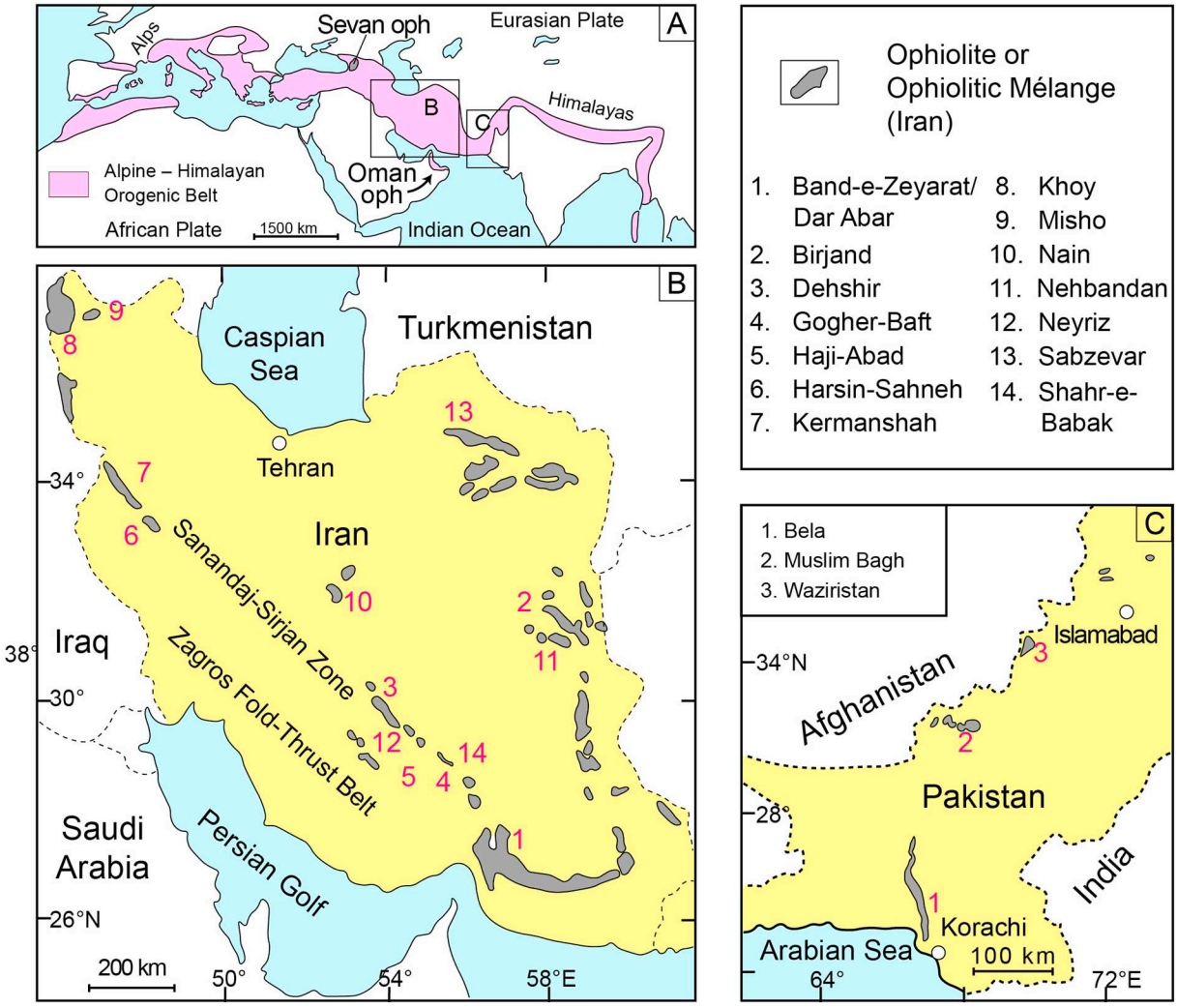

Fig. 4. A. Tectonic map showing the geographical extent of the Alpine-Himalayan Orogenic Belt (AHOB), and the location of maps B and C.
B. Map of Iran showing the location of the fourteen complexes of ophiolite or ophiolitic mélange, arranged in alphabetical order. All relevant references used in the compilation are shown in Table 1. The major tectonic features, i.e. the Zagros Fold-Trust Belt, and the Samandaj-Sirjan Zone are taken from Moghadam et al. (2014a).
C. Map of Pakistan showing the location of the Bela (Khan et al., 2018), Muslim Bagh (Khan et al., 2007a)) and Waziristan (Khan et al., 2007b) ophiolites.

separate subduction-related from subduction-unrelated basalts. All basalts that plot within the mantle array are considered as subduction-unrelated, whereas those plotting above it (oceanic and continental arc types) are interpreted to have been variably enriched in elements transported by hydrous fluids +/- melts released from subducting oceanic slab (Fig. 7A). Following this classification scheme, ophiolitic basalts are first divided into two main groups: subduction-unrelated and subduction-related (Dilek and Furnes, 2011, 2014; Furnes and Dilek, 2017). Basalts that plot within the mantle (MORB-OIB) array of the Th/Yb – Nb/Yb diagram were further evaluated in the TiO_2/Yb – Nb/Yb diagram (Step 2), because the TiO_2/Yb ratio functions as a good indicator of the depth of mantle melting (Pearce, 2014). Basalts that plot in the OIB or MORB arrays thus represent deep- and shallow-generated melts, respectively (Fig. 7B). The subduction-unrelated group can be further discriminated into Rift/Continental Margin, Mid-Ocean Ridge (MOR), and Plume types, a subdivision that is defined by their grouping in the TiO_2/Yb-Nb/Yb diagram (Fig. 7B). MOR type basalts plot within the MORB array, whereas plume-related basalts plot within the OIB array and the Rift/Continental Margin types fall into the alkaline field of the OIB array.

A third step involves further discrimination of the basalts using the V/Ti ratio as a proxy for SSZ derivation (Shervais, 1982). The modified V-Ti diagram (Pearce, 2014) discriminates between magmas of boninite, island-arc tholeiite (IAT), MORB and alkali basalt affinity, in which the MORB and boninite represent the tectonic environment for the most distant and the closest from a trench and the associated subduction zone, respectively. The subduction-related basalts can thus be subdivided into Backarc (BA), Backarc to Forearc (BA-FA), Forearc (FA), and Volcanic Arc (VA) types. The BA, BA-FA, and FA types are recognized, among which the majority of their compositions plot in the oceanic arc (as well as overlap the oceanic arc/continental arc) field of the Th/Yb-Nb/Yb diagram (Fig. 7A). Further, the BA, BA-FA, and FA types are characterized by a dominance of MORB, IAT and boninite compositions, respectively, in the V-Ti diagram (Fig. 7C). For the samples that we classify as VA basalts, the data also plot in the continental arc field of the Th/Yb-Nb/Yb diagram and within the IAT and boninite fields in the V-Ti diagram.

Another useful and appropriate discrimination diagram is provided by the MORB-normalized values of Th and Nb (Saccani, 2015). Of major importance here is the distinction between basalts of subduction-influenced and subduction-noninfluenced backarc basins (Fig. 8). About half of the backarc field overlaps largely with those of N-MORB and E-MORB without subduction influence. This is important to keep in mind when classifying ophiolites, because those ophiolites classified as MOR-type (D-MORB, N-MORB and E-MORB) may also be part of a trench-distal backarc system.

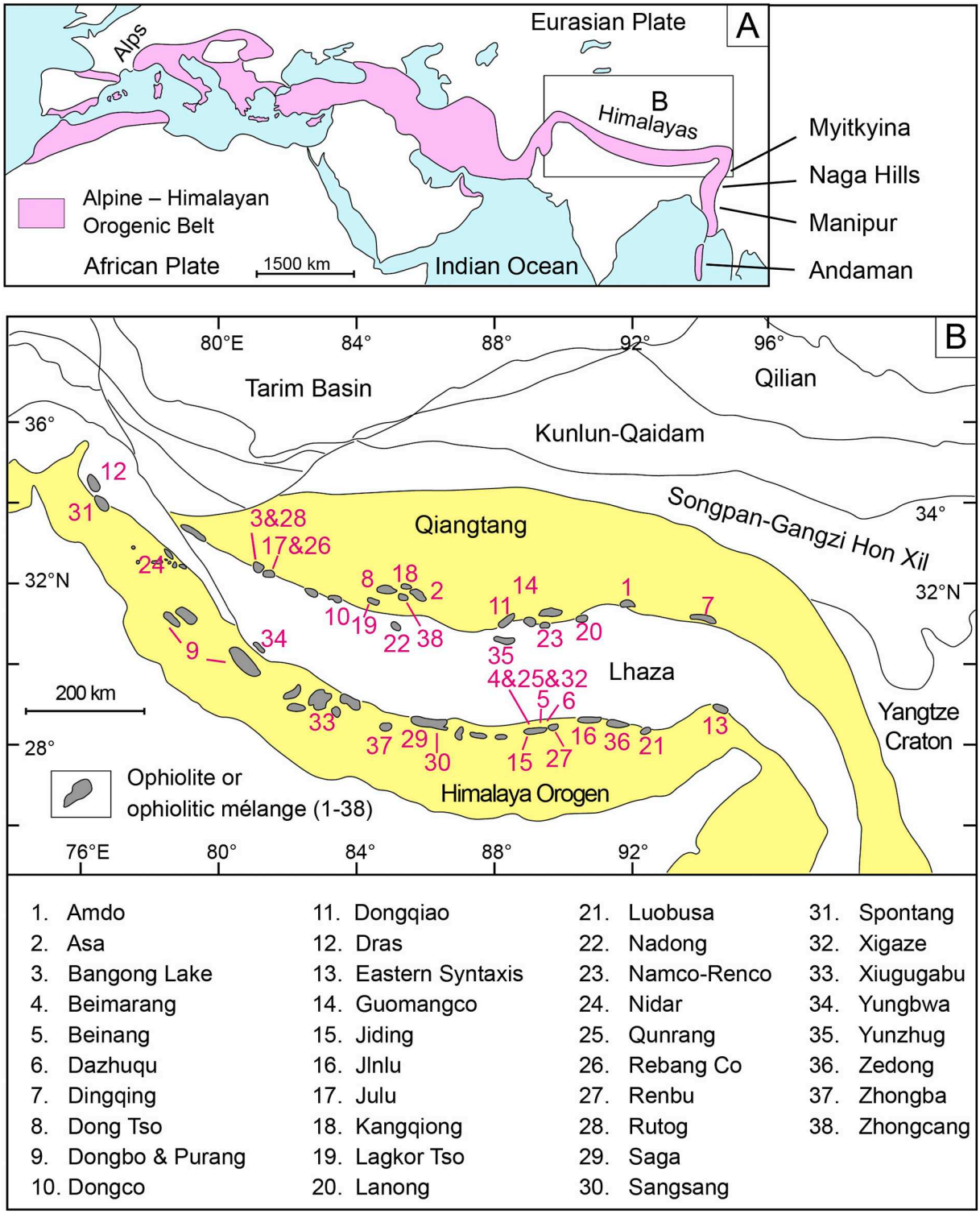

Fig. 5. A. Tectonic map showing the geographical extent of the Alpine-Himalayan Orogenic Belt (AHOB), and the location of map B. On this map the location of four of the ophiolite complexes included in the paper, i.e. the Myitkyina ophiolite in Myanmar (Xu et al., 2017), the Naga Hills ophiolite in NE India (Dey et al., 2018), the Manipur ophiolite in NE India (Singh et al., 2012), and the Andaman ophiolite in Andaman Island (Pedersen et al., 2010).
B. Map of the Tibetan plateau showing the location of the thirty-eight ophiolite complexes. The various terranes shown on the map are taken from Xiong et al. (2018).

4. Geological summary of the AHOB ophiolites

In this study, we have examined 137 ophiolite and island arc complexes in the Alpine-Himalayan Orogenic Belt, distributed in 23 countries. Most of these ophiolites occur in central to eastern parts of the orogenic system. Upper mantle and crustal lithologies, metamorphic conditions, tectonic framework, and main reference(s) on each complex are summarized in Table 1. Upper mantle lithologies have been reported from 121 of the ophiolites. Harzburgite is the most common reported peridotite rock, followed by lherzolite and dunite. Wehrlite and pyroxenite are reported from only several ophiolites (Table 1). In some ophiolites, ultramafic rocks are only categorized as

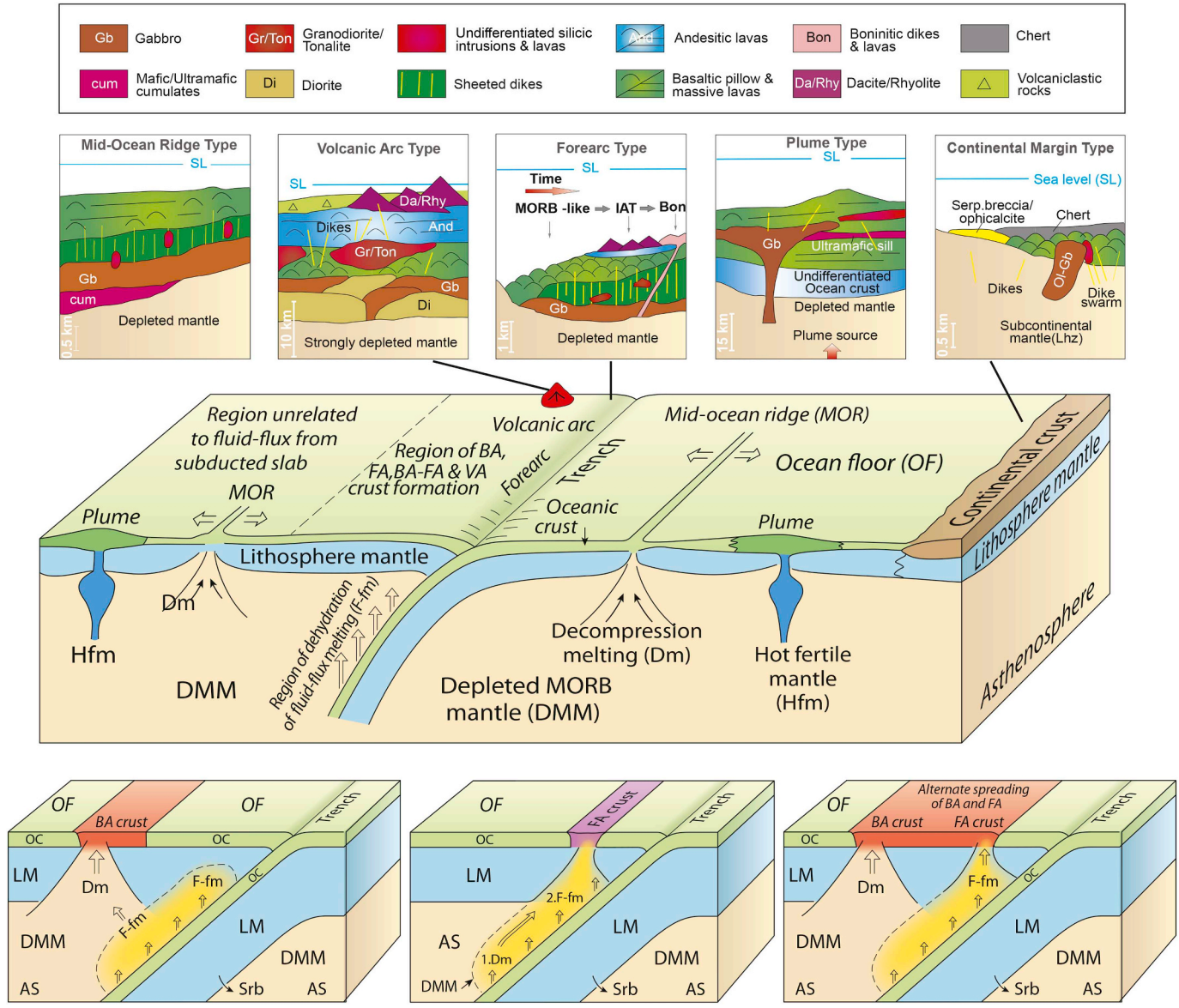

Fig. 6. Schematic plate tectonic illustration, depicting the major settings of magmatic construction of oceanic lithosphere (upper panel), the structural architecture of the types of oceanic lithosphere, developed in these settings (middle panel), and the details of magma production in the different settings (lower panel). Modified from Dilek and Furnes (2009), Furnes and Dilek (2017), Furnes and Safonova (2019).

unspecified peridotites, or as serpentinized peridotites due to their pervasive alteration. In their crustal sections, gabbro, basaltic dikes (often reported as sheeted dike complex) and basaltic lavas are reported in 111 of the ophiolites. Basaltic andesite, andesite, diorite and plagiogranite occur in some of the complexes (e.g., Dilek et al., 2005), whereas dacite and rhyolite are rare. Metamorphic grades of crustal rocks have been reported from 130 of the complexes (Table 1), and the majority (forty-two) of them display low grade, i.e., variable hydrothermal alteration and lower greenschist facies metamorphism. The remaining complexes are reported to have undergone upper greenschist-amphibolite-blueschist, blueschist to eclogite facies metamorphism (Table 1).

A major population of the AHOB ophiolites exhibits a complete crustal pseudostratigraphy, starting with a sedimentary cover on top, extrusive sequence of mainly pillowed and/or massive lavas, a sheeted dike complex, cumulate and isotropic gabbros, and ultramafic cumulates at the bottom; beneath the Moho are serpentinized peridotites, commonly intruded by doleritic dikes. In some of these ophiolites a several hundreds of meters thick metamorphic sole tectonically underlies the upper mantle peridotites (e.g., Dilek and Eddy, 1992; Dilek and Whitney, 1997; Dilek et al., 1999; Dilek et al., 2007; Dilek and Thy, 2009; Dilek and Furnes, 2011, 2014; Furnes and Dilek, 2017; Safonova et al., 2017). Some ophiolites are strongly deformed and dismembered during emplacement and post-emplacement stages during orogenic buildup, and they thus display a mélange character. The magmatic sequence in many ophiolites is capped by pelagic chert, hemipelagic siliceous mud/siltstone, turbiditic/greywacke sandstone, limestone and/or volcaniclastic rocks as part of their original sedimentary cover. It is not uncommon to find some ophiolitic subunits making up significant components of ocean plate stratigraphy (OPS), which is well–preserved in exhumed subduction–accretion complexes at paleo–convergent margins (Isozaki et al., 1990; Maruyama et al., 2010; Santosh, 2010; Wakita, 2012; Safonova and Santosh, 2014; Safonova et al., 2016; Zhang et al., 2018a, 2018b).

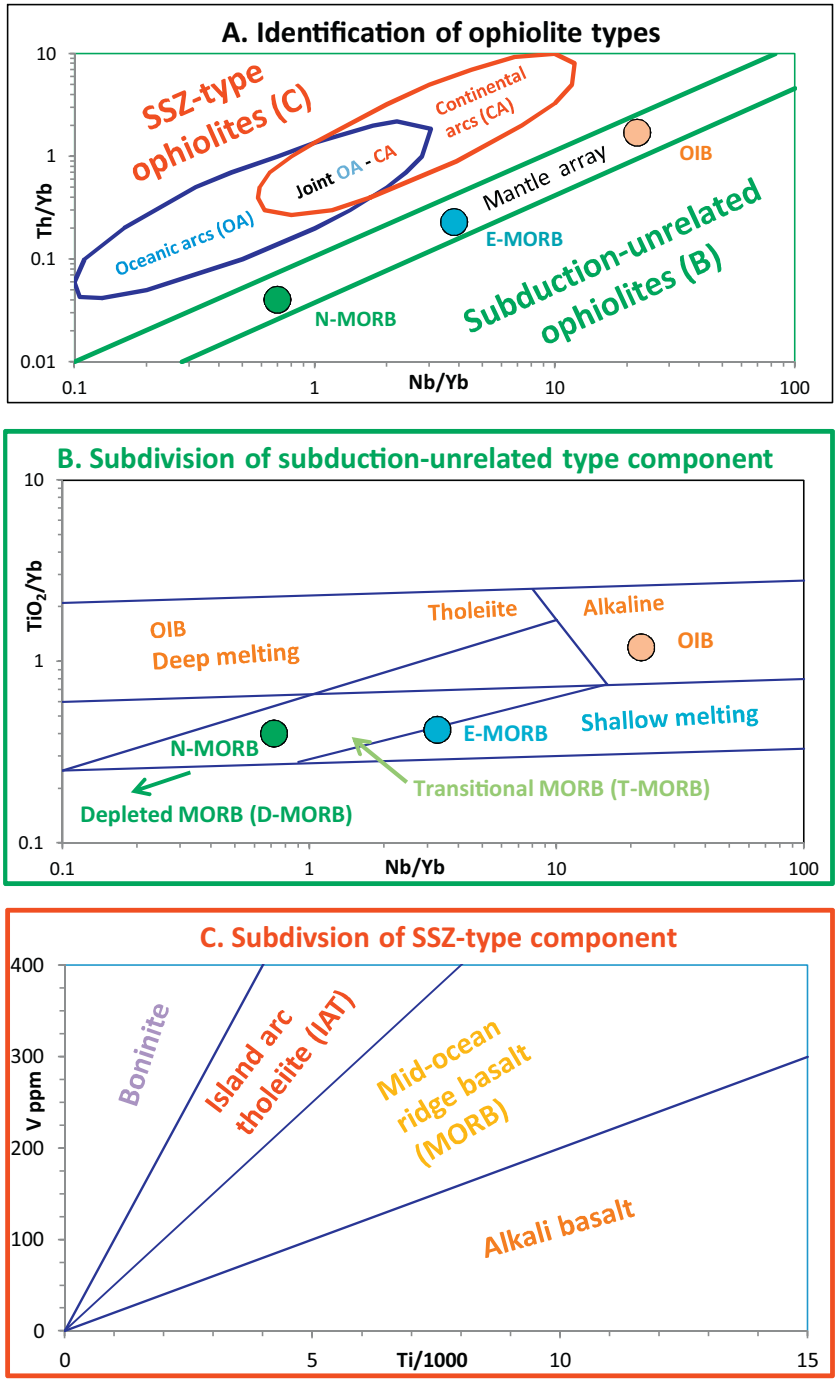

Fig. 7. Templates for various discrimination diagrams used for the geochemical discrimination of tectonic settings of formation of ophiolitic crustal units (after Pearce, 2014). (A) Nb/Yb – Th/Yb; (B) Nb/Yb – TiO_2/Yb; and (C) Ti/1000 – V diagrams.

5. Geochemical characteristics of basaltic rocks from the AHOB ophiolites

For the establishment of the database used in this compilation (Table 1) we have examined the bulk rock geochemical data of basaltic lavas and dikes, as well as a minor amount of isotropic gabbros from 152 published papers, comprising a total of 2179 analyses; in most of the cases ten or more analyses are available from each ophiolite complex. Most of these published papers (97%) are recent (2000–2019), and hence the geochemical data reported in them are more complete and of higher quality in comparison to the geochemical data published in the 1980s and 1990s. It is important to note, however, that the literature-based geochemical data used in our synthesis here have been produced in various laboratories, with different precisions and accuracies. Nevertheless, we have employed the same techniques of data processing (i.e., using the same diagrams for all collected data), which should help smoothen any major uncertainties.

5.1. Element mobility

In our classification of ophiolitic basalts and isotropic gabbros, we have applied seven elements (Ti, V, Zr, Y, Nb, Th and Yb). The majority of the investigated ophiolites experienced alteration and/or various degrees of metamorphism (Table 1), ranging from sub-greenschist to

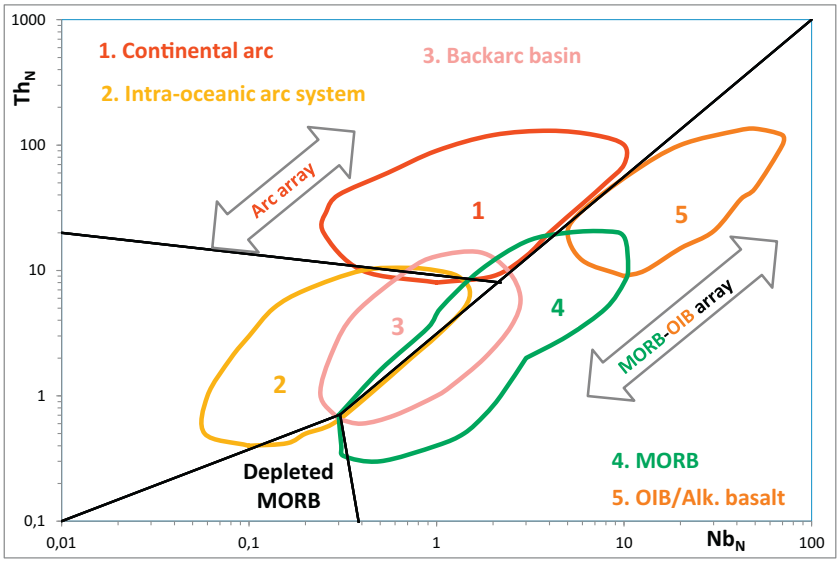

Fig. 8. Template for the Nb_N – Th_N discrimination diagram. Modified after Saccani et al. (2015).

eclogite facies. Sub-greenschist and greenschist facies are the dominant types of metamorphism for all various ophiolite types, adding between 72 and 82 percent. We review below how these seven elements in our classification respond to alteration and metamorphism.

Alteration and metamorphic processes that affect the element mobility in basaltic and gabbroic rocks in ophiolites are controlled by several factors such as the composition and stability of mineral phases, temperatures and fluxes (volumes) of fluid phases that circulate through the upper oceanic crust. Several low- to high-temperature experimental studies, related to these topics have been performed, as well as studies on natural systems (in particular submarine pillow lavas). It is widely accepted that Ti, V, Y, Zr, Nb, REE (particularly HREE), as well as Th are little mobile during alteration (e.g., Humphris and Thompson, 1978; Staudigel and Hart, 1983; Seyfried et al., 1988; Hofmann and Wilson, 2007; Furnes et al., 2012). A most critical element in the distinction between subduction-related and subduction-unrelated character is thorium (Th), and thus the Th/Yb ratio at any given Nb/Yb value is a significant indicator (Fig. 7A). Leaching experiments (Verma, 1992) have shown that Th remains almost constant at most conditions, but that it is depleted during palagonitisation. Studies on the behavior of U and Th (Valsami-Jones and Ragnarsdottir, 1997) during various conditions of sea-floor alteration indicate mobility of Th during high-temperature alteration, but that this element is mainly redistributed locally within an altered rock rather than being lost. Thus, for the vast majority of samples displaying low-grade metamorphic overprint, as well as no reports of presented palagonite, we have taken Th and the Th/Yb ratio of each given analysis as a near proxy for that of the originally fresh rock. None of the ophiolites we have examined contained palagonite as reported in the literature.

5.2. Magmatic character

For the distinction between alkaline, tholeiitic and calc-alkaline magmatic series, the alkali – total iron – magnesium (AFM) diagram (Irvine and Baragar, 1971) and the total alkali–silica (TAS) diagram (Le Maitre, 1989) have traditionally been applied. However, most of the analyzed samples in our synthesis are altered (with a dominant H_2O content ranging between ca. 2 – 5 wt.%), and metamorphosed (mostly in greenschist, but also medium-to high grade facies; see Table 1), and hence classification based on mobile major elements including Na, K, and Mg may be unreliable. Instead, we have used the relatively immobile elements Ti, Zr, Y, Nb, Th and Yb to test the magmatic character of ophiolitic lavas. As a first step, we employ the Nb/Y – Zr/Ti diagram of Winchester and Floyd (1977) to distinguish between subalkaline and alkaline basalts (Fig. 9). Thereafter, we isolate all the subalkaline basalts and plot those in the Zr/Y – Th/Yb discrimination diagram of Ross and Bedard (2009) to distinguish between tholeiitic and calc-alkaline character (Fig. 10). Subalkaline basalts are by far the most dominant compared to those of alkaline character (Fig. 9); the latter comprising between ca. 5 and 11 percent (Table 2), and with Jurassic ophiolites defining the highest proportion. A minor population of the Jurassic ophiolites, represented by some basaltic pillow lavas and dolerite samples of the Bangong Lake ophiolite in Tibet define very low Zr/Y numbers, due to extremely low Zr values, as reported by Shi et al. (2008). Of the subalkaline basalts, tholeiitic to transitional-type basalts are the dominant, whereas calc-alkaline basalts in general are subordinate (Fig. 10, and Table 2). The highest proportion of calc-alkaline basalts (16 percent) is represented by the Permo-Triassic examples.

5.3. Multi-element character of the ophiolite types

Primitive mantle (PM)-normalized multi-element diagrams, representing a collection of samples from the subduction-unrelated (Pl/CM/R and MOR) and subduction-related (BA, BA-FA, FA and VA) ophiolites are shown in Fig. 11. In general the subduction-unrelated ophiolite types show Th-enriched (Pl/CM/R-type) to Th-enriched/depleted (MOR-type) patterns. For the subduction-related types, like those of the MOR-type, the spread in the most incompatible elements (Th, Nb, La, Ce) is large, and negative Nb-anomalies are common, particularly for the FA- and VA-types.

In order to make the characterization of the multi-element character of the basaltic rocks (as shown in Fig. 11) more distinguishable, and hence to emphasize the differences between the various ophiolite types more effectively, we have calculated the Nb-anomalies and the PM-normalized La/Yb ratios [(La/Yb)N] for all the available data (Fig. 12). The Nb-anomaly, calculated as $[(Th_N + La_N)/2] - Nb_N$ for each sample, show that 80 % of the Pl/CM/R-type ophiolites, and 60 % of the MOR-type ophiolites have positive Nb-anomalies. For the subduction-related ophiolite types, on the other hand, the negative Nb-anomalies are the dominant feature. The BA- and BA-FA-type ophiolites display similar results, i.e. 73% and 77%, respectively, the FA-type 93%, and the VA-type 100% negative Nb-anomalies (Fig. 12). As to the PM-normalized La/Yb patterns, the main part (60%) define La-enriched nature (between 1 and 10), and the MOR-type ophiolites also exhibit a significant (35%) La-depleted character, with $(La/Yb)_N$ ratios between 0.1 and 1. For the basalts of the subduction-related BA-, BA-FA- and FA-type

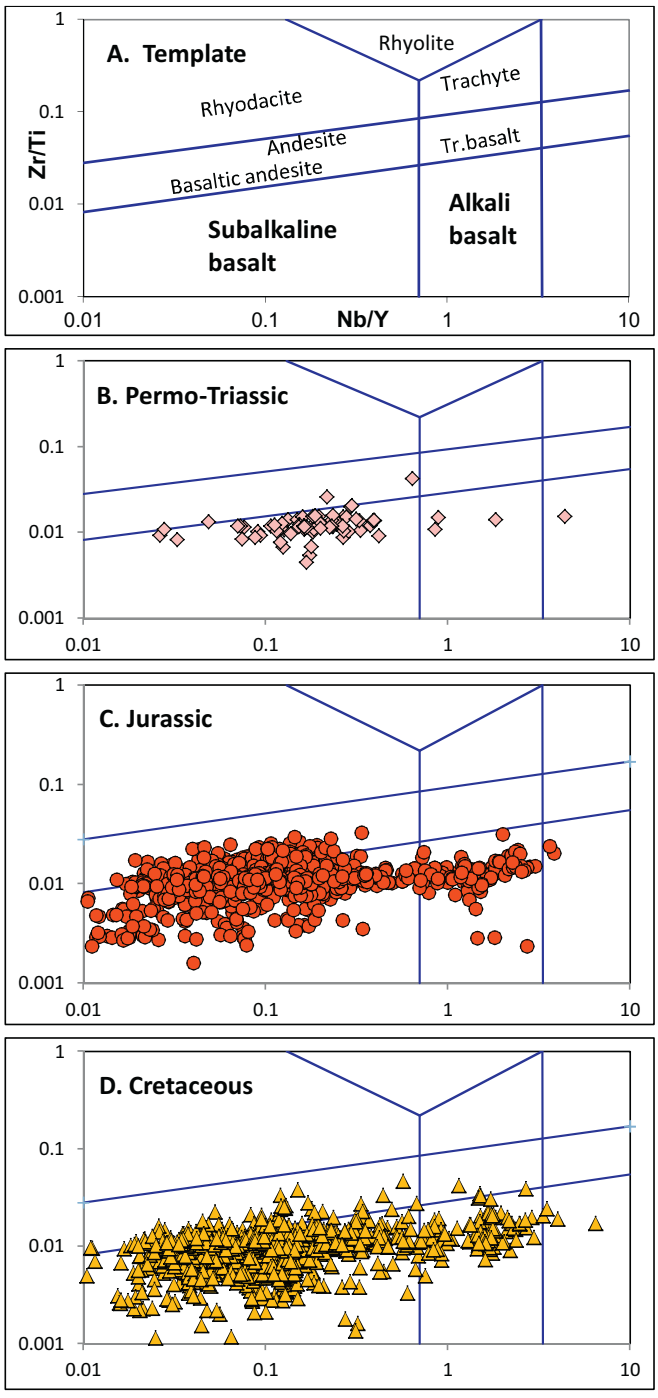

Fig. 9. Nb/Y – Zr/Ti diagram to distinguish between subalkaline and alkaline basalts (modified after Floyd and Winchester, 1975).

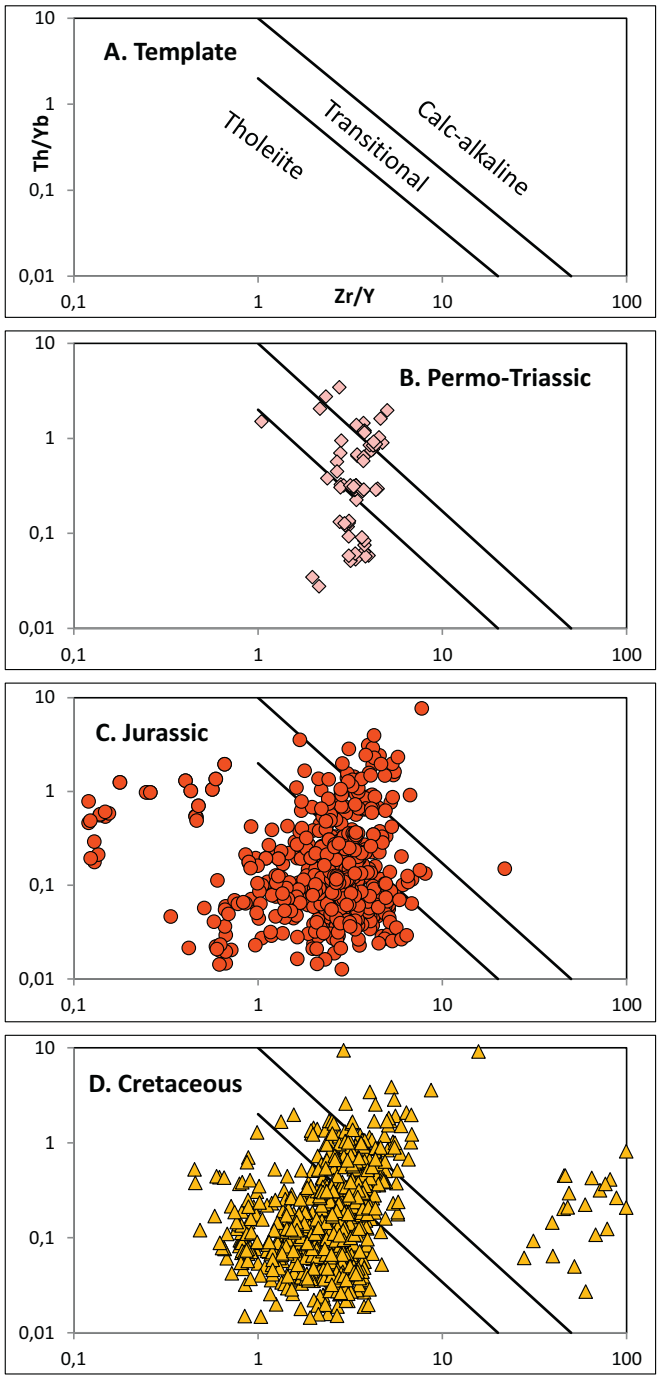

Fig. 10. Zr/Y – Th/Yb diagram to distinguish between tholeiitic and calc-alkaline basalts.

ophiolites the La/Yb_N ratios show a dominantly depleted nature, 55%, 70%, and 76%, respectively, whereas the VA-types define a predominantly enriched nature (Fig. 12).

5.4. Discrimination diagrams

We have plotted the elements Ti, Y, Zr, Nb, V, Th and Yb, applied either as various ratios (Nb/Yb – Th/Yb, Nb/Yb – TiO_2/Yb), and element concentrations (Ti – V), or as MORB-normalized elements (Nb_N – Th_N) of the basaltic rocks, in the discrimination diagrams of Pearce (2014) and Saccani et al. (2015). Before presenting the results of the complete data set, we introduce a selection of the various subtypes of the subduction-unrelated and subduction-related ophiolites, demonstrating their different positions in the various discrimination diagrams (Fig. 13). For the subduction-unrelated category, we chose three examples demonstrating a complete range from OIB-transitional E-MORB (Pl/CM/R-type) and two MOR-type examples representing typical E-MORB and N-MORB (Fig. 13A–D). For the subduction-related types a representative example of each of the four types (BA, BA-FA, FA and VA) were selected and plotted in the appropriate diagrams of Fig. 13. The ophiolites classified as BA and BA-FA types plot rather similarly in the Th/Yb-Nb/Yb diagram, whereas in the V-Ti diagram the BA type plot predominantly in the MORB field, while the BA-FA types show a much wider spread plotting in the boninite, IAT and MORB fields

Table 2
Magmatic character of the basalts of the investigated AHOB ophiolite complexes.

Age	Number of sequences and analyses in parantesis	Magmatic affinity (in %)				
		Alkaline Nb/Y > 0.7	Subalkaline Nb/Y < 0.7	Subalkaline division based on Zr/Y vs Th/Yb character		
				Tholeiite	Transitional	Calc-alkaline
Triassic-Permian	8 (79)	5	95	26	58	16
Jurassic	53 (857)	10.7	89.7	83	12	5
Cretaceous	67 (1341)	7.8	92.2	73	21	6

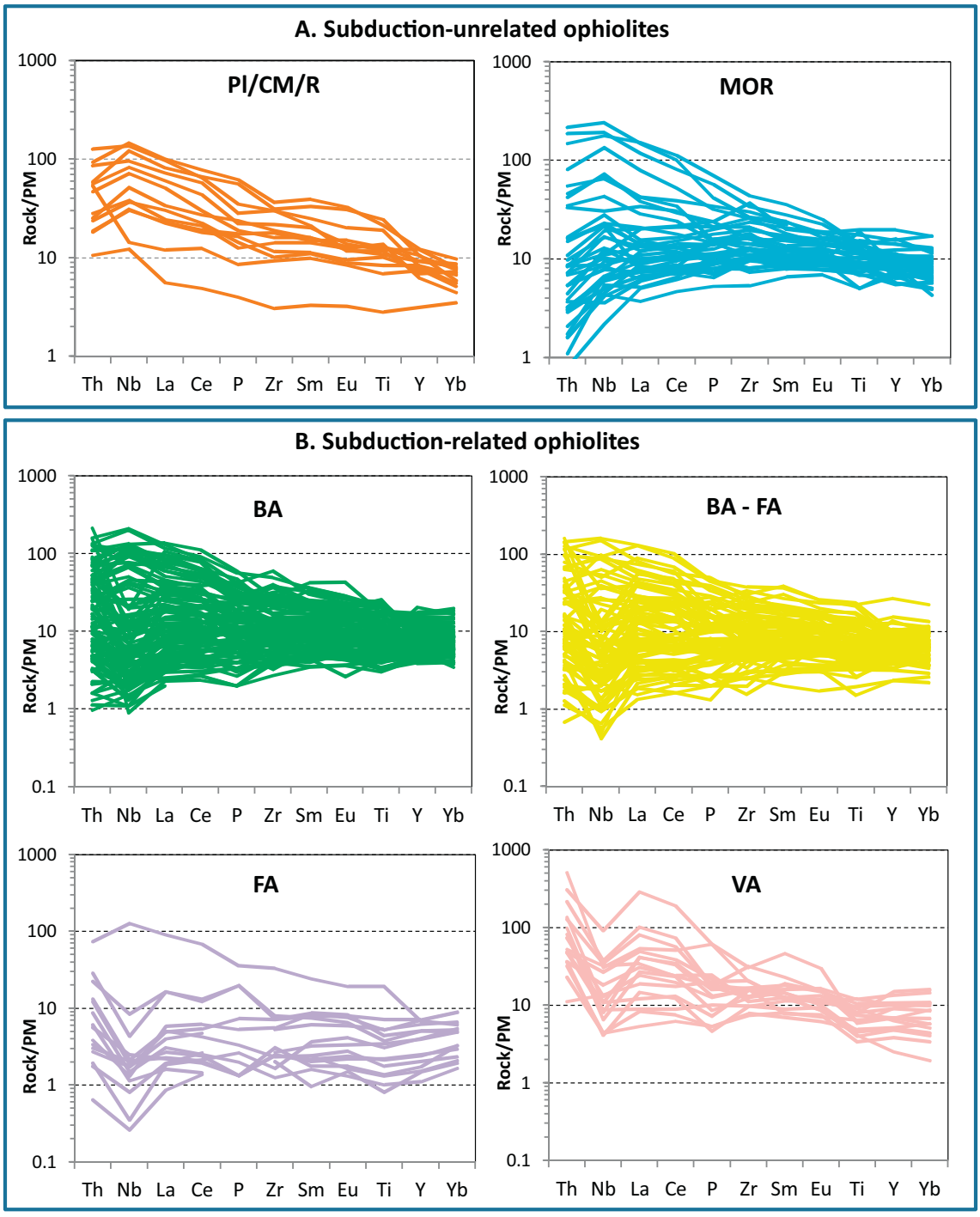

Fig. 11. Representative PM-normalized multi-element diagram of the subduction-unrelated (Pl/CM/R- and MOR-type) and subduction-related (BA-, BA-FA-, FA- and VA-type) ophiolites. References to geochemical data are given in Supplementary Table 1. The PM values are from Lyubetskaya and Korenaga (2007): Th: 62.6 ppb; Nb: 460 ppb; La: 508 ppb; Ce: 1340 ppb; P: 66 ppm; Zr: 8.42 ppm; Sm: 324 ppb; Eu: 123 ppb; Ti: 950 ppm; Y: 3.37 ppm; Yb: 346 ppb).

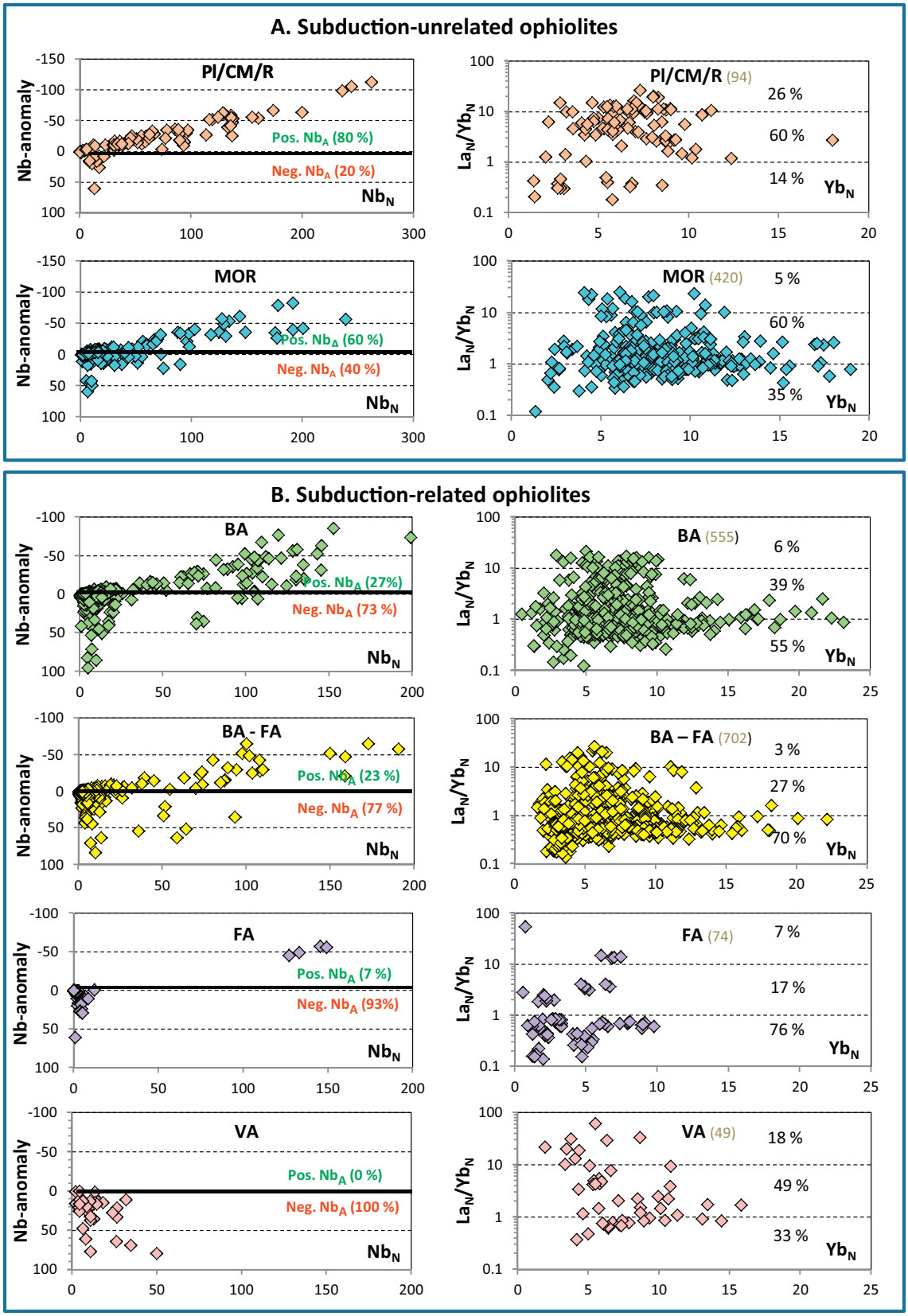

Fig. 12. Nb-anomalies (left column) and PM-normalized La/Yb-ratios (right column) for the subduction-unrelated and subduction-related ophiolite types. The Nb-anomaly is calculated as PM-normalized Th, Nb and La values according to the formula as $((Th_N + La_N)/2) - Nb_N$. The number in brackets show the number of analyses represented.

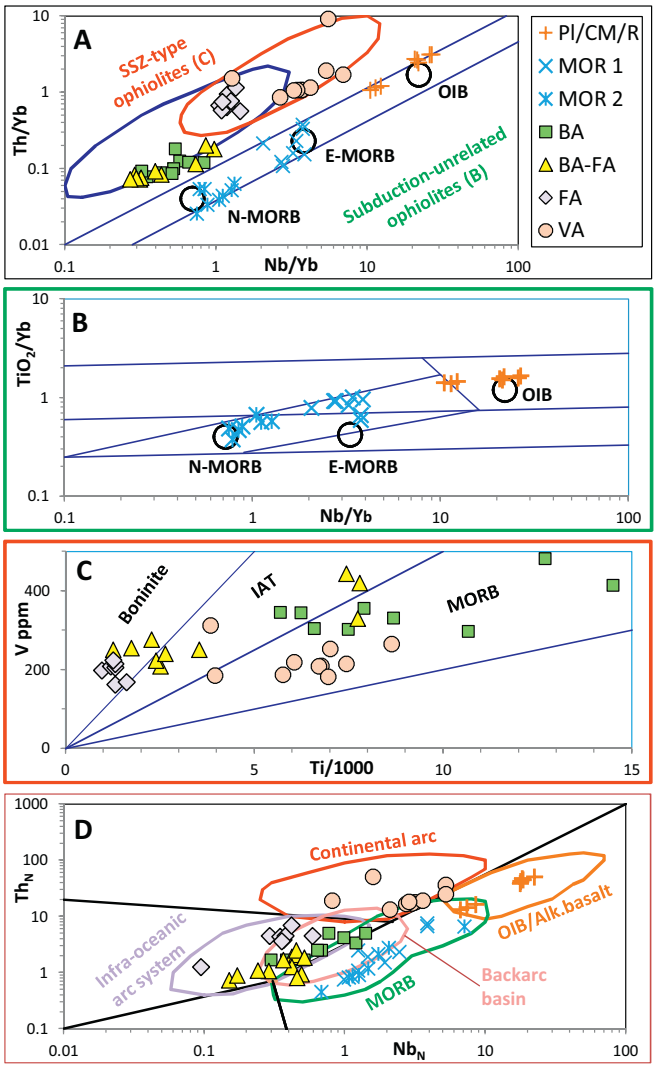

Fig. 13. Representative samples of the subduction-unrelated (Pl/CM/R and MOR types) and subduction-related (BA, BA-FA, FA and VA types) AHOB ophiolites plotted in Th/Yb-Nb/Yb (A), TiO_2/Yb-Nb/Yb (B), V-Ti (C), and Th_N-Nb_N (D) discrimination diagrams. The selected ophiolites are: Pl/CM/R type: Zhongba ophiolite, southern Tibet; MOR 1 type: Betic ophiolite, Spain; MOR 2 type: Elba ophiolite, Elba Island, Italy; BA type: Karadag ophiolite, Turkey; BA-FA type: Troodos, Cyprus; FA type ophiolite: Dingqing ophiolite, Tibet; VA type: Penjween ophiolite, Iraq. For further information on these ophiolite examples: see Tables 1 and 4, and Supplementary Tables 1 and 2.

(Fig. 13A and C). The samples of the selected FA–type ophiolite plot exclusively on the joint oceanic arc/continental arc field of the Th/Yb-Nb/Yb diagram, and in the boninite field of the V-Ti diagram. The VA–type ophiolite plots in the continental arc field of the Th/Yb-Nb/Yb diagram, and predominantly in the MORB field of the V-Ti diagram.

The results of our synthesis of the complete data sets are shown in Figs. 14–18. In each of the ophiolite complexes, as expressed in the discrimination diagrams of Pearce (2014), the subduction influence (0–100%) has been estimated (see Supplementary Table 1). All samples that plot within the mantle array (at any Nb/Yb value) have been taken as non-influenced by subduction. Thus, when all basalt samples from an ophiolite plot within the mantle array, they are featured as 0% subduction-influenced, and 100% subduction-influenced when they all plot above the mantle array (see further explanation as footnotes for Supplementary Tables 1 and 2. Samples that plot above the mantle array, i.e., in the Th/Yb – Nb/Yb diagram of Fig. 15, and in the field of the volcanic arc array of Fig. 16, have been taken as influenced by subduction processes. The results are shown as histograms in Fig. 14A. This calculation shows that those ophiolites that are negligibly or entirely unaffected (0–10%) by subduction-related processes comprise a significant part; those substantially to entirely subduction-influenced (90–100%) constitute the major part, as well. The samples that plot in the mantle array were further plotted in the Nb/Yb versus TiO_2/Yb diagram of Fig. 16. This diagram separates the basalts that have originated as a result of shallow–depth melting (MORB array) from those of a deep melting origin (OIB array). The results are illustrated by two histograms in Fig. 14B1 and B2, showing approximately equal proportions of MORB and alkali basalts.

We have also plotted all samples showing subduction-influence in the Th/Yb–Nb/Yb diagram of Fig. 15 in the V–Ti diagram of Fig. 17. They fall into the fields of boninite, IAT, MORB and alkali basalts. The results of this compilation are shown in four histograms (for boninite, IAT, MORB and alkali basalt) in Fig. 14. IAT and MORB are the dominant basalt types, occurring in various proportions in all of the complexes we have examined (Fig. 14C2 and C3). Boninite occurs in minor amounts and are absent in most of the complexes, and alkali basalts are rare (Fig. 14C1 and C2).

The calculated percentages of each of the occupied fields of the discrimination diagrams (Figs. 15–18), represented by the Permo-Triassic, Jurassic and Cretaceous time periods, are shown in Table 3. The calculated values for each of the 136 ophiolites are presented in Supplementary Tables 1 and 2. The Th/Yb - Nb/Yb relationships for the Permo-Triassic through Cretaceous ophiolites are shown in Fig.15. The majority of the analyzed samples are subduction-influenced, in particular those of the Cretaceous complexes that add up to ca 60%. The smallest contribution, apart from the Permo-Triassic samples, is represented by the continental arc composition (Table 3). Isolating the data of the OIB-MORB array (Fig. 7A) in the Nb/Yb – TiO_2/Yb diagram (Fig. 16), we see that the majority of the ophiolites define N-MORB character, whereas alkali basalts are dominant among the OIB types indicating deep melting for their origin. In further distinguishing the subduction-related ophiolites, we plot them in the V-Ti diagram (Fig. 17). The Jurassic and Cretaceous ophiolites mostly define an IAT character, whereas the Permo-Triassic ophiolites dominantly show a MORB character on this diagram (see Table 3).

The MORB-normalized Nb and Th values of the Permo-Triassic, Jurassic and Cretaceous ophiolites have been plotted in a simplified version of the Saccani et al. (2015) discrimination diagram (Fig. 18), and the estimated proportions of subduction-related and subduction-unrelated data are shown in Table 3. The Permo-Triassic and Jurassic ophiolites demonstrate the dominance of a subduction-unrelated character (particularly those of Jurassic age), whereas those Cretaceous ophiolites mostly display a subduction-related character (Table 3).

5.5. Nd-isotope data of basaltic rocks

Nd-isotope data were assembled from 49 of the 137 investigated ophiolite complexes, comprising altogether 450 analyses. The references to the isotope data are shown in Table 1. Each of the MOR-, Pl/CM/R-, BA-, BA-FA-, FA- and VA- ophiolite types, classified as such based on the discrimination diagrams (Figs. 15–18), has been isolated and the Nd-isotope data for different ophiolite types are compared and discussed regarding the nature of their melt sources. To this end we have plotted the ε_{Nd}-values versus Sm/Nd ratios, and have made histograms of the ε_{Nd}-values; the results of this compilation are presented in Fig. 19.

The ε_{Nd} - Sm/Nd diagrams of the basalt to basaltic andesite samples define a pronounced scatter in the Sm/Nd ratios at any given ε_{Nd} -value. An explanation for this pattern may be given by the behavior of the two elements in question. Since Nd is a more incompatible element than Sm, the Sm/Nd ratio of a melt decreases during crystal fractionation (CF), compared to the original value of the melt prior to fractionation. The

Fig. 14. Histograms summarizing: (A) the percentage of subduction influence (all samples); (B) melt regime (shallow or deep) of the subduction-unrelated basalts; (C) the percentage of boninite, IAT, MORB, and alkali basalts of the subduction-influenced basalts.

Sm/Nd ratio of melts also decreases during partial melting (particularly low-degree of melting), but increases during repeated melting of a progressively and strongly depleted mantle. The ε_{Nd} -values of ca. +7 to +11.5, as defined by the black stippled lines of the ε_{Nd} - Sm/Nd diagrams (Fig. 19), represent depleted mantle (DM) values of the mantle growth curve at the Jurassic to Cretaceous time range (ca. 100 Ma) as defined by the given samples (Shaw et al., 1987; Vervoort and Blichert-Ioft, 1999).

The ε_{Nd} -values of most of the MOR-type ophiolites fall within the DM (depleted mantle)-range, whereas for the Pl/CM/R-, BA-, BA-FA-, FA + VA-type ophiolites the majority define lower ε_{Nd} values than defined by the DM range (Fig. 19). We attribute this pattern to mixing of mantle-generated melts with variable amounts of melts generated from continental crustal material (CM) and/or global subducted sediments (GLOSS), defining, in general, very low, negative ε_{Nd} -values (Plank and Langmuir, 1998). As to the Pl/CM/R-types ophiolites, the generally low ε_{Nd} -values might be due to contamination by crustal continental material during ascent to the surface. These ophiolites, hence, more likely represent Continental Margin (CM)- and/or Rift (R)-type, rather than Plume (Pl)-type ophiolites. However, caution should be taken, since we do not know where and how the low epsilon Nd material was obtained by the magmas.

For the subduction-related ophiolites, the pattern can easily be explained by subduction of sediments (GLOSS), of which the main component (ca. 76 %) is terrigenous material, compositionally similar to upper continental crust (Plank and Langmuir, 1998). The BA and BA-FA ophiolites are similar with respect to their DM-contribution, and with the FA and VA types showing the lowest DM-values. However, the BA-FA types display the lowest ε_{Nd} -values registered, and thus demonstrate the close connection to subduction zone influence.

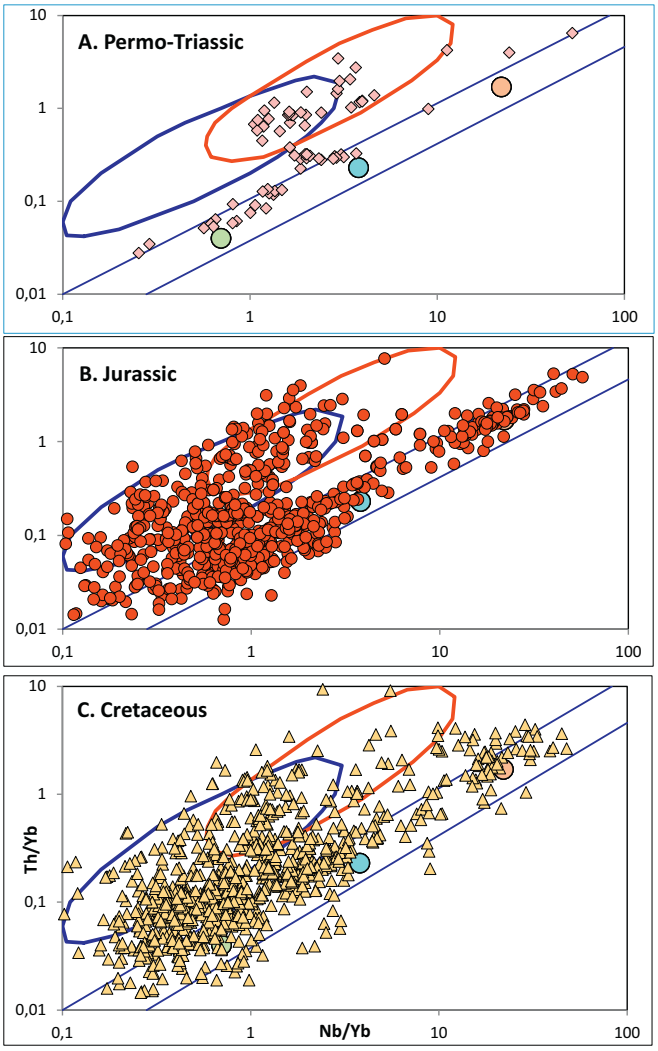

Fig. 15. Nb/Yb – Th/Yb plots of the basaltic rocks of the Permo-Triassic, Jurassic, and Cretaceous ophiolites of the Alpine-Himalayan Orogenic Belt.

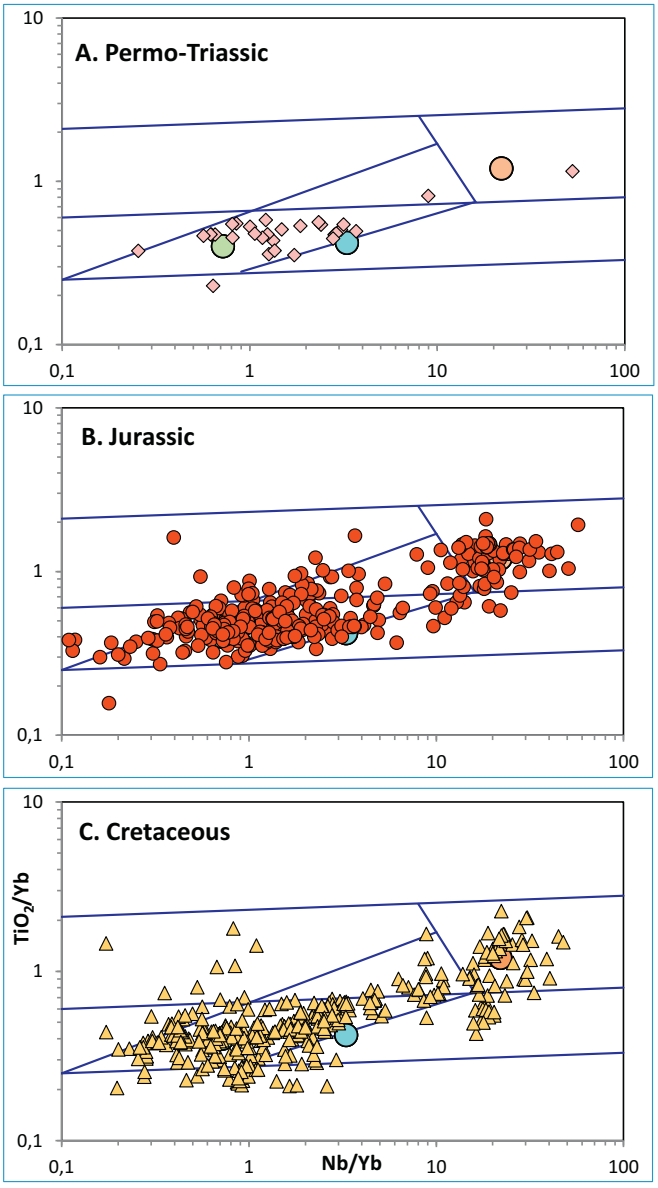

Fig. 16. Nb/Yb – TiO_2/Yb plots of the basaltic rocks of the Permo-Triassic, Jurassic, and Cretaceous ophiolites of the Alpine-Himalayan Orogenic Belt.

As to the basalts of the MOR-type ophiolites and their ε_{Nd} -values, which are lower than that of the depleted mantle, this pattern cannot be explained by active subducted sediment contribution. However, global recycling and differentiation of the mantle have occurred as long as some form of plate tectonic process has been active, likely dating back to the early Archean (e.g., Dilek and Polat, 2008; Furnes et al., 2009, 2012; Komiya et al., 2015; Maruyama et al., 2016; De Wit et al., 2018; Santosh et al., 2020), making it progressively heterogeneous (Kimura et al., 2017). The mantle under some parts of subduction-unrelated mid-ocean ridges may thus contain material from former subduction-related regimes, yielding melts with low ε_{Nd} -values, and may thus provide an explanation to the low ε_{Nd} -values of the MOR-type ophiolites shown in Fig.19.

5.6. Chemical character versus age and geography

The Permo-Triassic, Jurassic and Cretaceous ophiolites were organized in an approximately East-West order along the length of the AHOB, and Fig. 20 displays the relationship between the level of subduction influence (between 0 and 100%) and geographic position of the AHOB ophiolites. Most of the ten Permo-Triassic ophiolites occur in the western part of the AHOB, and a few in the easternmost part. Six of these are moderately to non-subduction influenced, and three are 100% subduction-influenced. The Jurassic ophiolites occur principally in the western and eastern parts, and are mostly absent in the middle part of the AHOB. Subduction-unrelated MOR–type ophiolites dominate in the western part, but from the Balkan Peninsula onwards to the east the AHOB ophiolites become more subduction-related. However, in the eastern part of the AHOB, we see a substantial number of subduction-unrelated ophiolites exposed again. The Cretaceous ophiolites dominate in the central domain of the orogen, i.e. from the Greek islands in the Aegean Sea and the eastern Mediterranean regions through the eastward extent of the AHOB (Dilek and Furnes, 2019). A fairly high proportion of ophiolites is 100% subduction-influenced, particularly those in Anatolia.

Ophiolites that exhibit OIB signature occur in all three age groups, but are most common in the Cretaceous age category (Fig. 21).

6. Lithology versus geochemistry

6.1. Crustal rock

The relationships between crustal lithological components of the

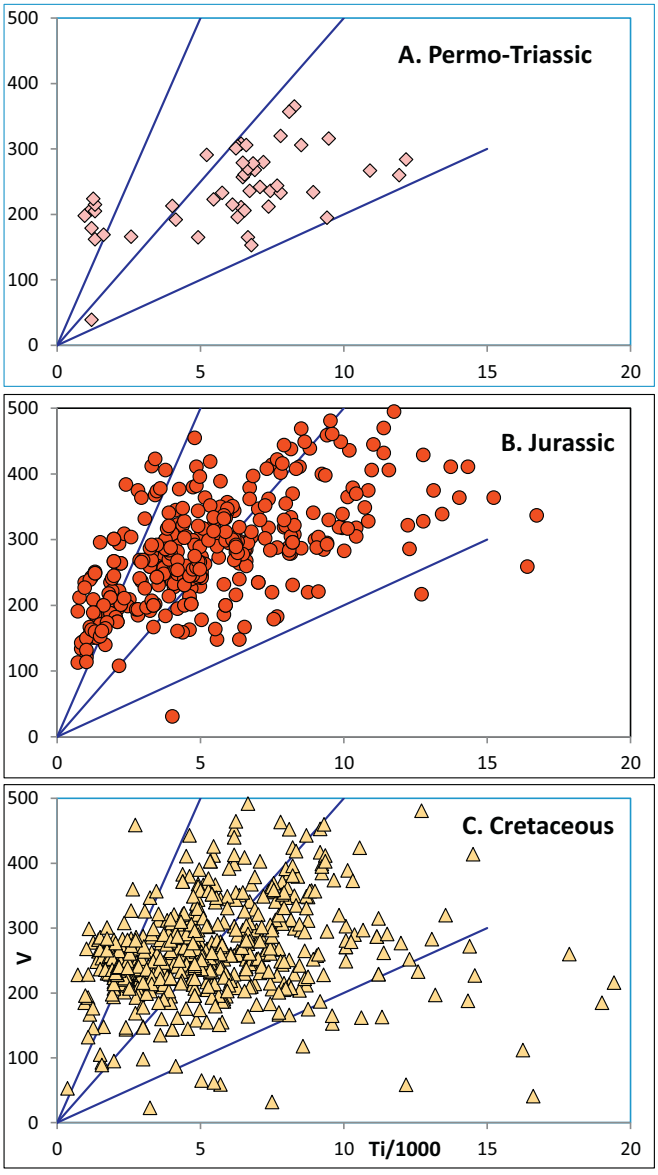

Fig. 17. Ti/1000 – V plots of the basaltic rocks of the Permo-Triassic, Jurassic, and Cretaceous ophiolites of the Alpine-Himalayan Orogenic Belt.

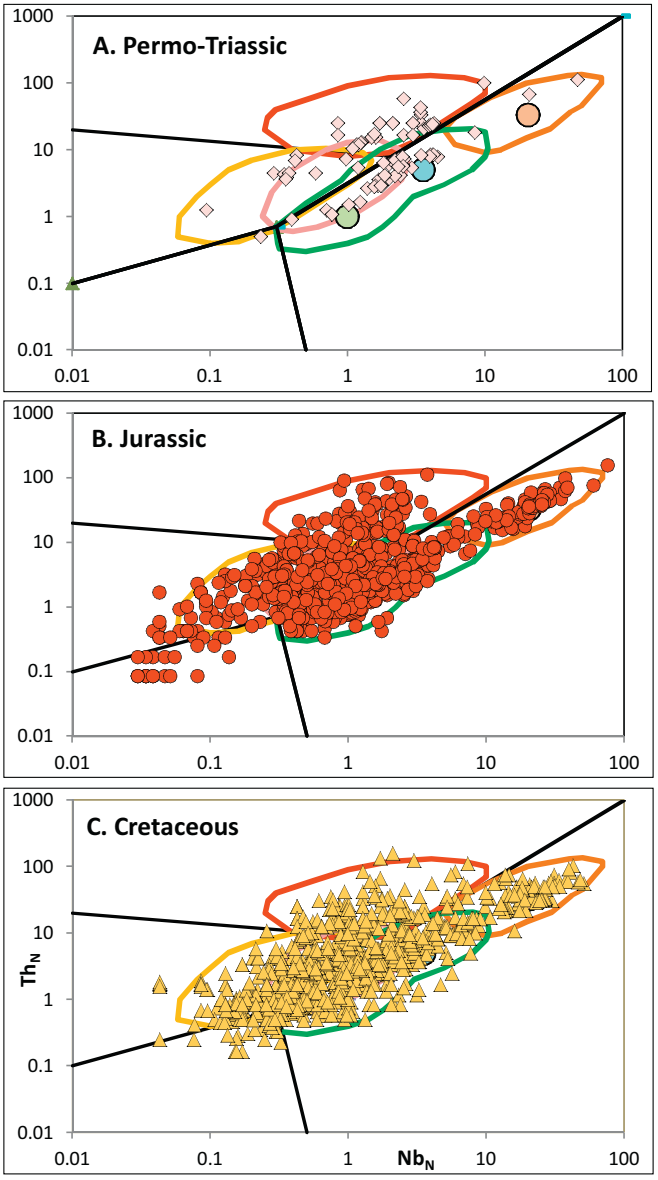

Fig. 18. Nb_N – Th_N plots of the basaltic rocks of the Permo-Triassic, Jurassic, and Cretaceous ophiolites of the Alpine-Himalayan Orogenic Belt.

ophiolites examined in this study are listed in Table 1, and their characterization based on the geochemical characteristics (shown in Figs. 15–18) is displayed in Fig. 22. There is a caveat, however, that the samples presented in the literature that we used for our database collection in this paper are not necessarily random samples and may reflect a sampling bias. Therefore, the rock type distributions may to some extent be based on potentially unrepresentative sampling.

For all the ophiolite complexes we have examined, the occurrence of gabbro and basalt is a common feature, representing the most abundant ophiolitic subunits. The Backarc (BA) type oceanic crust is structurally like MOR–generated oceanic lithosphere, and their rock type abundances are, hence, similar; the Backarc-Forearc (BA-FA)–type ophiolites also display a similar lithostratigraphy to that in BA–type ophiolites (Fig. 22). The Forearc (FA) and Volcanic Arc (VA) type ophiolites exhibit slightly higher abundances of basaltic andesite and andesite (Fig. 22). Boninite is more frequently reported from FA–type ophiolites in comparison to the other types. Even though many of the ophiolite complexes do not contain all subunits of a typical Penrose ophiolite stratigraphy (Dilek, 2003a; Robinson et al., 2008), the geochemical classification as shown in Table 4 largely reflects the lithological construction of the investigated ophiolites.

6.2. Mantle rocks

The mantle rocks of all the ophiolite types are dominated by harzburgite, lherzolite and dunite. Wehrlite and pyroxenite also occur in some complexes (Fig. 23). All the ophiolites also contain peridotites and serpentinite of unspecified type as reported in the literature. The VA-type ophiolites only have unspecified peridotites; however, the number of examples is limited (only 4) and may not be representative.

6.3. Metamorphic grade

The metamorphic facies of the reported ophiolites varies from low-grade through blueschist and eclogite. The term *low-grade* includes variants such as “non-metamorphic to weakly metamorphosed, sub-greenschist, low-T alteration and hydrothermal alteration” (Table 1), we refer to all these categories as sub-greenschist facies metamorphic overprint in this paper. The majority of the ophiolites of all different types have undergone sub-greenschist and greenschist facies

Table 3
Summary of discrimination character (Pearce, 2014; Saccani, 2015) of the basaltic rocks of the Alpine-Himalayan Orogenic Belt.

Discrimination (Pearce 2014)		Triassic-Permian	Jurassic	Cretaceous
Nb/Yb - Th/Yb proxy (in %)				
Mantle		47	58	38
Weak subduction influence		13	13	28
Oceanic arc (OA)		0	18	21
Continental arc (CA)		12	2	3
Joint OC-CA		28	9	10
Ti/V proxy(in %)				
Bon		14	17	18
IAT		6	48	43
MORB		80	34	35
Alk. Basalt			1	4
Nb/Yb - TiO_2/Yb proxy (in %)				
D-MORB	MORB array	3.4	5.5	6.4
N-MORB	MORB array	53.3	48.3	38.9
E-MORB	MORB array	36.7	21	29.6
OIB-tholeiite	OIB array	3.3	12	7.5
OIB-alkaline	OIB array	3.3	13.2	17.6
Discrimination (Saccani 2015)				
Subduction-related (in %)				
IAT & Bon & BAB		13.6	26.4	37.7
CAB		33.3	10.4	11.6
Sum		46.9	36.8	49.3
Subduction-unrelated (in %)				
MORB & BAB		49.4	53.3	42.6
OIB		3.7	9.9	8.1
Sum		53.1	63.2	50.7

metamorphism of ocean floor origin (Fig. 24). Only the subduction-unrelated (MOR and Pl/CM/Rift) and BA type ophiolites exhibit amphibolite to blueschist to eclogite facies metamorphic overprint because of their post–magmatic involvement in subduction related burial and subsequent exhumation at the interface between a downgoing plate and an upper plate (Fig. 24; Table 1). Subduction-related ophiolites commonly originate from the upper plates of subduction zones, whereas subduction-unrelated ophiolites have their origins in down-going plates (Dilek and Furnes, 2014). Therefore, the protoliths of these subduction–unrelated ophiolites became subjected to high-P metamorphism (blueschist to eclogite facies) as they started subducting with downgoing plates.

7. Ophiolite types of the Alpine-Himalayan Orogenic Belt

The geochemical proxies for the different ophiolite types (as shown in Supplementary Tables 1 and 2) demonstrate that the AHOB ophiolites vary significantly. Ophiolite types may grade into each other, and admittedly, in some cases it may be difficult to assign an ophiolite to one specific type. Different ophiolite types with zero to 100% subduction contribution may occur within the same suture zone.

We have treated the geochemical data as outlined in Figs. 9–10 and Figs. 13–18 and classified the examined ophiolite sequences of the AHOB according to the various tectonic settings as outlined in Fig. 6. The compilation is shown in Table 4, and also illustrated in a pie-diagram (Fig. 25). The ophiolite types classified as Backarc (BA), Backarc to Forearc (BA-FA), Forearc (FA), and Volcanic Arc (VA) constitute 43%, 19%, 8% and 6%, respectively, making the subduction-related ophiolites a dominant group (76%). Of the remaining 24%, the MOR type makes up the major part (19%) and the Pl/CM/R type the last 5% (Fig. 25).

It is important to note that not all ophiolites examined in this study have the required geochemical data to be fully processed through the discrimination procedure as outlined in Figs. 7 and 8. In Fig. 26 we have selected most of the ophiolite complexes from which complete geochemical datasets are available. We have further split these data into three age groups, Permo-Triassic, Jurassic and Cretaceous, and plotted the ophiolite types of the three time periods onto the spatial map of the AHOB (Fig. 26A–C). The Permo-Triassic (Fig. 26A) ophiolites predominantly occur in the Balkan Peninsula (Albania and Greece), and are exclusively of subduction-unrelated character. An exception is the Dingqing ophiolite in the eastern part of the AHOB in central Tibet. It should be emphasized, however, that this ophiolite is considerably younger than the others in the Balkan Peninsula, and that it straddles

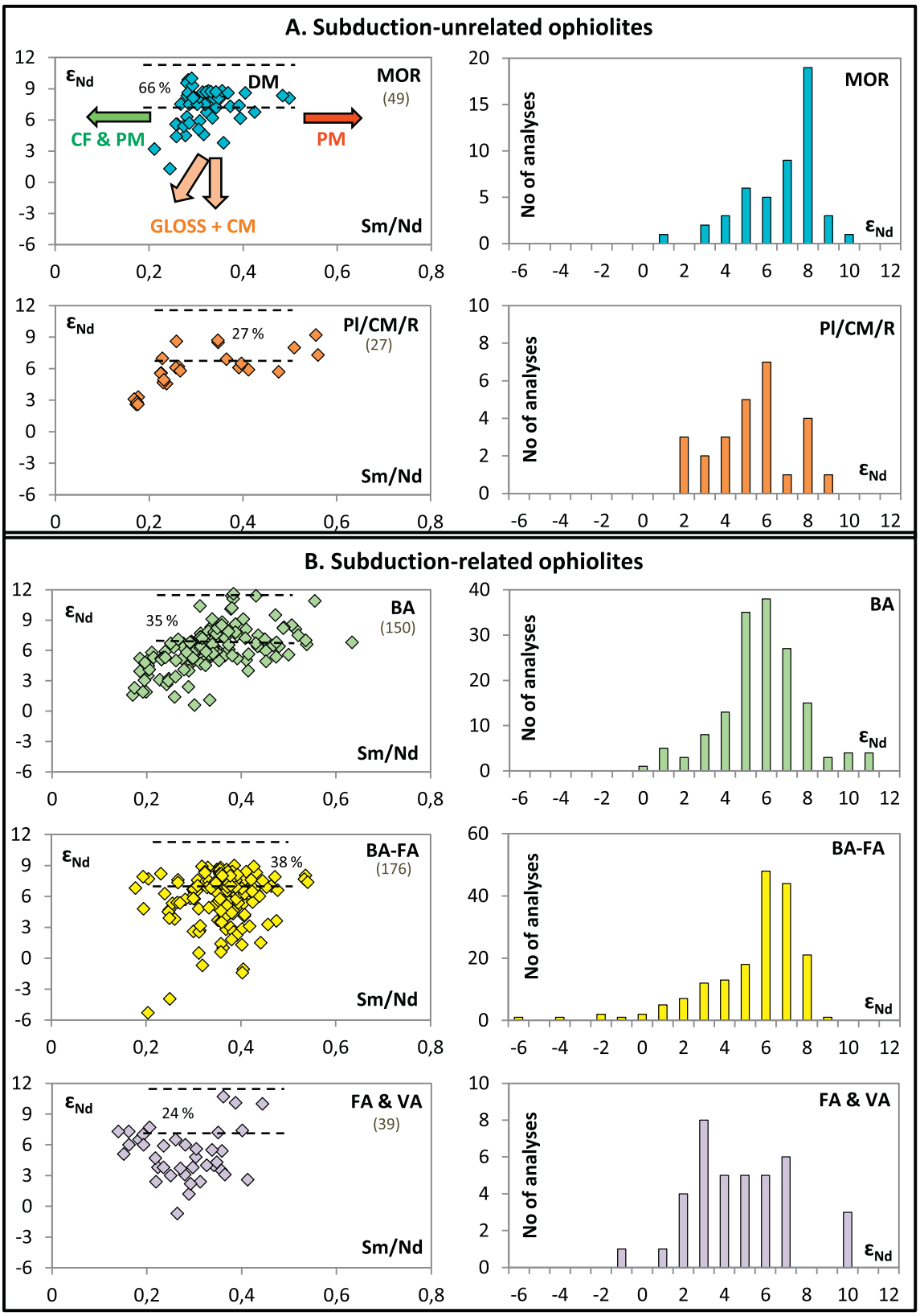

Fig. 19. ε_{Nd} - Sm/Nd diagrams and histograms of the ε_{Nd} – values for the subduction-unrelated and subduction-related ophiolite types. The number in brackets show the number of analyses represented.

the Triassic-Jurassic boundary.

The Jurassic ophiolites of the western AHOB (Betic–Spain, Western Alps–France, Italy and Switzerland) and part of the Balkan Peninsula, are exclusively of MOR type. Some Jurassic ophiolites also exist in the Himalayan–Tibetan region (Fig. 26B). Jurassic ophiolites are scarcely documented from the central part of the AHOB, but they are abundantly

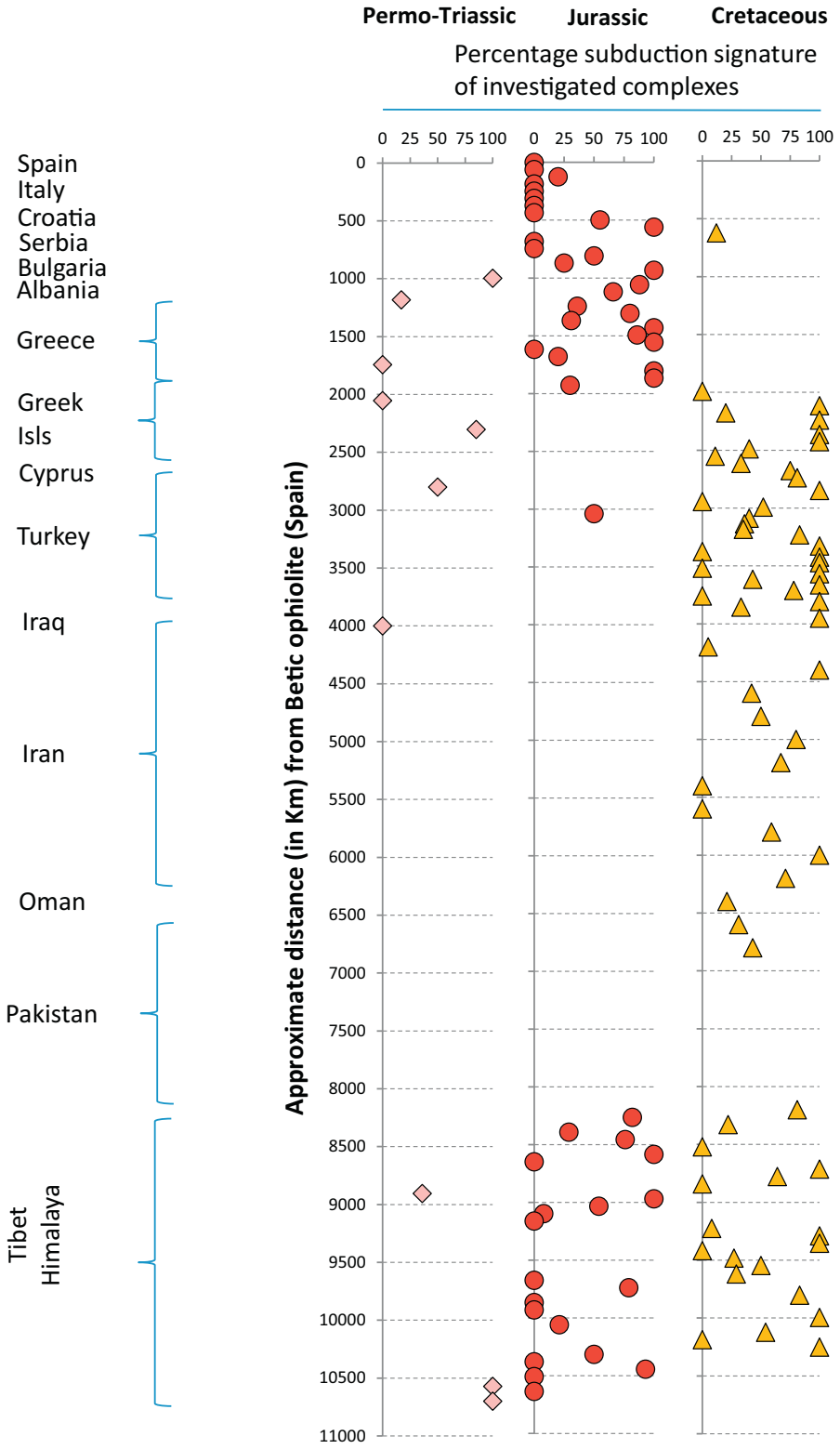

Fig. 20. Subduction-signature of the basaltic rocks of the Permo-Triassic, Jurassic, and Cretaceous ophiolites along the Alpine-Himalayan Orogenic Belt, from Spain to eastern Himalaya. Based on the Saccani et al. (2015) classification as shown in Supplementary Table 2.

represented in the Himalayan region by both subduction-unrelated and subduction-related types, though most of these belong to the latter type. In addition to the MOR-type ophiolite, BA- and BA-FA-types are the predominant types of the subduction-related Jurassic ophiolites. The Cretaceous ophiolites (Fig. 26C) are abundant in the central to eastern domains of the orogenic belt (Anatolia, Cyprus, Zagros, SE Arabian Peninsula–Oman and UAE), and are mostly represented by subduction-related types, i.e. predominantly the BA and BA-FA types (Fig. 26C).

8. Discussion

We have documented thusfar in this paper the distribution of the

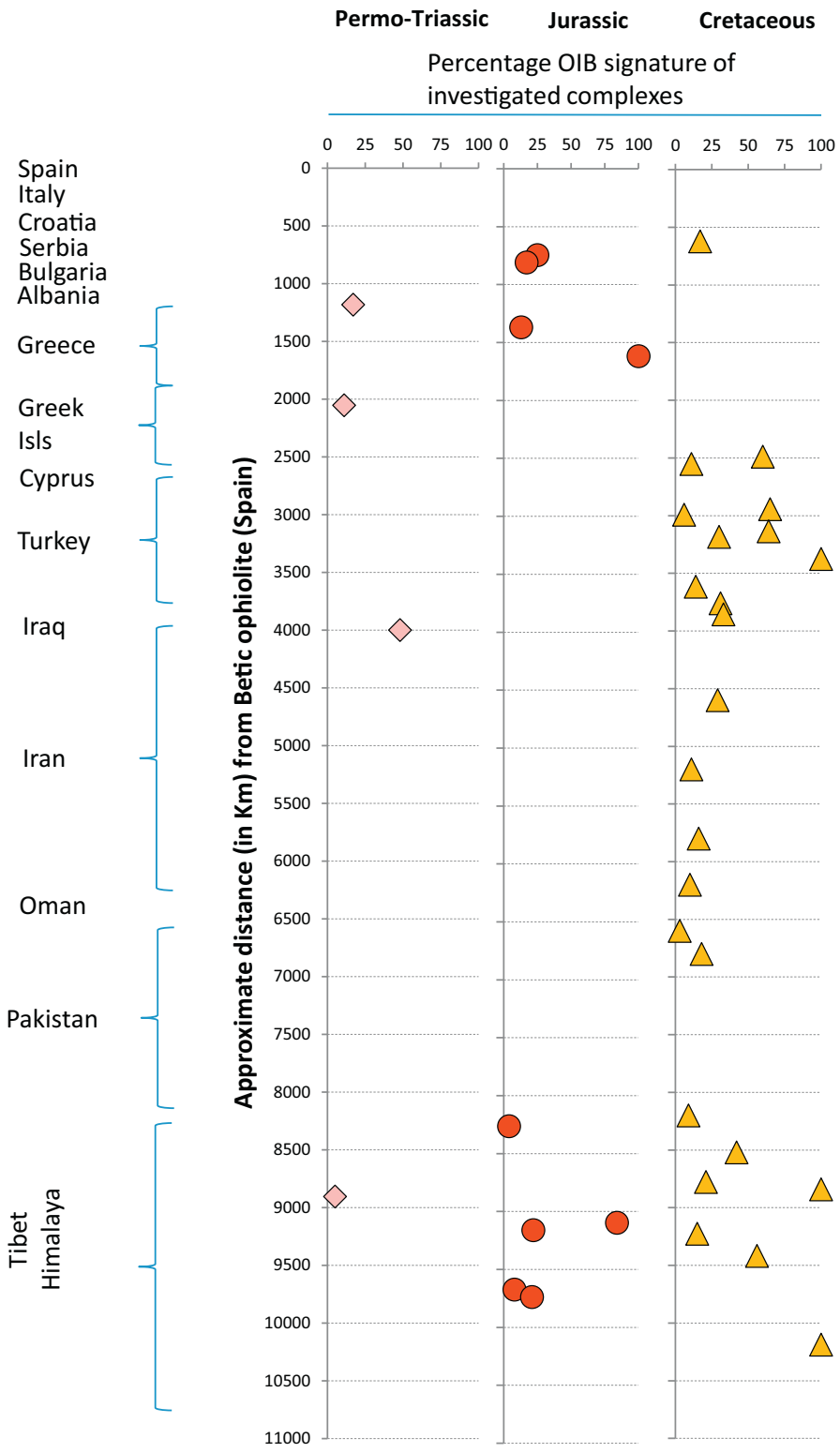

Fig. 21. OIB-signature of the basaltic rocks of the Permo-Triassic, Jurassic, and Cretaceous ophiolites along the Alpine-Himalayan Orogenic Belt, from Spain to eastern Himalaya. Based on the Saccani et al. (2015) classification as shown in Supplementary Table 2.

Mesozoic Neotethyan ophiolite suites within the Alpine-Himalayan Orogenic Belt based on their age groups and geochemical characteristics, and have classified them into various types as outlined in Fig. 6. We now discuss briefly the environment in which the subduction-unrelated group of ophiolites were generated, and the processes that led to the diversity of the subduction-related group of ophiolites.

8.1. Subduction-unrelated ophiolites

Mid-ocean ridge (MOR) ophiolites and rifted continental margin– or

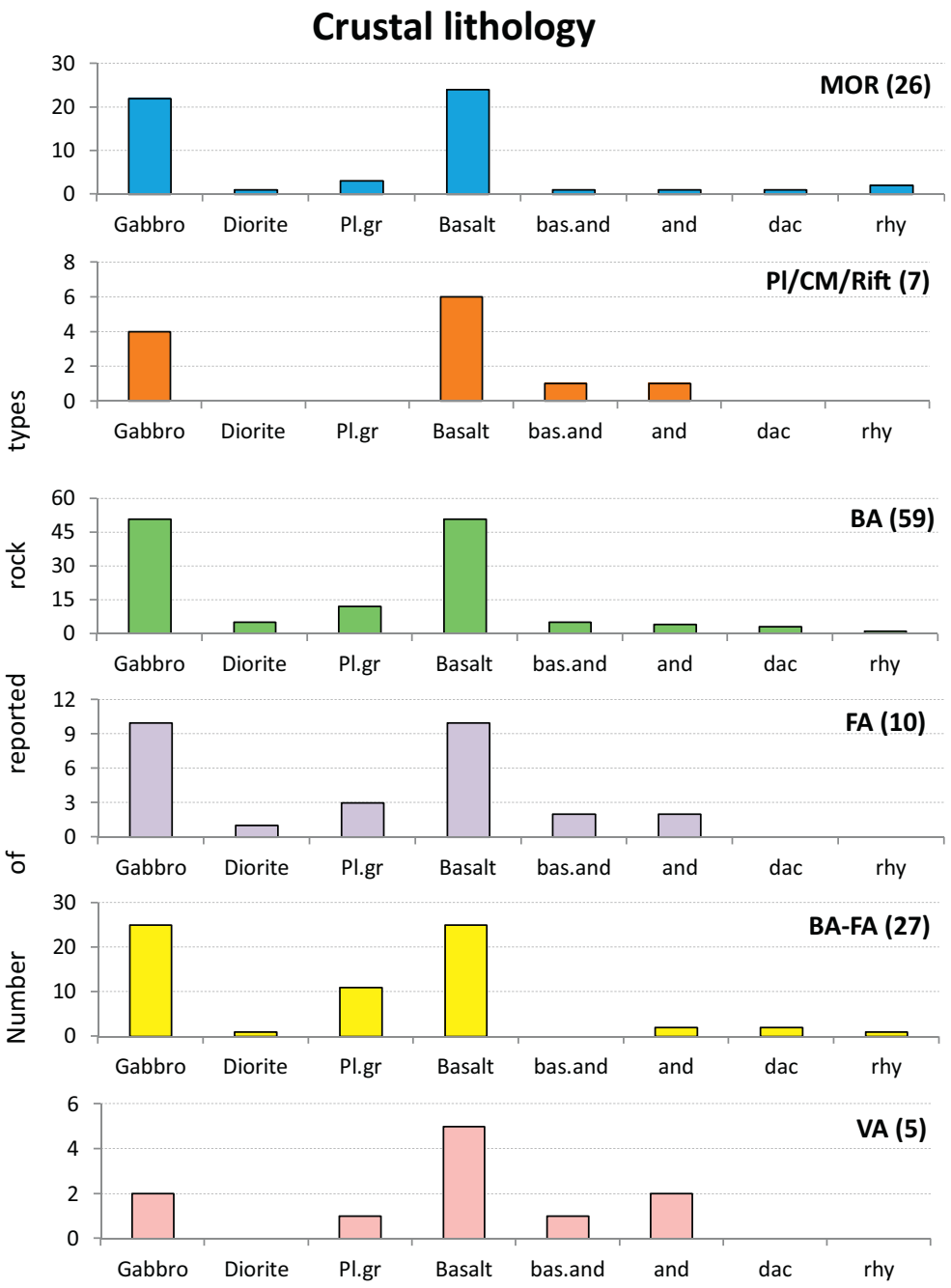

Fig. 22. Relationship between crustal rock types of the investigated Permo-Triassic, Jurassic, and Cretaceous ophiolites and their geochemical composition. The number in parenthesis (after each ophiolite type) denotes the number of complexes.

plume–type ophiolites make up 19% and 5%, respectively, of the subduction-unrelated ophiolites (Fig. 25). Some ophiolites in this last category may have started their development as magma-poor rifted continental margin products (e.g. Hess-type oceanic crust of the rifted Iberian continental margin; Dilek, 2003a) and subsequently transitioned into a typical MOR-type within a major ocean basin (as for example, the Atlantic Ocean), or alternatively they may have evolved within a trench–distal backarc basin in which the parental mantle was not influenced by subduction processes (Fig. 6A–C). An example of the latter-mentioned case, although of relatively minor volumetric significance, is represented by some segments of the Scotia Sea backarc basin oceanic crust (Fretzdorff et al., 2002).

As shown in Table 4, rock suites defined as ocean-island basalts (OIB) are commonly associated with the AHOB ophiolites. Of the twenty-six OIBs recorded (applying the Nb/Yb-TiO_2/Yb discriminant diagram; Fig. 16), four are associated with MOR, eight with BA-FA, thirteen with BA, and one with FA. It, thus, appears that OIBs are associated with any of the subduction-related ophiolite types, except the VA type. Seamounts and ocean islands, that may have a plume origin, are shown to have been common in all the major modern and former ocean basins (e.g., Hofmann, 1997; Dilek, 2003b; Regelous et al., 2003; Staudigel and Clague, 2010; Safonova and Santosh, 2014; Sarıfakıoğlu et al., 2017), as well as in in-situ (active or fossil) backarc basins (Staudigel and Koppers, 2015). Compositionally, the basaltic rocks of oceanic islands, seamounts and backarc basins define a wide range, representing tholeiitic to alkaline and calc-alkaline character (see Furnes and Safonova, 2019 and appropriate references therein). Thus, some backarc basins may host seamounts that represent magmatic

Table 4
Proposed ophiolite types and associated complexes of the Alpine-Himalayan Orogenic Belt.

Complex/area	Reference(s) to geochemical data and previously suggested tectonic setting For Nd-isotope data, the reference is marked with (i)	Suggested opiolite typebased on discrimination diagrams of Pearce (2014) and Saccani et al. (2015)	Associted magmatic complex
Spain			
Betic	Mid-ocean ridge; Puga et al. (2011, 2017)	Mid-ocean ridge	
France & Italy			
Chenaillet	Slow-spread mid-ocean ridge: Manatschal et al. (2011)	Mid-ocean ridge	
Switzerland-Italy			
Zermatt-Saas	Continental rifting: Kramer et al. (2003)	Rift/Mid-ocean ridge?	
Italy			
Calabrian	Rift stage: Liberi et al. (2006); Tortorici et al. (2009)	Rift/Mid-ocean ridge?	
Corsica	Rift stage to ocean opening: Saccani et al. (2008a)	Rift to Mid-ocean ridge	Ocean island
Elba	Slow-spreading mid-ocean ridge: Saccani and Principi (2016)	Mid-ocean ridge	
External Ligurides	Different stages in evolution from rifting to ocean floor stage: Montanini et al. (2008)	Mid-ocean ridge	Arc?
Internal Ligurides	MORB-type oceanic crust: Rampone et al. (1998)	Mid-ocean ridge	
Croatia			
Banija	Backarc spreading: Lugović et al. (1991)	Mid-ocean ridge	
Kalnik	Ensimatic backarc margial basin: Lugović et al. (et al. (2015)	Backarc	
Medvednica	Forearc in intra-oceanic basin: Slovenec and Šegvić (2018)	Forearc	
Bosnia			
Kozara	Plume-influenced mid-ocean ridge: Cvetković et al. (2014)	Mid-ocean ridge	
Krivaja-Konjuh	Mid-ocean ridge: Trubelja et al. (1995)	Mid-ocean ridge	
Serbia			
Maljen Massif	Subduction-related oceanic basin: Chiari et al. (2011)	Backarc to forearc	Ocean island
Zlatibor Massif	Subduction-related oceanic basin: Chiari et al. (2011)	Backarc	
Romania			
SAM (South Apuseni Mountains)	Mid-ocean ridge spreading centre: Saccani et al. (2001)	Backarc	
Bulgaria			
Satovcha	Suprasubduction: Froitzheim et al. (2014)	Backarc to forearc	
W. Rhodope massif	Intra-continental rifting: Bonev and Dilek (2010)	Rift/continetal margin	
Armenia			
Sevan	Mid-ocean ridge: Galoyan et al. (2009)	Backarc to forearc	
Albania			
Mirdita (North)	Suprasubduction: Dilek et al. (2008)	Backarc to forearc	
Mirdita (South)	Mid-ocean ridge setting: Bortolotti et al. (2006)	Mid-ocean ridge	Ocean island
Greece (mainland)			
Almopias	Ocean-continental transition zone, and associated volcanic arc: Saccani et al. (2015)	Backarc to forearc	Ocean island
Argolis	Embryonic ocean (Red Sea type): Saccani et al. (2003)	Mid-ocean ridge	
Evros	Intra-ocean subduction: Koglin (2008)	Backarc to forearc	
Guevgueli	Backarc basin: Zachariadis (2007); Saccani et al. (2008a, 2008b, 2008c)	Backarc	
Kassandra-Sithonia	Supra-subduction setting: Zachariadis (2007)	Volcanic arc	
Koziakas	Rift stage: Pomonis et al. (2004); Chiari et al. (2012)	Rift	
Oraeokastron	Supra-subduction setting: Zachariadis, 2007)	Backarc	
Othris	Subduction-related ocean basin: Koutsovitis and Magganas (2010)	Backarc	
Pindos	Backarc setting: Pe-Piper et al. (2004); Dilek and Furnes (2009)	Backarc to forearc	
Rhodiani	Backarc basin: Saccani et al. (2008a, 2008b, 2008c)	Backarc	
Thessaloniki	Supra-subduction setting: Zachariadis (2007)	Forearc	
Greek Islands			
Andros	Backarc basin: Bulle et al. (2010)	Backarc	
Crete oph.	Subduction-related setting: Koepke et al. (2002)	Backarc?	
Evia	Uncertain tectonic setting: Bröcker et al. (2014	Mid-ocean ridge	
Ikaria	Oceanic crust: Pe-Piper and Photiades (2006)	Backarc	Ocean island
Lesvos	Incipient rift: Koglin (2008); Koglin et al. (2009a)	Rift/Mid-ocean ridge	
Naxos	Supra-subduction: Stouraiti et al. (2017)	Backarc?	
Paros	Supra-subduction: Stouraiti et al. (2017)	Backarc?	
Samos	Supra-subduction: Stouraiti et al. (2017)	Backarc	
Samothraki	Evolved backarc basin: Koglin et al. (2009b)	Backarc	
Serifos	Backarc: Stouraiti (2010)	Backarc?	
Siphnos	Backarc: Mocek (2001)	Volcanic arc	
Skyros	Supra-subduction setting: Karkalis et al. (2016); Stouraiti et al. (2017)	Forearc?	
Syros	Backarc: Seck et al. (1996)	Backarc	
Tinos	Backarc: Bulle et al. (2010); Lamont et al. (2019)	Backarc	

(*continued on next page*)

Table 4 (*continued*)

Complex/area	Reference(s) to geochemical data and previously suggested tectonic setting For Nd-isotope data, the reference is marked with (i)	Suggested opiolite typebased on discrimination diagrams of Pearce (2014) and Saccani et al. (2015)	Associted magmatic complex
Cyprus			
Troodos	Supra-subduction: Rautenschlein et al. (1985), Dilek and Furnes (2009), Pearce and Robinson (2010), Woelki et al. (2019)	Backarc to forearc	
Turkey			
Anatolian	Supra-subduction, mid-ocean ridge: Colakuglo et al. (2012)	Backarc	Ocean island
Ankara	Mantle plume to mid-ocean ridge: Bortolotti et al. (2018)	Mid-ocean ridge	Ocean island
Antalya	Supra-subduction: Bağci et al. (2006)	Forearc?	
Beysehir-Hoyran	Rift-drift to intra-oceanic subduction: Elitok and Drüppel (2008)	Rift to Mid-ocean ridge	Ocean island?
Boğazköy	Supra-subduction: Topuz et al. (2018)	Mid-ocean ridge	
Çiçekdağ	Supra-subduction: Yaliniz et al. (2000)	Backarc	
Eldivan	Intra-oceanic subduction: Dangerfield et al. (2011)	Backarc?	
Göksun	Supra-subduction: Rizaoğlu (2017), Parlak et al. (2020)	Backarc?	
Guleman	Intra-oceanic subduction: Özek et al. (2017)	Backarc	
Ispendere	Supra-subduction: Parlak et al. (2012)	Volcanic arc	
Kahramanmaras	Supra-subduction: Bağci (2013)	Backarc?	Ocean island
Karadağ	Supra-subduction: Parlak et al. (2013)	Backarc	
Kizildag	Supra-subduction: Dilek and Thy (2009)	Backarc to forearc	
Kömürhan	Supra-subduction: Beyarslan and Bingöl (2000)	Backarc?	
Konya	Intra-oceanic subduction: Dașçi et al. (2015)	Backarc to forearc	Ocean island
Küre	Continental backarc basin: Alparslan and Dilek (2018)	Backarc	
Lycian	Subduction-related setting: Çelik and Chiaradia (2008)	Backarc?	
Mersin	Supra-subduction: Çelik (2008); Ishimaru et al. (2018)	Backarc to forearc	Ocean island
Meydan	Supra-subduction: Yildirim (2015)	Backarc to forearc	
Pinarbaşi	Subduction-related: Vergili and Parlak (2005)	Backarc	
Pozanti-Karsanti	Intra-oceanic subduction: Lian et al. (2017, 2019)	Backarc	
Refahiye	Forearc setting: Parlak et al. (2013)	Backarc to forearc	Ocean island
Şahvelet	Forearc setting: Parlak et al. (2013)	Backarc	
Sarikaraman	Supra-subduction: Yaliniz et al. (1996)	Backarc to forearc	
Sivas	Intra-oceanic subduction: Kavak et al. (2017)	Backarc	
Syria			
Baer-Bassit	Subduction-related setting: Al-Riyami et al. (2002)	Forearc?	
Iraq			
Bulfat	Arc tectonic seting: Ali (2015)	Volcanic arc?	
Mawat	Mantle plume: Azizi et al. (2013)	Mantle plume?	
Penjween	Supra-subduction: Hadi et al. (2013)	Volcanic arc	
Iran			
Band-e-Zeyarat/Dar Abar	Mid-ocean ridge: Ghazi et al. (2004)	Backarc	
Birjand	Mid-ocean ridge: Zarrinkoub et al. (2012)	Backarc	Ocean island
Deshir	Supra-subduction: Moghadam et al. (2010, 2012)	Backarc to forearc	
Gogher-Baft	Supra-subduction: Moghadam et al. (2013a)	Backarc to forearc	Ocean island
Haji-Abad	Supra-subduction: Moghadam et al. (2013b)	Backarc	Ocean island
Harsin-Sahneh	Supra-subduction: Sahamich and Miradpour (2015)	Backarc	
Kermanshah	Continental rifted margin to oceanic spreading: Saccani et al. (2013a)	Rift to mid-ocean ridge	
Khoy	Oceanic spreading: Hassanipak and Ghazi, (2000), Khalatbari-Jafari et al. (2006), Moghadam et al. (2019)	Mid-ocean ridge	Arc
Misho	Plume activity: Saccani et al. (2013a, 2013b)	Plume	
Nain	Backarc oceanic basin: Moghadam et al. (2009)	Backarc to forearc	
Nehbandan	Mid-ocean ridge to suprasubduction zone: Saccani et al. (2010)	Mid-ocean ridge	
Neyriz	Supra-subduction: Babaie et al. (2006), Rajabzadeh et al. (2013), Moghadam et al. (2014a), Monsef et al. (2018)	Backarc	
Sabzevar	Backarc basin: Shojaat et al. (2003); Moghadam et al. (2014b)	Backarc to forearc	Ocean island
Shahr-e-Babak	Backarc oceanic basin: Moghadam et al. (2009)	Backarc to forearc	
Oman			
Oman	Supra-subduction: Goodenough et al. (2010, 2014), Ambrose and Searle (2019)	Backarc to forearc	
Pakistan			
Bela	Fast-spreading mid-ocean ridge: Sarwar (1992); Khan et al. (2018)	Mid-ocean ridge	
Muslim Bagh	Supra-subduction: Kakar et al. (2014)	Backarc to forearc	Ocean island
Waziristan	Backarc basin: Khan et al. (2007b)	Backarc?	
Yarlung-Zangbo and Bangong Lake – Lijiang ophiolite belts Tibet & India (I)			
Amdo	Intra-oceanic backarc: Wang et al. (2016)	Backarc	
Asa	Oceanic backarc basin: Zeng et al. (2018a)	Backarc to Volcanic arc	
Bangong Lake	MOR and SSZ: Shi et al. (2004, 2008)	Backarc to forearc	
Beimarang	Backarc basin: Huot et al. (2002), Dubois-Côté et al. (2005)	Backarc	
Beinang	Backarc basin: Dubois-Côté et al. (2005)	Backarc	
Dazhuqu	Intraoceanic arc: Bao et al. (2013); Dubois-Côté et al. (2005)	Backarc	
Dingqing	Forearc: Liu et al. (2002, Xiong et al. (2018)	Forearc	
Dong Tso	Continental backarc basin: Wang et al. (2008)	Backarc to forearc	
Dongbo & Purang	Continental margin: Liu et al. (2013, 2015)	Rift/Continental Margin	

(*continued on next page*)

Table 4 (*continued*)

Complex/area	Reference(s) to geochemical data and previously suggested tectonic setting For Nd-isotope data, the reference is marked with (i)	Suggested opiolite typebased on discrimination diagrams of Pearce (2014) and Saccani et al. (2015)	Associted magmatic complex
Dongco	Supra-subduction: Wang et al. (2016)	Backarc	Ocean island
Dongqiao	Mid-ocean ridge, ocean island and island arc: Liu et al. (2016)	Backarc	Ocean island
Dras (I)	Intraoceanic arc: Corfield et al. (2001); Clift et al. (2002)	Volcanic Arc	
Eastern Syntaxis	Intraoceanic arc: Saha et al. (2012)	Backarc	
Guomangco	Backarc basin: Xu et al. (2014)	Mid-ocean ridge	
Jiding	Backarc basin: Bao et al. (2013); Dubois-Côté et al. (2005)	Backarc	
Jinlu	Intraoceanic arc: Dubois-Côté et al. (2005)	Forearc	
Julu	Backarc basin: Liu et al. (2014)	Backarc	
Kangqiong	Backarc basin: Xu et al. (2015b)	Forearc	
Lagkor Tso	Continental backarc basin: Wang et al. (2008)	Backarc to forearc	
Lanong	Rifting and continental fore-arc setting: Zhong et al. (2017)	Backarc	Ocean island
Luobusa	Mid-ocean ridge: Zhang et al. (2016a)	Backarc	
Nadong	Ocean island: Fan et al. (2014)	Backarc	Ocean island
Namco-Renco	Continental marginal basin (178 Ma) to mature backarc basin (150 Ma): Zhong et al. (2015)	Mid-ocean ridge	
Nidar (I)	Intraoceanic arc: Mahéo et al. (2004)	Backarc	
Qunrang	Backarc basin: Dubois-Côté et al. (2005)	Backarc	
Rebang Co	Backarc basin: Liu et al. (2014)	Backarc	
Renbu	Plume-influenced ocean crust: Xia et al. (2008)	Rift/Continental Margin	
Rutog	Intra-oceanic backarc basin: Wang et al. (2016)	Backarc	
Saga	Backarc - arc: Bédard et al. (2009)	Backarc	Ocean island
SangSang	Backarc - arc: Bédard et al. (2009)	Backarc	Ocean island
Spontang (I)	Intraoceanic arc: Mahéo et al. (2004), Corfield et al. (2001), Pedersen et al. (2001)	Backarc to forearc	
Taoxinghu	Continental backarc basin: Wu et al. (2016)	Backarc	
Xigaze	Suprasubduction zone: Malpas et al. (2003), Chen and Xia (2008), Dai et al. (2013)	Backarc to forearc	
Xiugugabu	Backarc basin: Bezard et al. (2011)	Backarc	Ocean island
Yungbwa	N-MORB: Miller et al. (2003)	Mid-ocean ridge	
Yunzhug	Slow spreading oceanic setting or an embryonic ocean: Zeng et al. (2018b)	Mid-ocean ridge	
Yushu	Trench-arc-backarc system: Zhang et al. (2017)	Backarc	
Zedong	Intraoceanic arc: Malpas et al. (2003) Active continental margin: Zhang et al. (2014) Proto-forearc: Liu et al. (2019)	Forearc	
Zhongba	Intra-oceanic suprasubduction zone: Dai et al. (2012)	Rift/plume	
Zhongcang	Subduction-related setting: Tang et al. (2018)	Forearc	Ocean island
India			
Andaman	Arc-related setting: Pal, 2011), Rasool et al. (2015)	Backarc?	
Manipur	Mid-ocean ridge: Singh et al. (2012)	Mid-ocean ridge	
Naga Hills	Oceanic crust generated above subduction zone: Abdullah et al. (2018); Dey et al. (2018)	Backarc	Ocean island
Myanmar			
Myitkyina	Supra-subduction: Yang et al. (2012); Xu et al. (2017)	Forearc	

products associated with slab dynamics (e.g., Regelous et al., 2003; Staudigel and Koppers, 2015), whereas some others may include magmatic construction associated with backarc spreading centers and/or plume activities (Leat et al., 2000; Fretzdorff et al., 2002; Keller et al., 2002; Regelous et al., 2003; Tararin et al., 2003; Pearce et al., 2005). Also, tholeiitic to alkaline seamounts with an origin of plume magmatism, occurring on the seafloor of backarc basins, might represent traces of former plumes that originally were responsible for the opening of some backarc basins (e.g., Hickey-Vargas, 1998; Macpherson and Hall, 2001; Deschamps and Lallemand, 2002; Sdrolias et al., 2004; Deschamps et al., 2008; Barnes, 2008; Ishizuka et al., 2013: Chang et al., 2016).

8.2. Subduction-related ophiolites

Among the investigated ophiolites in the AHOB we have demonstrated large geochemical variations in the extent of slab signature in the origin of subduction-related ophiolites (Figs. 15–18). In this section, we briefly discuss several parameters that may directly affect the chemical geodynamics of oceanic crust formation in subduction zone environments: (1) variation in slab dip-angles, (2) ridge jumps, (3) subduction rates, (4) spreading rates, (5) thermal structure, (6) and orientation of spreading axis. We propose that each of these processes, or a combination of them, may be responsible for the observed geochemical variations.

The slab dip-angle of the modern backarc subduction systems in the westen Pacific Ocean exhibit large variations from less than 30 degrees to near vertical (e.g., Gvirtzman and Stern, 2004; Lallemand et al., 2005). Furthermore, the slab geometry in these subduction zone environments may vary laterally as well as vertically through time (Guillaume et al., 2013). Lateral variations in dip-angles of a subducting slab beneath a backarc basin are anticipated to affect the extent of subduction influence on its mantle under its spreading center(s). This scenario may explain, in part, the existence geochemical heterogeneities in the backarc mantle and its melt products, as observed in many of the BA–SSZ ophiolites in the AHOB.

A second important parameter involves a change in the geometry and kinematics of spreading centres within backarc basins via ridge jumping and ridge propagation. These processes are well documented at fast-spreading mid-ocean ridges in major oceans (e.g., Mittelstaedt et al., 2008), in modern backarc basins (Deschamps et al., 2008; Maldonado et al., 2014; Stern and Dickinson, 2010), and even in some ophiolites (Dilek et al., 1997). Melt regimes associated with ridge propagation and ridge jump processes may cause significant

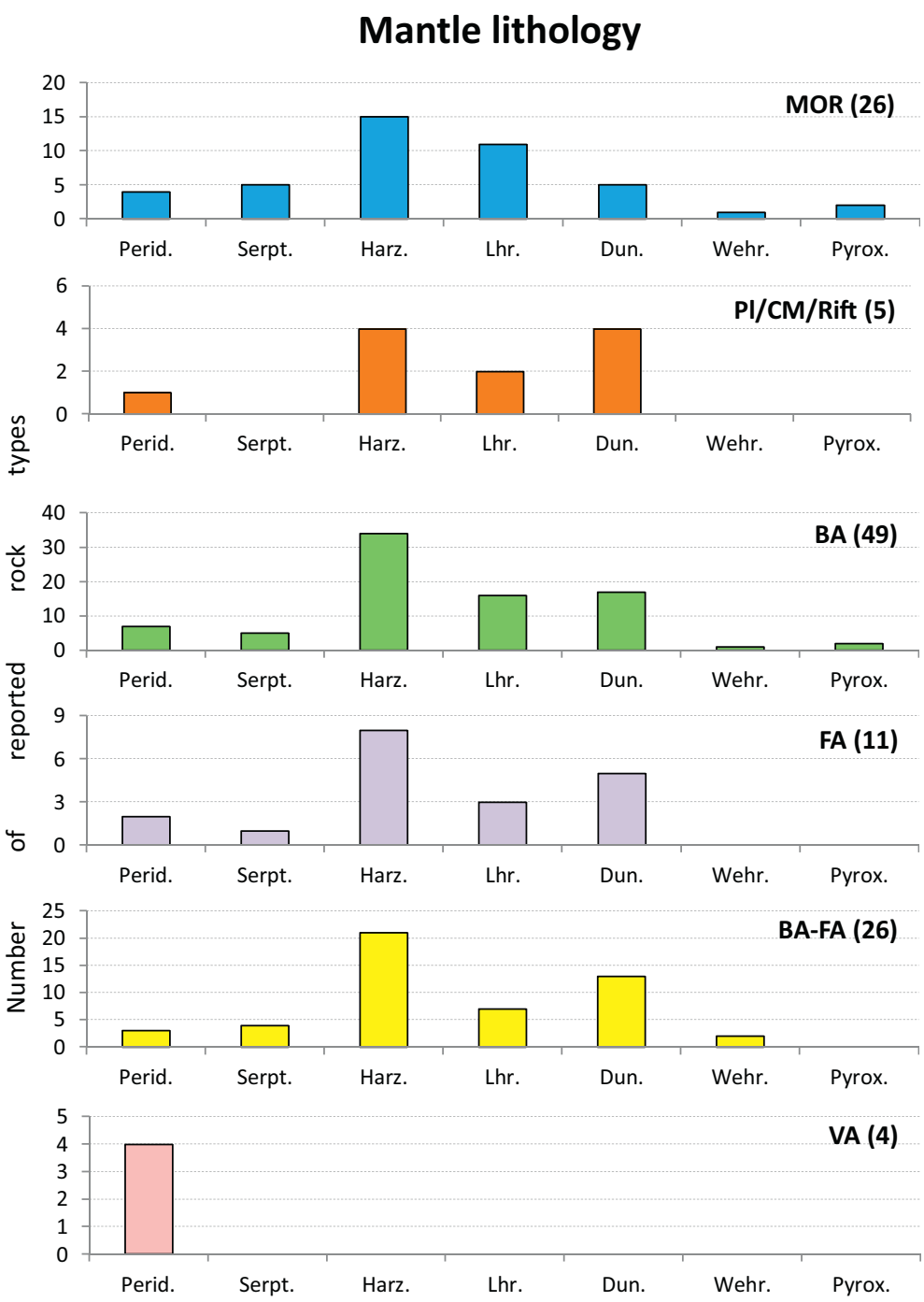

Fig. 23. Relationship between mantle rock types of the investigated Permo-Triassic, Jurassic, and Cretaceous ophiolites and their geochemical composition. The number in parenthesis (after each ophiolite type) denotes the number of complexes.

fluctuations in magma outputs and their chemical makeups both laterally and vertically along spreading centers.

A third parameter, which contributes to lateral differences in slab contribution to melt regimes beneath SSZ spreading centers, is the rate of subduction. The global subduction rates during the Cenozoic have varied from ca. 1.5 cm/year to 16 cm/year (Hoareau et al., 2015). In an extreme case, in a single subduction system the rates may vary by ca. 2 cm/year within short time intervals of 1–2 million years (Hoareau et al., 2015). The amount of sediments that is carried down within a subduction zone (e.g., Von Huene and Scholl, 1991; Clift and Vannucchi, 2004; Scholl and van Huene, 2007; Safonova et al., 2015) and the concentration of important slab derived elements in such sediments (e.g., Th, see Plank and Langmuir, 1998) may vary significantly. Such fluctuations contribute significantly to varied geochemical fingerprints of SSZ ophiolites, as represented by the four (BA, BA-FA, FA, and VA) subduction-related types in the AHOB.

A fourth parameter is the spreading rate within backarc basins that affects magma production rates and geochemical characteristics of magmas. Examples of slow- and fast-spreading backarc basins are documented from the Mariana Trough (e.g., Pearce et al., 2005; Anderson et al., 2017) and the Lau Basin (e.g., Baker et al., 2019), respectively. Different spreading rates along individual segments of the

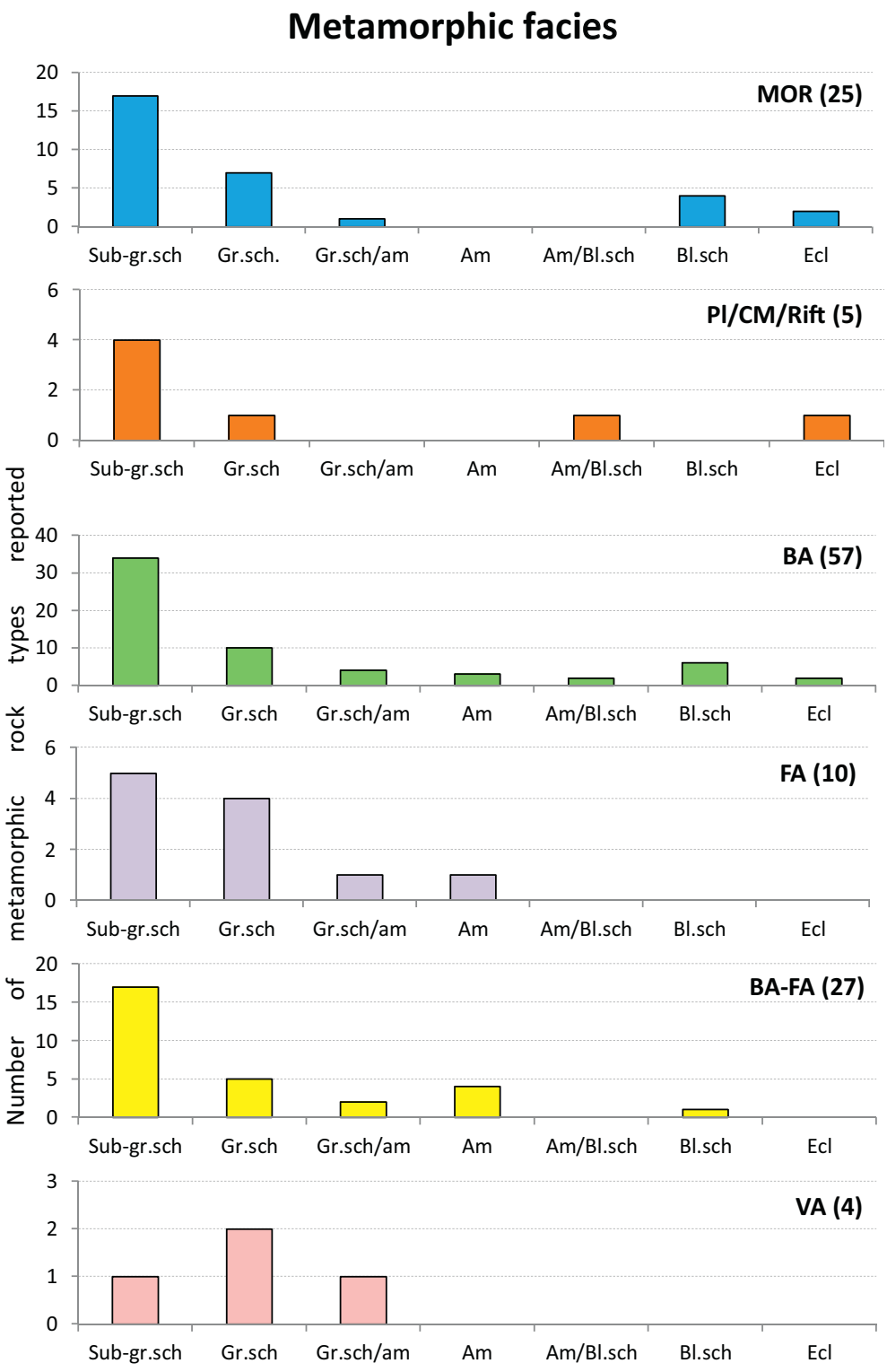

Fig. 24. Relationship between metamorphic rock types of the investigated Permo-Triassic, Jurassic, and Cretaceous ophiolites and their geochemical composition. The number in parenthesis (after each ophiolite type) denotes the number of complexes.

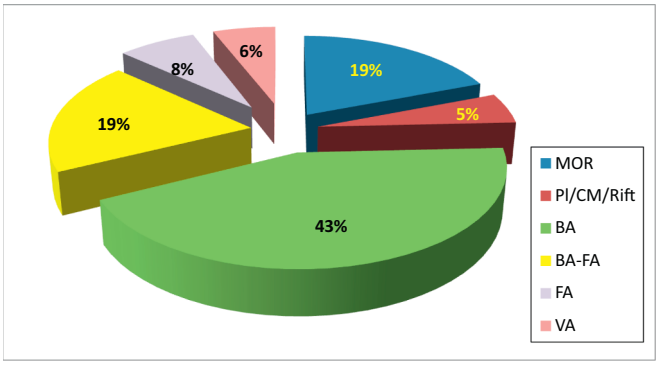

Fig. 25. Pie diagram showing the proportion (in %) of each ophiolite type.

seafloor spreading centers in these backarc basins have produced significantly different morphological features and internal structures of the SSZ oceanic lithosphere.

The thermal structure of a subducting slab (mainly a function of slab age) affects metamorphic dehydration P-T-t paths, and hence the spatial distribution of slab-derived components in the suprasubduction zone environment (Van Keken, 2003). Thus, this parameter has a strong control on the nature and mode of fluid and melt flux from a slab into the overlying mantle wedge.

The sixth parameter, the orientation of the spreading axis within a backarc basin relative to the trench/arc orientation, may play a significant role in geochemical signatures of ophiolitic magmas. In such cases the distance between the sites of magma production along the spreading center and the subduction zone will be different. An Example of such a case is represented by the North Fiji Basin (Price et al., 1990). As a result, magmas produced along the same spreading axis may be influenced differently by melts/fluids derived from a subduction slab.

8.3. Proportions of subduction-related and subduction-unrelated ophiolites in the AHOB

Fig. 25 shows the proportions of subduction-related and subduction-unrelated ophiolites of the AHOB. The ophiolites in the former group [Backarc (BA), Forearc (FA), Backarc to Forearc (BA-FA), and Volcanic Arc (VA)], define the majority of ophiolite occurrences in the AHOB, constituting 43%, 8%, 19%, and 6%, respectively, adding up to 76%. Mid-ocean ridge (MOR) and plume + continental margin + rift (Pl/CM/R) types of the subduction–unrelated category define 24% of the total, with the MOR-type as the dominant (19%) group. Contribution by continental material to mantle melts (Yamamoto et al., 2009; Safonova et al., 2015) is also supported by the Nd-isotope data, i.e., low proportion (27%) of the basalt data that plot within the field of depleted mantle (DM) (Fig. 19). However, although we must consider the MOR–generated oceanic lithosphere and their ophiolite derivatives in the earth's rock record, it is widely accepted that MOR–originated oceanic lithosphere was mostly subducted entirely and recycled into the deep mantle due to slab-pull forces throughout the evolution of the earth (Cloos, 1993). It appears, then, that subduction-related ophiolites are by far the most dominant ophiolite occurrences that became part of the rock record through all times, even in the very early stages of the earth (Furnes et al., 2014, 2015).

8.4. Comparison with other orogenic belts

Orogenic belts can be classified into (a) collisional and (2) accretionary types (Windley, 1992; Maruyama et al., 1996; Cawood et al., 2009). In the case of a collisional orogen, the classic model involves opening of an ocean and its subsequent closure (also referred to as the Wilson cycle) leading to orogenesis, caused by collision between either two continental blocks or a continent and an island arc. Accretionary orogens are produced by subduction of an oceanic plate beneath a continental plate or along an archipelago of island arcs (e.g. Japanese Islands). Such orogens form at both intraoceanic convergent margins and Andean–type, active continental margins. SSZ backarc to forearc ophiolites are common in accretionary–type orogenic belts.

Orogens of both types have developed through most of the earth history (e.g. Collins et al., 2011). We present below a comparison of the AHOB ophiolites in the collisional Alpine-Himalayan Orogenic Belt with the ophiolites in the accretionary-type Central Asian Orogenic Belt (CAOB; Furnes and Safonova, 2019). This comparison is shown in Fig. 27, in which the ophiolite types, as well as the proportion of basalt types generated within mantle arrays are displayed. The subduction-unrelated category is slightly higher in the AHOB (24%) in comparison to the CAOB (21%), whereas the sum of FA + VA is significantly higher in the latter (22%) than in the AHOB (14%). As to the generation of basaltic melts in the mantle array, there is also a significant difference between the AHOB and CAOB ophiolites. For the AHOB ophiolites, 77% contain basalts that were asthenospheric mantle-array-produced, compared to 64% for those of the CAOB, and the proportion of samples is 45% and 33%, respectively. It is highly probable that this low record is a reflection of preservation in the case of the CAOB, as much of MOR–generated oceanic lithosphere in its multiple seaways was mostly recycled into the deep mantle without leaving a trace at the surface.

The asthenospheric mantle-array-produced, shallow-melting generated MORB basalts have been divided into depleted (D), normal (N), transitional (T), enriched (E) types, and the deep-mantle generated OIB basalts have been divided into tholeiitic (OIB-Th) and alkaline (OIB-alk) types (See Fig. 7). Geochemical characterization of basaltic rocks of the AHOB (Fig. 27) shows that the N-type basalt is the dominant one among the MOR-ophiolites of the AHOB (with insignificant amount of D-type). For the D-type MOR-ophiolites, the pattern is different, with only minor N-type but significant D-, T-, and OIB-type basalts. For the BA ophiolite types of both AHOB and CAOB, the proportion of D-type basalts becomes higher, particularly for those of the CAOB. For the ophiolites of the BA-FA category of the CAOB, the T- and E-type basalt is dominant compared to those of the AHOB. As to the FA and VA ophiolite types of both orogens, the number of examples with reliable data is too low in order to allow meaningful categorization.

In an investigation of ophiolite types globally (Furnes et al., 2014), a classification of 17 examples of the accretionary Western Pacific-Cordilleran Orogenic Belt shows that the proportion of subduction-unrelated and subduction-related types is 24% and 76%, respectively. Further, a compilation of 105 ophiolite occurrences of the Eoarchean through Archean and Proterozoic Eons indicates that 85% of them are subduction-influenced (Furnes et al., 2015). These observations suggest that plate tectonics and plate subduction played a significant role in the production of oceanic lithosphere throughout the earth history (Dilek and Furnes, 2011).

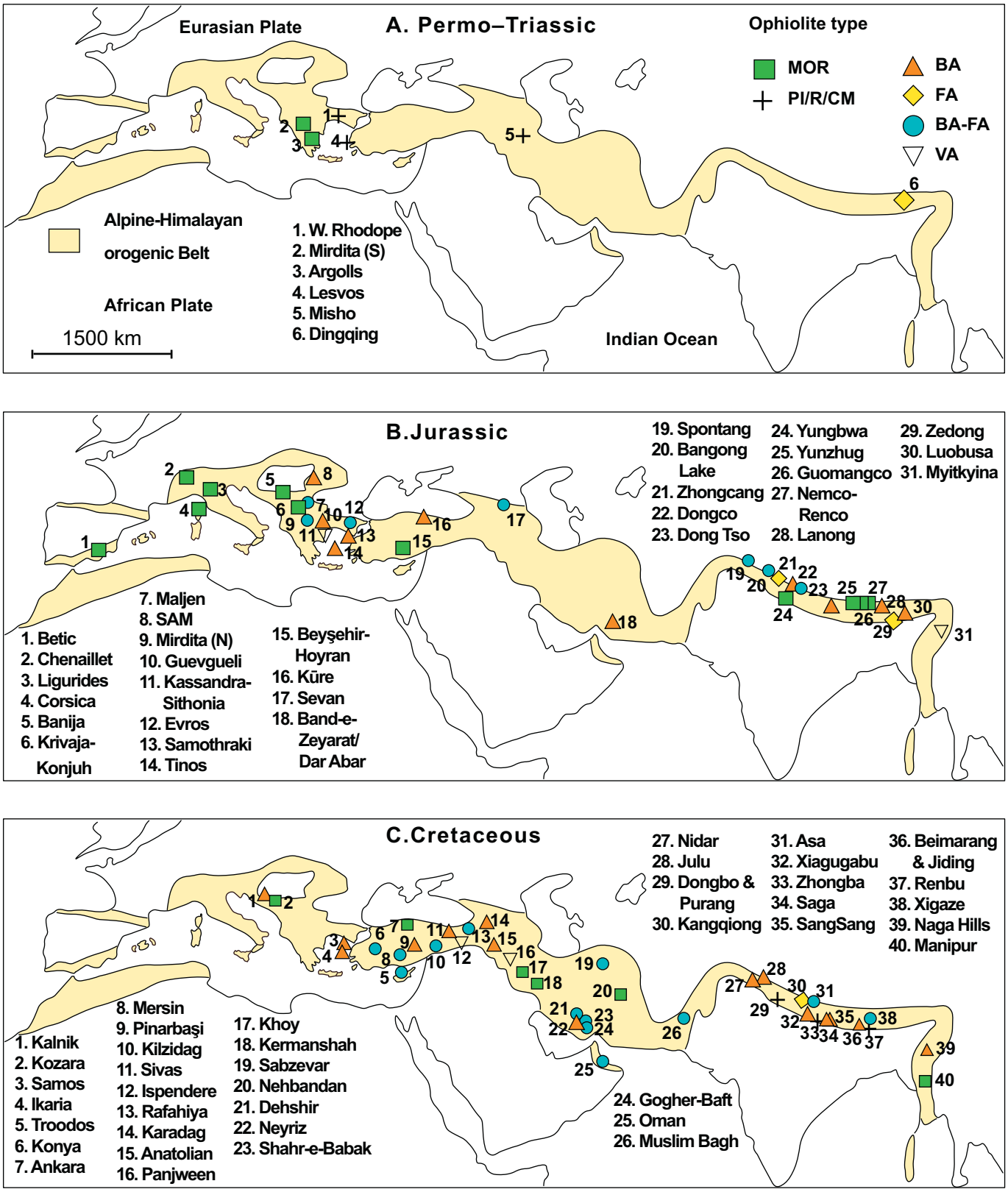

Fig. 26. Geographical outline of the Alpine-Himalayan Orogenic Belt, onto which ophiolites of various ages (A: Permo-Triassic; B: Jurassic; C: Cretaceous) have been plotted. For the more precise location of each ophiolite, the reader is referred to the various maps of Figs. 1–5.

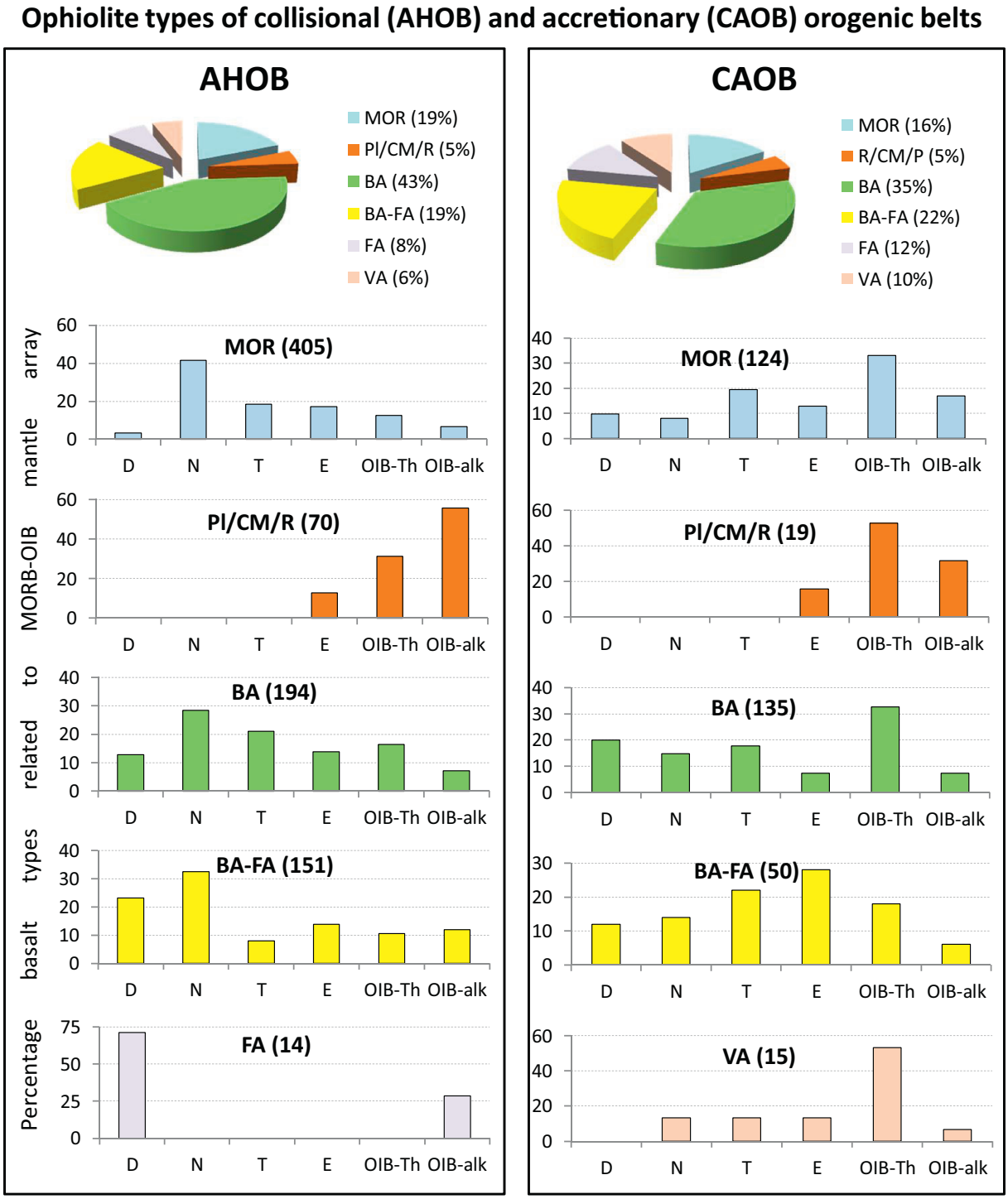

Fig. 27. Comparison of ophiolite types of the collisional Alpine-Himalayan orogenic Belt (AHOB) and the accretionary Central Asian Orogenic Belt (CAOB). The histograms of the two categories show the proportions of mantle-array-basalts (D = depleted, N = normal, T = transitional. E = enriched MOR-types), and tholeiitic and alkaline ocean island basalts (OIBs) of the various ophiolite types.

9. Summary

Geochemical characterization of basaltic rocks from 137 ophiolite occurrences within the Alpine-Himalayan Orogenic Belt with ages ranging from the Triassic through Cretaceous shows a variety of subduction-unrelated and subduction-related ophiolite types, and hence a wide diversity in oceanic crust generation during the evolution of the Mesozoic Neotethys.

1. The ophiolites of subduction-related origin, subdivided as *Backarc* (BA), *Forearc* (FA), *Backarc to Forearc* (BA-FA) and *Volcanic Arc* (VA) types, comprise the major group (about 76%). Thus, subduction zone processes contributed significantly to magmatic construction of SSZ oceanic lithosphere within the Neotethyan realm.
2. The BA ophiolite is the dominant type (43%), followed by BA-FA (19%), and subordinate occurrences of FA (8%) and VA (6%) types.
3. Subduction influence is highly variable among the BA-type ophiolites, generally high in the FA type. The BA-FA and VA types define intermediate levels of subduction influence between the two end-member types (BA and FA).
4. The subduction-unrelated group of ophiolites (24%) are subdivided

as mid-ocean-ridge (MOR) type and a combined group of *rift* (R), *continental margin* (CM) and *plume* (Pl) type (referred to as Pl/CM/R type). The MOR-type ophiolites are dominant (19%), particularly in the westernmost trunk of the AHOB.

5. The Jurassic ophiolites constitute the dominant population of subduction-unrelated examples, whereas the Cretaceous ophiolites are almost entirely made of subduction-related types.
6. Low-grade to greenschist metamorphic grade is the most common in all ophiolite types and commonly reflect ocean floor (hydrothermal) metamorphism of the original oceanic lithosphere. High-grade (eclogite) metamorphic overprint is also preserved in the subduction-unrelated category and the BA-type of the subduction-related category.
7. Highly variable subduction influence in the basalts between adjacent ophiolite complexes along the same suture zone may be explained by lateral variations in the slab dip angles, as well as by variable amounts of hydrated sediments and subduction-important elements (such as Th) incorporated into mantle wedges. Such variable quantities of material and fluid flux into the mantle should affect the compositions of melts generated above subducting slabs.
8. The ε_{Nd} -values of most of the MOR-type ophiolites fall within the range of depleted mantle, whereas the ε_{Nd} -values of the plume/rift/continental margin types and the subduction-related BA-, BA-FA-, FA + VA-type ophiolites define values lower than those defined by the DM range. This phenomenon may be the result of mixing of sediments and/or sediment-contaminated mantle with the rising melt column beneath spreading centers.

Supplementary data to this article can be found online at https://doi.org/10.1016/j.earscirev.2020.103258.

Declaration of competing interest

We have no conflict of interest involving this study and our reporting of its findings in this paper.

Acknowledgements

Financial support over many years of fieldwork in ophiolites and greenstone belts in different orogenic belts have been supported by the Norwegian Research Council and the Meltzer Foundation at the University of Bergen to HF, and by the National Science Foundation (NSF-USA), the NATO Science for Peace Programme, the National Geographic Society, and Miami University Research Funds to YD; and the Ministry of Education and Science of the Russian Federation (project no. 14.Y26.31.0018) and State Assignment Scientific Project of IGM SB RAS to IS. We gratefully acknowledge these funds and all the financial support. Our discussions in the field with many colleagues over the years on the internal structure, magmatic and petrological features, regional geology and tectonic evolution of the ophiolites in Italy, Albania, Greece, Turkey, Cyprus, Syria, Iran, Tibet and India were indispensable for our interpretations and synthesis presented in this paper; we express our sincere thanks to all those colleagues and collaborators for their insights and great memories. We extend our thanks and gratitude to Tim Horscroft at Elsevier for inviting us to contribute this paper in Earth-Science Reviews. We further thank Tatsuki Tsujimori and John Encarnacion for their insightful and constructive reviews for the journal that helped us improve the paper, and Zhang Hui for assisting in the production of Figs. 1–6, and Fig. 26.

References

Abbate, E., Bortolotti, V., Passerini, P., Principi, G., 1985. The rhythm of Phanerozoic ophiolites. Ofioliti 10, 109–138.
Abdullah, S., Misra, S., Ghosh, B., 2018. Melt-rock interaction and fractional crystallization in the Moho transition Zone: evidence from the Cretaceous Naga Hills Ophiolite, North-East India. Lithos 322, 197–211.
Ahmad, T., Tanaka, T., Sachan, H.K., Asahara, Y., Islam, R., Khanna, P.P., 2008. Geochemical and isotopic constraints on the age and origin of the Nidar Ophiolitic Complex, Ladakh, India: implications for the Neo-Tethyan subduction along the Indus suture zone. Tectonophysics 451, 206–224.
Aitchison, J.C., Davis, A.M., Liu, J., Luo, H., Malpas, J.G., McDermid, I.R.C., Wu, H., 2000. Remnants of the Cretaceous intra-oceanic subduction system within the Yarlung-Zangbo suture (southern Tibet). Earth Planet. Sci. Lett. 183, 231–244.
Ali, S.A., 2015. Petrogenesis of metabasalt rocks in the Bulfat complex, Kurdistan region, Iraqi Zagros Suture Zone. Kirkuk Univ. J. Sci. Stud. 10 (3), 242–258.
Alparslan, G., Dilek, Y., 2018. Seafloor spreading structure, geochronology, and tectonic evolution of the Küre ophiolite, Turkey: a Jurassic continental backarc basin oceanic lithosphere in southern Eurasia. Lithosphere 10 (1), 14–34. https://doi.org/10.1130/L641.1.
Al-Riyami, K., Robertson, A., Dixon, J., Xenophontos, C., 2002. Origin and emplacement of the Late Cretaceous Baer-Bassit ophiolite and its metamorphic sole in NW Syria. Lithos 65, 225–260.
Ambrose, T.K., Searle, M.P., 2019. 3-D structure of the northern Oman-UAE ophiolite: widespread, short-lived, suprasubduction zone magmatism. Tectonics 38. https://doi.org/10.1029/2018TC005038.
Anderson, M.O., Chadwick Jr., W., Hannington, M.D., Merle, S.G., Resing, J.A., Baker, E.T., Butterfield, D.A., Walker, S.L., Augustin, N., 2017. Geological interpretation of volcanism and segmentation of the Mariana back-arc spreading center between 12.7°N and 18.3°N. Geochem. Geophys. Geosyst. 18, 2240–2274. https://doi.org/10.1002/2017GC006813.
Anonymous, 1972. Penrose field conference on ophiolites. Geotimes 17, 24–25.
Ao, A., Bhowmik, S.K., 2014. Cold subduction of the Neotethys: the metamorphic record from finely banded lawsonite and epidote blueschists and associated metabasalts of the Nagaland Ophiolite Complex, India. J. Met. Geol. 32, 829–850.
Azizi, H., Hadi, A., Asahara, Y., Mohammad, Y.O., 2013. Geochemistry and geodynamics of the Mawat mafic complex in the Zagros Suture zone, northeast Iraq. Cent. Eur. J. Geosci. 5 (4), 523–537.
Babaie, H.A., Babaei, A., Ghazi, A.M., Arvin, M., 2006. Geochemical, $^{40}Ar/^{39}Ar$ age, and isotopic data for crustal rocks of the Neyriz ophiolite. Iran. Can. J. Earth Sci. 43, 57–70.
Bağci, U., 2013. The geochemistry and petrology of the ophiolitic rock from the Kahramanmaras region, southern Turkey. Turk. J. Earth Sci. 22, 536–562.
Bağci, U., Parlak, O., Höck, V., 2006. Geochemical character and tectonic environment of ultramafic to mafic cumulate rocks from the Tekirova (Antalya) ophiolite (southern Turkey). Geol. J. 41, 193–219.
Baker, E.T., Walker, S.L., Massoth, G.J., Resing, J.A., 2019. The NE Lau Basin: widespread and abundant hydrothermal venting in the back-arc region behind a superfast subduction zone. Front. Mar. Sci. https://doi.org/10.33897/fmars.2019.00382.
Balestro, G., Festa, A., Dilek, Y., Tartarotti, P., 2015. Pre-alpine extensional Tectonics of a Peridotite-Localized oceanic core complex in the Late Jurassic, high-pressure Monviso ophiolite (Western Alps). Episodes 38 (4), 266–282. https://doi.org/10.18814/epiiugs/2015/v38i4/82421.
Bao, P., Su, L., Wang, J., Zhai, Q., 2013. Study on the tectonic setting for the ophiolites in Xigaze, Tibet. Acta Geol. Sinica 87 (2), 395–425.
Barnes, G.L., 2008. The making of the Japan Sea and the Japanese Mountains: understanding Japan's volcanism in structural context. Japan Rev. 20, 3–52.
Barth, M.G., Mason, P.R.D., Davies, G.R., Dijkstra, A.H., Drury, M.R., 2003. Geochemistry of the Othris ophiolite, Greece: evidence for refertilization? J. Petrol. 44 (10), 1759–1785.
Bashir, E., Naseem, S., Kaleem, M., Khan, Y., Hamza, S., 2012. Study of serpentinized ultramafic rocks of Bela ophiolite, Balochistan, Pakistan. J. Geogr. Geol. 4 (1), 79–89.
Bédard, É., Hébert, R., Guilmette, C., Lesage, G., Wang, C.S., Dostal, J., 2009. Petrology and geochemistry of the Saga and Sangsang ophiolitic massifs, Yarlung Zangbo Suture Zone, Southern Tibet: evidence for an arc-back-arc origin. Lithos 113, 48–67.
Beyarslan, M., Bingöl, A.F., 2000. Petrology of a supra-subduction zone ophiolite (Elaziğ, Turkey). Can. J. Earth Sci. 37, 1411–1424.
Beyarslan, M., Bingöl, A.F., 2014. Petrology of the Ispendere, Kømurhan and Guleman Ophiolites (Southeast Turkey): subduction initiation rule (SIR) ophiolites and arc related magmatics. In: 3rd Annual international Conference on Geological & Earth Sciences (GEOS 2014), Singapore, pp. 50–59.
Bezard, R., Hébert, R., Wang, C., Dostal, J., Dai, J., Zhong, H., 2011. Petrology and geochemistry of the Xiugugabu ophiolitic massif, western Yarlung Zangbo suture zone, Tibet. Lithos 125, 347–367.
Bonev, N., Dilek, Y., 2010. Geochemistry and tectonic significance of proto-ophiolitic metamafic units from the Serbo-Macedonian and western Rhodope massifs (Bulgaria-Greece). Int. Geol. Rev. 52 (2-3), 298–335.
Bortolotti, V., Chiari, M., Kodra, A., Marcucci, M., Marroni, M., Mustafa, F., Prela, M., Pandolfi, L., Principi, G., Saccani, E., 2006. Triassic MORB magmatism in southern Mirdita zone (Albania). Ofioliti 31, 1–9.
Bortolotti, V., Chiari, M., Marroni, M., Pandolfi, L., Principi, G., Saccani, E., 2013. Geodynamic evolution of ophiolites from Albania and Greece (Dinaric-Hellenic belt): one, two, or more oceanic basins? Int. J. Earth Sci. 102, 783–811.
Bortolotti, V., Chiari, M., Göncüoglu, M.C., Principi, G., Saccani, E., Tekin, U.K., Tassinari, R., 2018. The Jurassic-Early Cretaceous basalt-chert association in the ophiolites of the Ankara Mélange, east of Ankara, Turkey: age and geochemistry. Geol. Mag. 155 (2), 451–478.
Bröcker, M., Löwen, K., Rodionov, N., 2014. Unraveling protolith ages of meta-gabbros from Samos and the Attic-Cycladic Crystalline Belt, Greece: results of a U-Pb zircon and Sr-Nd whole rock study. Lithos 198-199, 234–248.
Bucher, K., Grapes, R., 2009. The eclogite-facies Allalin Gabbro of the Zermatt-Saas Ophiolite, Western Alps: a record of subduction zone hydration. J. Petrol. 50 (8), 1405–1442.
Bucher, K., Fazis, Y., De Capitani, C., Grapes, R., 2005. Blueschists, eclogites, and decompression assemblages of the Zermatt-Saas ophiolite: high-pressure metamorphism of subducted Tethys lithosphere. Am. Mineral. 90, 821–835.
Buda, G.Y., 1993. Igneous Petrology of the Bulfat area (North-East Iraqi Zagros Thrust Zone). Acta Mineralogica-Petrographica, Szeged, pp. 21–39 XXXIV.
Bulle, F., Brökner, M., Gärtnes, C., Keasling, A., 2010. Geochemistry and geochronology of HP mélanges from Tinos and Andros, cycladic blueschist belt, Greece. Lithos 117, 61–81.
Cawood, P.A., Kröner, A., Collins, W.J., Kusky, T.M., Mooney, W.D., Windley, B.F., 2009. Accretionary orogens through Earth history. Geol. Soc. Lond. Spec. Publ. 318, 1–36.

https://doi.org/10.1144/SP318.1.
Çelik, Ö.F., 2008. Detailed geochemistry and K-Ar geochronology of the metamorphic sole rocks and their mafic dykes from the Merson ophiolite, Southern Turkey. Turk. J. Earth Sci. 17, 685–708.
Çelik, Ö.F., Chiaradia, M., 2008. Geochemical and petrological aspects of dike intrusions in the Lycian ophiolites (SW Turkey): a case study for the dike emplacement along the Tauride Belt Ophiolites. Int. J. Earth Sci. 97, 1151–1164.
Çelik, Ö.F., Chiaradia, M., Marzoli, A., Billor, Z., Marschik, R., 2013. The Eldivan ophiolite and volcanic rocks in the Izmir-Ankara-Erzincan suture zone, Northern Turkey: geochronology, whole-rock geochemical and Nd-Sr-Pb characteristics. Lithos 172-173, 31–46.
Chang, S.-J., Ferreira, A.M.G., Faccenda, M., 2016. Upper and mid-mantle interaction between the Samoan plume and the Tonga-Kermadec slabs. Nat. Comm. 7. https://doi.org/10.1038/ncomms10799.
Charlot-Prat, F., 2005. An undeformed ophiolite in the Alps: field and geochemical evidence for a link between volcanism and shallow plate tectonic processes. In: Foulger, G.R., Natland, J.H., Presnall, D.C., Anderson, D.L. (Eds.), Plates Plumes and Paradigms. Geol. Soc. Am. Spec. Pap Vol. 388. pp. 751–780.
Chen, G., Xia, B., 2008. Platinum-group elemental geochemistry of mafic and ultramafic rocks from Xigaze ophiolite, southern Tibet. J. Asian Earth Sci. 32, 406–422.
Chen, N.H.-C., Zhao, G., Jahn, B.-m., Zhou, H., Sun, M., 2017. Geochemistry and geochronology of the Delinggou Intrusion: implications for the subduction of the Paleo-Asian Ocean beneath the North China Craton. Gondwana Res. 43, 178–192.
Chiari, M., Djerić, N., Garfagnoli, F., Hrvatoić, H., Krstić, M., Levi, N., Malasoma, A., Marroni, M., Menna, F., Nirta, G., Pandolfi, L., Principi, G., Saccani, E., Stojadinović, U., Trivić, B., 2011. The geology of the Zlatibor-Maljen area (western Serbia): a geotraverse aross the ophiolites of the Dinari-Hellenic collisional belt. Ofioliti 36 (2), 139–166.
Chiari, M., Bortolotti, V., Marcucci, M., Photiades, A., Principi, G., Saccani, E., 2012. Radiolarian biostratigraphy and geochemistry of the Koziakas massif ophiolites (Greece). Bull. Soc. Géol. France 183 (4), 287–306.
Clark, S.R., Stegman, D., Müller, R.D., 2008. Episodicity in back-arc tectonic regimes. Phys. Earth Planet. Inter. 171, 265–279.
Clift, R., Vannucchi, P., 2004. Controls on tectonic accretion versus erosion and recycling of the continental crust. Rev. Geophys. 42https://doi.org/10.1029/2003RG000127. RG2001.
Clift, P.D., Hannigan, R., Blusztajn, J., Draut, A.E., 2002. Geochemical evolution of the Dras-Kohistan Arc during collision with Eurasia: evidence from the Ladakh Himalaya, India. Island Arc 11, 255–273.
Cloos, M., 1993. Lithospheric buoyancy and collisional orogenesis: subduction of oceanic plateaus, continental margins, island arcs, spreading ridges, and seamounts. Geol. Soc. Am. Bull. 105 (6), 715–737.
Colakuglo, A.R., Sayit, K., Günay, K., Göncüolgu, M.C., 2012. Geochemistry of mafic dykes from the Southeast Anatolian ophiolites, Turkey: implications for an intra-oceanic arc-basin system. Lithos 132-133, 113–126.
Coleman, R.G., 1977. Ophiolites, Ancient Oceanic Lithosphere? Springer-Verlag, Berlin, Heidelberg, New York, pp. 229.
Collins, W.J., Belousova, E.A., Kemp, A.I.S., Murphy, B., 2011. Two contrasting Phanerozoic orogenic systems revealed by hafnium isotope data. Nat. Geosci. 4, 333–337.
Corfield, R.I., Searle, M.P., Pedersen, R.B., 2001. Tectonic setting, origin, and obduction history of the Spontang Ophiolite, Ladakh Himalaya, NW India. J. Geol. 109, 715–736.
Cvetković, V., Šarić, K., Grubić, A., Cvijić, R., Milošević, A., 2014. The Upper Cretaceous ophiolite of North Kozara – remnants of an anomalous mid-ocean ridge segment of the Neotethys? Geol. Carpath. 65 (2), 117–130.
Dai, J., Wang, C., Li, Y., 2012. Relicts of the Early Cretaceous seamounts in the central-western Yarlung Zangbo Suture Zone, southern Tibet. J. Asian Earth Sci. 53, 25–37.
Dai, J., Wang, C., Polat, A., Santosh, M., Li, Y., Ge, Y., 2013. Rapid forearc spreading between 130 and 120 Ma: evidence from geochronology and geochemistry of the Xigaze ophiolite, southern Tibet. Lithos 172-173, 1–16.
Dangerfield, A., Harris, R., Sarifakioğlu, E., Dilek, Y., 2011. Tectonic evolution of the Ankara Mélange and associated Eldivan ophiolite near Hançili, central Turkey. In: Wakabayashi, J., Dilek, Y. (Eds.), Melanges: Processes of Formation and Societal Significance. Geol. Soc. Am. Spec. Pap. Vol. 480. pp. 143–169.
Daşçi, H.T., Parlak, O., Nurlu, N., Billor, Z., 2015. Geochemical characteristics and age of metamorphic sole rocks within a Neotethyan ophiolitic mélange from Konya region (central southern Turkey). Geodin. Acta 27 (4), 223–243.
De Wit, M., Furnes, H., MacLennan, S., Doucoure, M., Schoene, B., Weckmann, U., Martinez, U., Bowring, S., 2018. Paleoarchean bedrock lithologies across the Makhonjwa Mountains of South Africa and Swaziland linked to geochemical, magnetic and tectonic data revel early plate tectonic genes flanking subduction margins. Geosci. Front. 9, 603–665.
Deschamps, A., Lallemand, S., 2002. The West Philippine Basin: a Paleocene-Oligocene backarc basin opened between two opposed subduction zones. J. Geophys. Res. 107 (12). https://doi.org/10.1029/72001JB001706.
Deschamps, A., Shinjo, R., Matsumoto, T., Lee, C.-S., Lallemand, S.E., Wu, S., Scientific party of KR03 and KR04 cruises, 2008. Propagators and ridge jumps in a back-arc basin, the west Philippine Basin. Terra Nova 20, 327–332.
Dey, A., Hussain, M.F., Barman, M.N., 2018. Geochemical characteristics of mafic and ultramafic rocks from the Naga Hills Ophiolite, India: implications for petrogenesis. Geosci. Front. 9, 517–529.
Dilek, Y., 2003a. Ophiolite concept and its evolution. In: Dilek, Y., Newcomb, S. (Eds.), Ophiolite Concept and the Evolution of Geological Thought. Geol. Soc. Am. Spec. Pap. Vol. 373. pp. 1–16.
Dilek, Y., 2003b. Ophiolites, plumes and orogeny. In: Dilek, Y., Robinson, P.T. (Eds.), Ophiolites in Earth History. Geol. Soc. London, Spec. Publ. Vol. 218. pp. 9–19.
Dilek, Y., 2006. Collision tectonics of the Eastern Mediterranian region: causes and consequences. Geol. Soc. Am. Spec. Pap. 409, 1–13.
Dilek, Y., Eddy, C.A., 1992. The Troodos (Cyprus) and Kizidag (S.Turkey) ophiolites as structural models for slow-spreading ridge segments. J. Geol. 100, 305–322.
Dilek, Y., Flower, M.F.J., 2003. Arc-trench rollback and forearc accretion: 2. Model template for Albania, Cyprus and Oman. In: Dilek, Y., Robinson, P.T. (Eds.), Ophiolites in Earth History. Geological Society of London Special Publication Vol. 218. pp. 43–68.
Dilek, Y., Furnes, H., 2009. Structure and geochemistry of Tethyan ophiolites and their petrogenesis in subduction rollback systems. Lithos 113, 1–20.
Dilek, Y., Furnes, H., 2011. Ophiolite genesis and global tectonics: geochemical and tectonic fingerprinting of ancient oceanic lithosphere. Geol. Soc. Am. Bull. 123 (3/4), 387–411. https://doi.org/10.1130/B30446.1.
Dilek, Y., Furnes, H., 2014. Ophiolites and their origins. Elements 10, 93–100.
Dilek, Y., Furnes, H., 2019. Tethyan ophiolites and Tethyan seaways. J. Geol. Soc. Lond. 176, 899–912.
Dilek, Y., Moores, E.M., 1990. Regional tectonics of the Eastern Mediterranean ophiolites. In: Malpas, J., Moores, E.M., Panayiotou, A., Xenophontos, C. (Eds.), Ophiolites, Oceanic Crustal Analogues. Proceedings of the Symposium "Troodos 1987", Nicosia, Cyprus. The Geological Survey Department, pp. 295–309.
Dilek, Y., Polat, A., 2008. Suprasubduction zone ophiolites and Archean tectonics. Geology 36 (5), 431–432.
Dilek, Y., Thy, P., 1998. Structure, petrology and seafloor spreading tectonics of the Kizildag ophiolite, Turkey. Geol. Soc. Lond. Spec. Publ. 148, 43–69.
Dilek, Y., Thy, P., 2009. Island arc tholeiite to boninitic melt evolution of the Cretaceous Kizildag (Turkey) ophiolite: model for multi-stage early arc–forearc magmatism in Tethyan subduction factories. Lithos 113 (1-2), 68–87.
Dilek, Y., Whitney, D.L., 1997. Counterclockwise *PTt* trajectory from the metamorphic sole of a Neo-Tethyan ophiolite (Turkey). Tectonophysics 280 (3-4), 295–301. https://doi.org/10.1076/S00401951(97)00038-3.
Dilek, Y., Yang, J.-S., 2018. Ophiolites, diamonds, and ultrahigh-pressure minerals: new discoveries and concepts on upper mantle petrogenesis. Lithosphere 10 (1), 3–13. https://doi.org/10.1130/L715.1.
Dilek, Y., Thy, P., Moores, E.M., Ramsden, T.W., 1990. Tectonic evolution of the Troodos ophiolite within the Tethyan framework. Tectonics 9 (4), 811–823.
Dilek, Y., Furnes, H., Skjerlie, K., 1997. Propagating rift tectonics of a Caledonian marginal basin: multi-stage seafloor spreading history of the Solund-Stavfjord ophiolite in western Norway. Tectonophysics 280 (3-4), 213–238. https://doi.org/10.1016/S0040-1951(97)00036-X.
Dilek, Y., Thy, P., Hacker, B., Grundvig, S., 1999. Structure and petrology of Tauride ophiolites and mafic dike intrusions (Turkey): implications for the Neotethyan ocean. Geol. Soc. Am. Bull. 111 (8), 1192–1216. https://doi.org/10.1130/0016-7606(1999)111<1192:SAPOTO>2.3.CO;2.
Dilek, Y., Shallo, M., Furnes, H., 2005. Rift-drift spreading and subduction zone tectonics of Albanian ophiolites. Int. Geol. Rev. 47, 147–176. https://doi.org/10.2747/00206814.47.2.147.
Dilek, Y., Furnes, H., Shallo, M., 2007. Suprasubduction zone ophiolite formation along the periphery of Mesozoic Gondwana. Gondwana Res. 11, 453–475. https://doi.org/10.1016/j.gr.2007.01.005.
Dilek, Y., Furnes, H., Shallo, M., 2008. Geochemistry of the Jurassic Mirdita Ophiolite (Albania) and the MORB to SSZ evolution of a marginal basin oceanic crust. Lithos 100, 174–209.
Dubois-Côté, V., Hébert, R., Dupuis, C., Wang, C.S., Li, Y.L., Dostal, J., 2005. Petrology and geochemical evidence for the origin of the Yarlung Zangbo ophiolites, southern Tibet. Chem. Geol. 214, 265–286.
Elitok, Ö., Drüppel, K., 2008. Geochemistry and tectonic significance of metamorphic sole rocks beneath the Beyşehir-Hoyran ophiolite (SW-Turkey). Lithos 100, 322–353.
Fan, J.-J., Li, C., Xu, J.-J., Wang, M., 2014. Petrology, geochemistry, and geological significance of the Nadong ocean island, Banggongco-Nujiang suture, Tibetan plateau. Int. Geol. Rev. 56 (8), 915–928.
Festa, A., Balestro, G., Dilek, Y., Tartarotti, P., 2015. A Jurassic oceanic core complex in the high-P Monviso Ophiolite (Western Alps, NW Italy). Lithosphere 7 (6), 646–652.
Floyd, P.A., Winchester, J.A., 1975. Magma type and tectonic setting discrimination using immobile elements. Earth Panet. Sci. Lett. 27, 211–218.
Fretzdorff, S., Livermore, R.A., Devey, C.W., Leat, P.T., Stoffers, P., 2002. Petrogenesis of the back-arc East Scotia Ridge, South Atlantic Ocean. J. Petrol. 43 (8), 1435–1467.
Froitzheim, N., Jahn-Awe, S., Frei, D., Wainwright, A.N., Maas, R., Georgiev, N., Nagel, T.J., Pleuger, J., 2014. Age and composition of meta-ophiolite from Rhodope Middle Allochton (Satovcha, Bulgaria): a test for the maximum-allochthony hypothesis. Tectonics 32. https://doi.org/10.1002/2014TC003526.
Furnes, H., Dilek, Y., 2017. Geochemical characterization and petrogenesis of intermediate to silicic rocks in ophiolites: a global synthesis. Earth-Sci. Rev. 166, 1–37.
Furnes, H., Safonova, I., 2019. Ophiolites of the Central Asian Orogenic Belt: geochemical and petrological characterization and tectonic settings. Geosci. Front. 10, 1255–1284.
Furnes, H., Rosing, M., Dilek, Y., de Wit, M.J., 2009. Isua supracrustal belt (Greenland) – a vestige of a 3.8 Ga suprasubduction zone ophiolite, and the implications for Archean geology. Lithos 113, 115–132.
Furnes, H., Robins, B., de Wit, M.J., 2012. Geochemistry and petrology of lavas in the upper Onverwacht Suite, Barberton mountain land, South Africa. South Afr. J. Geol. 115 (2), 171–210.
Furnes, H., de Wit, M., Dilek, Y., 2014. Four billion years of ophiolites reveal secular trends in oceanic crust formation. Geosci. Front. 5, 571–603.
Furnes, H., Dilek, Y., de Wit, M., 2015. Precambrian greenstone sequences represent different ophiolite types. Gondwana Res. 27, 649–685.
Gallhofer, D., van Quadt, A., Schmid, S.D., Guillong, M., Peytcheva, I., Seghedi, I., 2016. Magmatic and tectonic history of Jurassic ophiolites and associated granitoids from South Apuseni Mountains (Romania). Swiss J. Geosci. https://doi.org/10.1007/s00015-016-0231-6.
Galoyan, G., Rolland, Y., Sosson, M., Corsini, M., Billo, S., Verati, C., Melkonyan, R., 2009. Geology, geochemistry and $^{40}Ar/^{39}Ar$ dating of Sevan ophiolites (Lesser Caucasus, Armenia): evidence for Jurassic back-arc opening and hot spot event between the South Armenian Block and Eurasia. J. Asian Earth Sci. 34, 135–153.

Garašič, V., Vrkljan, M., Majer, V., 2004. Mineral relationships and their chemistry in some basic magmatic rocks of Banija ophiolite complex, Croatia. Rudasko-geološko-naftni zbornik 16, 1–19.
Gass, I.G., 1968. Is the Troodos massif of Cyprus a fragment of Mesozoic ocean floor. Nature 221, 926–930.
Ghazi, A.M., Hassanipak, A.A., Mahoney, J.J., Duncan, R.A., 2004. Geochemical characteristics, ^{40}Ar - ^{39}Ar ages and original tectonic setting of the Band-e-Zeyarat/Dar Anar ophiolite, Makran accretionary prism, S.E. Iran. Tectonophysics 393, 175–196.
Gnos, E., Khan, M., Mahmood, K., Khan, A.S., Shafique, N.A., Villa, I.M., 1998. Bela oceanic lithosphere assemblage and its relation to the Réunion hotspot. Terra Nova 10, 90–95.
Godard, M., Dautria, J.-M., Perrin, M., 2003. Geochemical variability of the Oman ophiolite lavas: relationship with spatial distribution and paleomagnetic directions. Geochem. Geophys. Geosyst. 4 (6), 8609. https://doi.org/10.1029/2002GC00452.
Goodenough, M.K., Styles, M.T., Schofield, D., Thomas, R.J., Crowley, Q.C., Lilly, R.M., McKervey, J., Stephenson, D., Carney, J.N., 2010. Architecture of the Oman-UAE ophiolite: evidence for multi-phase magmatic history. Arab. J. Geosci. 3, 439–458.
Goodenough, K.M., Thomas, R.J., Styles, M.T., Schofield, D.I., MacLeod, C.J., 2014. Records of ocean growth and destruction in the Oman-UAE ophiolite. Elements 10, 109–114.
Guillaume, B., Husson, L., Funiciello, F., Faccenna, C., 2013. The dynamics of laterally variable subductions: laboratory models applied to the Hellenides. Solid Earth 4, 179–200.
Guilmette, C., Hébert, R., Dostal, J., Indares, A., Ullrich, T., Bédard, É., Wang, C., 2012. Discovery of a dismembered metamorphic sole in the Saga ophiolite mélange, South Tibet: assessing an Early Cretaceous disruption of the Neo-Tethyan supra-subduction zone and consequences on basin closing. Gondwana Res. 22, 398–414.
Gvirtzman, Z., Stern, R.J., 2004. Bathymetry of mariana trench-arc system and formation of the challenger deep as a consequence of weak plate coupling. Tectonics 23https://doi.org/10.1029/2003TC001581. TC2011.
Hadi, A., Kameraan, D., Ismael, S., 2013. Characteristics of the amphibolite rocks of Penjween area, Kurdistan Region, northeast Iraq: genetic implication and association with Penjween Ophiolite Complexes. J. Environ. Earth Sci. 3 (14), 22–44.
Hassanipak, A.A., Ghazi, A.M., 2000. Petrology, geochemistry and tectonic setting of the Khoy ophiolite, northwest Iran: implications for the Tethyan tectonics. J. Asian Earth Sci. 18, 109–121.
Hébert, R., Huot, F., Wang, C., Liu, Z., 2003. Yarlung Zangbo ophiolites (Southern Tibet) revisited: geodynamic implications from the mineral record. In: Dilek, Y., Robinson, P.T. (Eds.), Ophiolites in Earth History. Geol. Soc. Lond. Spec. Publ. Vol. 218. pp. 165–190.
Hébert, R., Bezard, R., Guilmette, C., Dostal, J., Wang, C.S., Liu, Z.F., 2012. The Indus–Yarlung Zangbo ophiolites from Nanga Parbat to Namche Barwa syntaxes, southern Tibet: first synthesis of petrology, geochemistry, and geochronology with incidences on geodynamic reconstructions of Neo-Tethys. Gondwana Res. 22, 377–397.
Herrmann, J., Müntener, O., Günther, D., 2001. Differentiation of mafic magma in a continental crust-to-mantle transition zone. J. Petrol. 42, 189–206. https://doi.org/10.1093/petrology/42.1.189.
Hickey-Vargas, R., 1998. Origin of the Indian Ocean-type isotopic signature in the basalts from Philippine Sea plate spreading centers: an assessment of local versus large-scale processes. J. Geophys. Res. 103 (B9), 20963–20979.
Hoareau, G., Bomou, B., van Hinsbergen, D.J.J., Carry, N., Marquer, D., Donnadieu, Y., Le Hir, G., Vrielynck, B., Walter-Simonnet, A.-V., 2015. Did high Neo-Tethyan subduction rates contribute to early Cenozoic warming? Clim. Past 11, 1751–1767.
Hofmann, A.W., 1997. Mantle geochemistry: the message from oceanic volcanism. Nature 385, 219–229.
Hofmann, A., Wilson, A.H., 2007. Silicified basalts, bedded cherts and other sea floor alteration phenomena of the 3.4 Ga Nondweni greenstone belt, South Africa. In: Van Kranendonk, M.J., Smithies, R.H., Bennett, V.C. (Eds.), Earth's Oldest Rocks. Developments in Precambrian Geology. Vol. 15. Elsevier, Amsterdam, pp. 571–605.
Humphris, S.E., Thompson, G., 1978. Trace element mobility during hydrothermal alteration of oceanic basalts. Geochim. Cosmochim. Acta 42, 127–136.
Huot, F., Hébert, R., Varfalvy, V., Beaudoin, G., Wang, C., Liu, Z., Dostal, J., 2002. The Beimarang mélange (southern Tibet) brings additional constraints in assessing the origin, metamorphic evolution and obduction processes of the Yarlung Zangbo ophiolite. J. Asian Earth Sci. 21, 307–322.
Irvine, T.N., Baragar, W.R.A., 1971. A guide to the chemical classification of common volcanic rocks. Can. J. Earth Sci. 8, 523–548.
Ishimaru, S., Saikawa, Y., Miura, M., Parlak, O., Arai, S., 2018. Decoding of mantle processes in the Mersin ophiolite, Turkey, of end-member arc type: location of the boninitic magma generation. Minerals 8, 464. https://doi.org/10.3390/min8100464.
Ishiwatari, A., 1994. Circum-Pacific Phanerozoic multiple ophiolite belts. In: Ishiwatari, A., Malpas, J., Ishizuka, M. (Eds.), Circum-Pacific Ophiolites. Proceedings of the 29th IGC, Kyoto, Part D. VSP, Utrecht, pp. 7–28.
Ishizuka, O., Taylor, R.N., Ohara, Y., Yuasa, M., 2013. Upwelling rifting and age-progressive magmatism from the Oki-Daito mantle plume. Geology 41 (9), 1011–1014. https://doi.org/10.1130/G34525.1.
Isozaki, Y., Maruyama, S., Fukuoka, F., 1990. Accreted oceanic materials in Japan. Tectonophysics 181, 179–205.
Kakar, M.I., Collins, A.S., Mahmood, K., Foden, J.D., Khan, M., 2012. U-Pb zircon crystallization age of the Muslim Bagh ophiolite: enigmatic remains of an extensive pre-Himalayan arc. Geology 40 (12), 1099–1102.
Kakar, M.I., Kerr, A.C., Mahmood, K., Collins, A.S., Khan, M., McDonald, L., 2014. Supra-subduction zone tectonic setting of the Muslim Bagh Ophiolite, northwestern Pakistan: insights from geochemistry and petrology. Lithos 202-203, 190–206.
Kakar, M.I., Mahmood, K., Khan, M., Plavsa, D., 2015a. Petrology and geochemistry of amphibolites and greenschists from the metamorphic sole of the Muslim Bagh ophiolite (Pakistan): implications for protolith and ophiolite emplacement. Arab. J. Geosci. 8, 6105–6120.
Kakar, M.I., Mahmood, K., Arif, M., Khan, M., Kerr, A.C., Mohibullah, M., Kasi, A.K., 2015b. Petrology and geochemistry of mafic dykes from the Muslim Bagh Ophiolite (Pakistan): implications for petrogenesis and emplacement. Turk. J. Earth Sci. 24, 165–178.
Kapsiotis, A., Rassios, A.E., Antonelou, A., Tzamos, E., 2016. Genesis and multi-episodic alteration of zircon-bearing chromitites from the Ayios Stefanos Mine, Othris Massif, Greece: assessment of an unconventional hypothesis on the origin of zircon in ophiolitic chromitites. Minerals 6. https://doi.org/10.3390/min6040124.
Karaoğlan, F., Parlak, O., Klötzli, U., Thöni, M., Koller, F., 2013. U-Pb and Sm-Nd geochronology of the Kizildağ (Hatay, Turkey) ophiolite: implications for the timing and duration of suprasubduction zone type oceanic crust formation in the southern Neotethys. Geol. Mag. 150 (2), 283–299.
Karkalis, C., Magganas, A., Koutsovitis, P., 2016. Petrological, mineralogical and geochemical data from the Eohellenic ophiolitic nappe in the island of Skyros, Greece. Bull. Geol. Soc. Greece 50, 1867–1877.
Katzir, Y., Matthews, A., Garfunkel, Z., Schliestedt, M., Avigad, D., 1996. The tectono-metamorphic evolution of a dismembered ophiolite (Tinos, Cyclades, Greece). Geol. Mag. 133 (3), 237–254.
Kavak, K.S., Parlak, O., Temiz, H., 2017. Geochemical characteristics of ophiolitic rocks from the southern margin of the Sivas basin and their implications for the inner Tauride Ocean, Central-Eastern Turkey. Geodin. Acta 29 (1), 160–180.
Keller, R.A., Fisk, M.R., Smellie, J.L., Strelin, J.A., Lawver, L.A., 2002. Geochemistry of back arc basin volcanism in Bransfield Strait, Antarctica: subducted contributions and along-axis variations. J. Geophys. Res. 107 (B8), 2171. https://doi.org/10.1029/2001JB000444.
Khalatbari-Jafari, M., Juteau, T., Cotten, J., 2006. Petrology and geochemical study of the Late Cretaceous ophiolite of Khoy (NW Iran), and related geological formations. J. Asian Earth Sci. 27, 465–502.
Khan, M., Kerr, A.C., Mahmood, K., 2007a. Formation and tectonic evolution of the Cretaceous-Jurassic Muslim Bagh ophiolite complex, Pakistan: implications for the composite tectonic setting of ophiolites. J. Asian Earth Sci. 31, 112–127.
Khan, S.R., Jan, M.Q., Khan, T., Khan, M.A., 2007b. Petrology of the dykes from the Waziristan Ophiolite, NW Pakistan. J. Asian Earth Sci. 29, 369–377.
Khan, M., Khan, M.J., Mahmood, K., Kakar, M.I., 2018. Geology and petrology of crustal section of Bela ophiolite, Balochistan, Pakistan. Bahria Univ. Res. J. Earth Sci. 3 (1), 1–5.
Kimura, J.-I., Gill, J.B., van Keken, P.E., Kawabata, H., Skora, S., 2017. Origin of geochemical mantle components: role of spreading ridges and thermal evolution of mantle. Geochem. Geophys. Geosyst. 18, 697–734. https://doi.org/10.1002/2016GC006696.
Koepke, J., Seidel, E., Kreuzer, H., 2002. Ophiolites on the Southern Aegean island Crete, Karpathos and Rhodes: composition, geochronology and composition within the ophiolite of the Eastern Mediterranean. Lithos 65, 183–203.
Koglin, N., 2008. Geochemistry, Petrogenesis and Tectonic Setting of Ophiolites and Mafic-Ultramafic Complexes in the Northeastern Aegean Region: New Trace-Element, Isotopic and Age Constraints. Ph.D thesis. Johannes Gutenberg-Universität 136 pp.
Koglin, N., Kostopoulos, D., Reichmann, T., 2009a. The Lesvos mafic-ultramafic complex, Greece: ophiolite or incipient rift? Lithos 108, 243–261.
Koglin, N., Kostopoulos, D., Reischmann, T., 2009b. Geochemistry, petrogenesis and tectonic setting of the Samothraki mafic suite, NE Greece: trace-element, isotopic and zircon age constraints. Tectonophysics 473, 53–68.
Komiya, T., Yamamoto, S., Aoki, S., Sawaki, Y., Ishikawa, A., Tashiro, T., Koshida, K., Shimojo, M., Aoki, K., Collerson, K.D., 2015. Geology of the Eoarchean. > 3.95 Ga, Nulliak supracrustal rocks in the Saglek Block, northern Labrador, Canada: the oldest geological evidence for plate tectonics. Tectonophysics 662, 40–66.
Koutsovitis, P., Magganas, A., 2010. The geochemistry and petrogenesis of volcanic rocks within ophiolitic formations at the northeast Othris region, Greece. In: Proceedings of the XIX CBGA Congress, Thessaloniki, Greece. Spec. vol. 99. Scientific Annals, School of Geology, Aristotle University of Thessaloniki, pp. 263–270.
Kramer, J., Abart, R., Müntener, O., Schmid, S.M., Stern, W.-B., 2003. Geochemistry of metabasalts from ophiolitic and adjacent distal continental margin units: evidence from the Monte Rosa region (Swiss and Italian Alps). Schweiz. Mineral. Petrogr. Mitt. 83, X1–X24.
Lallemand, S., Heuret, A., Boutelier, D., 2005. On the relationships between dip, back-arc stress, upper plate absolute motion, and crustal nature in subduction zones. Geochem. Geophys. Geosyst. 6 (9). https://doi.org/10.1029/2005GC000917. Q09006.
Lamont, T.N., Roberts, N.M.W., Searle, M.P., Gopon, P., Waters, D.J., Miller, I., 2019. The age, origin and emplacement of the Tsiknias Ophiolite, Tinos, Greece. Tectonics. https://doi.org/10.1029/2019TC005677.
Langosch, A., Seidel, E., Stosch, H.-G., Okrusch, M., 2000. Intrusive rocks in the ophiolitic mélange of Crete – witnesses to a Late Cretaceous thermal event of enigmatic geological position. Contrib. Mineral. Petrol. 139, 339–355.
Le Maitre, R.W., 1989. A Classification of Igneous Rocks and Glossary of Terms. Blackwell, Oxford, UK.
Leat, P.T., Livermore, R.A., Millar, I.L., Pearce, J.A., 2000. Magma supply in back-arc spreading centre segment E2, East Scotia Ridge. J. Petrol. 41 (6), 845–866.
Li, X.-H., Faure, M., Rossi, P., Lin, W., Lahondère, D., 2015. Age of Alpine Corsica ophiolites revisited: insights from *in situ* zircon U-Pb age and O-Hf isotopes. Lithos 220–223, 179–190.
Lian, D., Yang, J., Dilek, Y., Liu, F., Wu, W., Xiong, F., 2017. Geochemical, geochronological, and Sr-Nd Isotopic constraints on the origin of the mafic dikes from the Pozanti-Karsanti ophiolite: implications for tectonic evolution. J. Geol. 125, 223–239.
Lian, D., Yang, J., Dilek, Y., Rocholl, A., 2019. Mineralogy and geochemistry of peridotites and chromitites in the Aladag Ophiolite (southern Turkey): melt evolution of the Cretaceous Neotethyan mantle. J. Geol. Soc. Lond. 176, 958–974. https://doi.org/10.1144/jgs2018-060.
Liberi, F., Piluso, E., 2009. Tectonometamorphic evolution of the ophiolitic sequences from Northern Calabrian Arc. Ital. J. Geosci. 128 (2), 483–493.
Liberi, F., Morten, L., Piluso, E., 2006. Geodynamic significance of ophiolites within the Calabrian Arc. Island Arc 15, 26–43.
Lister, G.S., Forster, M.A., Rawling, T.J., 2001. Episodicity during orogenesis. In: Miller, J.A., Holdsworth, R.E., Buick, I.S., Hand, M. (Eds.), Continental Reactivation and Reworking.
Liu, W.B., Qian, Q., Yue, G.L., Li, Q.S., Zhang, Q., Zhou, M.F., 2002. The geochemical

characteristics of fore-arc ophiolite from Dingqing area, Tibet. Acta Petrol. Sin. 18 (3), 392–400.
Liu, F., Yang, J.S., Chen, S.Y., Liang, F.H., Niu, X.L., Li, Z.L., Lian, D.Y., 2013. Ascertainment and environment of the OIB-type basalts from the Dongbo ophiolite in the western part of the Yarlung Zangbo Suture Zone. Acta Petrol. Sin. 29 (6), 1909–1932.
Liu, W.-L., Xia, B., Zhong, Y., Cai, J.-X., Li, J.-F., Liu, H.-F., Cai, Z.-R., Sun, Z.-L., 2014. Age and composition of the Rebang Co and Julu ophiolites, central Tibet: implications for the evolution of the Bangong Meso-Tethys. Int. Geol. Rev. 56 (4), 430–447.
Liu, F., Yang, J.-s., Dilek, Y., Xu, Z.-q., Xu, X.-z., Liang, F.-h., Chen, S.-y., Lian, D.-y., 2015. Geochronology and geochemistry of basaltic lavas in the Dongbo and Purang ophiolites of the Yarlung-Zangbo Suture zone: plume-influenced continental margin-type oceanic lithosphere in southern Tibet. Gondwana Res. 27, 701–718.
Liu, T., Zhai, Q.-g., Wang, J., Bao, P.-s., Qiangba, Z., Tang, S.-h., Tang, Y., 2016. Tectonic significance of the Dongqiao ophiolite in the north-central Tibetan plateau: evidence from zircon dating, petrological geochemical and Sr-Nd-Hf isotopic characterization. J. Asian Earth Sci. 116, 139–154.
Liu, Y., Li, W., Feng, Z., Wen, Q., Neubauer, F., Liang, C., 2017. A review of the Paleozoic tectonics in the eastern part of the Central Asian Orogenic Belt. Gondwana Res. 43, 123–148.
Liu, T., Wu, F.-Y., Liu, C.-Z., Tribuzio, R., Ji, W.-B., Zhang, C., Xu, Y., Zhang, W.-Q., 2018. Variably evolved gabbroic intrusions within the Xigaze ophiolite (Tibet): new insights into the origin of ophiolite diversity. Contrib. Mineral. Petrol. 173, 91. https://doi.org/10.1007/s00410-018-1518-6.
Liu, W.-L., Zhong, Y., Gu, M., Tang, G.-J., Zhong, L.-F., Liu, H.-F., Xia, B., 2019. The Late Jurassic Zedong ophiolite: a remnant of subduction initiation within Yarlung Zangbo Suture Zone (southern Tibet) and its tectonic implications. Gondwana Res. https://doi.org/10.1016/j.gr.2019.09.002.
Lugović, B., Altherr, R., Raczek, I., Hofmann, A.W., Majer, V., 1991. Geochemistry of peridotites and mafic igneous rocks from the Central Dinaric Ophiolite Belt, Yugoslavia. Contrib. Mineral. Petrol. 106, 201–226.
Lugović, B., Slovenec, D., Schuster, R., Schwarz, W.H., Horwat, M., 2015. Petrology, geochemistry and tectono-magmatic affinity of gabbroic olistoliths from the ophiolite mélange in the NW Dinaric-Vardar ophiolite zone (Mts. Kalnik and Ivanščica, North Croatia). Geologia Croatica 68 (1), 25–49.
Lyubetskaya, T., Korenaga, J., 2007. Chemical composition of Earth's primitive mantle and its variance: 1. Method and results. J. Geophys. Res. 112https://doi.org/10.2029/2005JB004223. B03211.
Macpherson, C.G., Hall, R., 2001. Tectonic setting of Eocene boninite magmatism in the Izu-Bonin-Mariana forearc. Earth Planet. Sci. Lett. 186, 215–230.
Magni, V., 2019. The effects of back-arc spreading on arc magmatism. Earth Planet. Sci. Lett. 519, 141–151.
Mahéo, G., Bertrand, H., Guillot, S., Villa, I.M., 2004. The South Ladakh ophiolites (NW Himalaya, India): an intra-oceanic tholeiitic arc origin with implications for the closure of the Neo-Tethys. Chem. Geol. 203, 273–303.
Maldonado, A., Bohoyo, F., Galindo-Zaldívar, J., Hernández-Molina, F.J., Lobo, F.J., Lodolo, E., Martos, Y.M., Pérez, L.F., Schreider, A.A., Somoza, L., 2014. A model of oceanic development by ridge jumping: opening of the Scotia Sea. Glob. Planet. Chang. 123, 152–173.
Malpas, J., Zhou, M.-F., Robinson, P.T., Reynolds, P.H., 2003. Geochemical and geochronological constrains on the origin and replacement of the Yarlung-Zangbo ophiolites, southern Tibet. In: Dilek, Y., Robinson, P.T. (Eds.), Ophiolites in Earth History. Geol. Soc. London, Spec. Publ. Vol. 218. pp. 191–206.
Manatschal, G., Sauter, D., Karpoff, A.M., Masini, E., Mpohn, G., Lagabrielle, Y., 2011. The Chenaillet Ophiolite in the French/Italian Alps: an ancient analogue for an Oceanic Core Complex? Lithos 169–184.
Maruyama, S., Liou, J.G., Terbayashi, M., 1996. Blueschist and eclogites of the world, and their exhumation. Int. Geol. Rev. 38, 485–594.
Maruyama, S., Kawai, T., Windley, B.F., 2010. Ocean plate stratigraphy and its imbrication in an accretionary orogen: the Mona complex, Anglesey-Lleyn, Wales, UK. Geol. Soc. Lond. Spec. Publ. 338, 55–75.
Maruyama, S., Santosh, M., Azuma, S., 2016. Initiation of plate tectonics in the Hadean: eclogitization triggered ABEL bombardment. Geosci. Front. 7, 1–17. https://doi.org/10.1016/j.gsf.2016.11.009.
Metcalfe, I., 2013. Gondwana dispersion and Asian accretion: tectonic and palaeogeographic evolution of eastern Tethys. J. Asian Earth Sci. 66, 1–33.
Miller, C., Thöni, M., Frank, W., Schuster, R., Melcher, F., Meisel, T., Zanetti, A., 2003. Geochemistry and tectonomagmatic affinity of the Yungbwa ophiolite, SW Tibet. Lithos 66, 155–172.
Mirza, T.A., 2008. Petrogenesis of the Mawat Ophiolite Complex and the Associated Chromite, Kurdistan Region, NE Iraq. PhD thesis. University of Sulaimani 189 pp.
Mirza, T.A., Ismail, S.A., 2007. Origin of plagiogranites in the Mawat ophiolite Complex, Kurdistan region, NE Iraq. J. Kirkuk Univ. Sci. Stud. 2 (1), 1–20.
Mittelstaedt, E., Ito, G., Behn, M.D., 2008. Mid-ocean ridge jumps associated with hotspot magmatism. Earth Planet. Sci. Lett. 266, 256–270.
Miyashiro, A., 1973. The Troodos ophiolite complex was probably formed in an island arc. Earth Planet. Sci. Lett. 19, 218–224.
Mocek, B., 2001. Geochemical evidence for arc-type volcanism in the Aegean Sea: the blueschist unit of Siphnos, Cyclades (Greece). Lithos 57, 263–289.
Moghadam, H.S., Rahgoshay, M., Whitechurch, H., 2008. Mesozoic back-arc extension in the active margin of the Iranian continental block: constraints from age and geochemistry of the mafic lavas. Ofioliti 33, 95–103.
Moghadam, H.S., Whitechurch, H., Rahgoshay, M., Monsef, I., 2009. Significance of Nain-Baft ophiolitc belt (Iran): Shrt-lived, transtensional Cretaceous back-arc oceanic basins over the Tethyan subduction zone. Compt. Rendus Geosci. 341, 1016–1028.
Moghadam, H.S., Stern, R.J., Rahgoshay, M., 2010. The Dehshir ophiolite (central Iran): geochemical constraints on the origin and evolution of the Inner Zagros ophiolite belt. Geol. Soc. Am. Bull. 122 (9/10), 1516–1547.
Moghadam, H.S., Stern, R.J., Kimura, J.-I., Hirahara, Y., Senda, R., Miyazaki, T., 2012. Hf-Nd isotope constraints on the origin of Deshir Ophiolite, Central Iran. Island Arc 21, 202–214.
Moghadam, H.S., Stern, R.J., Chiaradia, M., Rahgoshay, M., 2013a. Geochemistry and tectonic evolution of the Late Cretaceous Gogher-Baft ophiolite, central Iran. Lithos 168-169, 33–47.
Moghadam, H.S., Mosaddegh, H., Santosh, M., 2013b. Geochemistryand petrogenesis of the Late Cretaceous Haji-Abad ophiolite (Outer Zagros Ophiolite Belt, Iran): implications for geodynamics of the Bitlis-Zagros suture zone. Geol. J. 48 (6), 579–602.
Moghadam, H.S., Khedr, M.Z., Chiaradia, M., Stern, R.J., Bakhshizad, F., Arai, S., Ottley, C.J., Tamura, A., 2014a. Supra-subduction zone magmatism of the Neyriz ophiolite, Iran: constraints from geochemistry and Sr-Nd-Pb isotopes. Int. Geol. Rev. 56 (11), 1395–1412.
Moghadam, H.S., Corfu, F., Chiaradia, M., Stern, R.J., Ghorbani, G., 2014b. Sabzevar Ophiolite, NE Iran: progress from embryonic oceanic lithosphere into magmatic arc constrained by new isotopic and geochemical data. Lithos 210-211, 224–241.
Moghadam, H.S., Corfu, F., Stern, R.J., Lotfibakhsh, A., 2019. The Eastern Khoy Metamorphic Complex of NW Iran: a Jurassic ophiolite or continuation of the Sanandaj-Sirjan Zone. J. Geol. Soc. Lond. 176, 517–529 10.144/jgs2018-081.
Mohn, G., Manatschal, G., Beltrando, M., Masini, M., Kusznir, N., 2012. Necking of continental crust in magma-poor rifted margins: evidence from the fossil Alpine Tethys margins. Tectonics 31https://doi.org/10.1029/2011TC002961. TC1012.
Monsef, I., Monsef, R., Mata, J., Zhang, Z., Pirouz, M., Rezaeian, M., Esmaeili, R., Xiao, W., 2018. Evidence for an early-MORB to fore-arc evolution within the Zagros suture zone: constraints from zircon U-Pb geochronology and geochemistry of the Neyriz ophiolite (South Iran). Gondwana Res. 62, 287–305.
Montanini, A., Tribuzio, R., Vernia, L., 2008. Petrogenesis of basalts and gabbros from an ancient continent – ocean transition (External Liguride ophiolites, Northern Italy). Lithos 101, 453–479.
Moores, E.M., 1982. Origin and emplacement of ophiolites. Rev. Geophys. 20 (4), 735–760. https://doi.org/10.1130/0016-7606(1999)111<1192:SAPOTO>2.3.CO;2.
Moores, E.M., Vine, F.J., 1971. The Troodos massif, Cyprus, and other ophiolites as oceanic crust: evaluation and implications. Phil. Trans. R. Soc. London 258A, 443–466.
Osozawa, S., Shinjo, R., Lo, C.-H., Jahn, B.-m., Hoang, N., Sasaki, M., Ishikawa, K., Kano, H., Hoshi, H., Xenophontos, C., Wakabayashi, J., 2012. Geochemistry and geochronology of the Troodos ophiolite: an SSZ ophiolite generated by subduction initiation and an extended episode of ridge subduction? Lithosphere 4 (6), 497–510.
Ottonello, G., Joron, J.L., Piccardo, G.B., 1984. Rare Earth and 3d transition element geochemistry of peridotitic rocks: II. Ligurian peridotites and associated basalts. J. Petrol. 25 (2), 373–393.
Özek, G., Akgül, M., Nurlu, N., Yapici, N., 2017. Tectonic setting and geochemical features of the Guleman ophiolite (Elazığ). KSU J. Eng. Sci. 20 (2), 29–44.
Pal, T., 2011. Petrology and geochemistry of the Andaman ophiolite: melt-rock interaction in a suprasubduction-zone setting. J. Geol. Soc. Lond. 168 (4), 1031–1045.
Parlak, O., Höck, V., Delaloye, M., 2002. The supra-subduction zone Pozanti-Karsanti ophiolite, southern Turkey: evidence for high-pressure crystal fractionation of ultramafic cumulates. Lithos 65, 205–224.
Parlak, O., Karaoğlan, F., Rizaoğlu, T., Nurlu, N., Bağci, U., Höck, V., Önal, A.Ő., Kürü, S., Topak, Y., 2012. Petrology of the İspendere (Malatya) ophiolite from Southeast Anatolia: implications for the Late Mesozoic evolution of the southern Neotethyan Ocean. In: Robertson, A.H.F., Parlak, O., Ünlügenç, U.C. (Eds.), Geological Development of Anatolia and the Easternmost Mediterranean Region. Geol. Soc. London, Spec. Publ. Vol. 372https://doi.org/10.1144/SP372.11.
Parlak, O., Çolakoğlu, A., Dönmez, C., Sayak, H., Yildirim, N., Türkel, A., Odabaşi, I., 2013. Geochemistry and tectonic significance of ophiolites along the Izmir-Ankara-Erzincan Suture Zone in northestern Anatolia. In: Robertson, A.H.F., Parlak, O., Ünlügnç, U.C. (Eds.), Geological Development of Anatolia and the Eastermost Mediterranean Region. Geol. Soc. London, Spec. Publ. Vol. 372. pp. 75–105.
Parlak, O., Bağci, U., Rizaoğlu, T., Ionescu, C., Önal, G., Höck, V., Kozlu, H., 2020. Petrology of ultramafic to mafic cumulate rocks from the Göksun (Kahramamaraş) ophiolite, southeast Turkey. Geosci. Front. 11 (1), 109–128.
Pearce, J.A., 2014. Ophiolites: immobile elements fingerprinting of ophiolites. Elements 10 (2), 101–108.
Pearce, J.A., Robinson, P.T., 2010. The Troodos ophiolite complex probably formed in a subduction initiation, slab edge setting. Gondwana Res. 18, 60–68.
Pearce, J.A., Lippard, S.J., Roberts, S., 1984. Characteristics and tectonic significance of supra-subduction zone ophiolites. Geol. Soc. Lond. Spec. Publ. 16, 77–94.
Pearce, J.A., Stern, R.J., Bloomer, S.H., Fryer, P., 2005. Geochemical mapping of the Mariana arc-basin system: implications for the nature and distribution of subduction components. Geochem. Geophys. Geosyst. 6 (7). https://doi.org/10.1029/2004GC000895. Q07006.
Pedersen, R.B., Searle, M.P., Corfield, R.I., 2001. U-Pb zircon ages of the Spontang Ophiolite,Ladakh Himalaya. J. Geol. Soc. Lond. 158, 513–520.
Pedersen, R.B., Searle, M.P., Carter, A., Bandopadhyay, P.C., 2010. U-Pb zircon age of the Andaman ophiolite: implications for the beginning of subduction beneath the Andaman-Sumatra arc. J. Geol. Soc. Lond. 167, 1105–1112.
Pe-Piper, G., Photiades, A., 2006. Geochemical characteristics of the Cretaceous ophiolitic rocks of Ikaria island, Greece. Geol. Mag. 143 (4), 417–429.
Pe-Piper, G., Tsikouras, B., Hatzipanagiotou, K., 2004. Evolution of boninites and island-arc tholeiites in the Pindos Ophiolite. Greece. Geol. Mag. 141 (4), 455–469.
Plank, T., Langmuir, C.H., 1998. The chemical composition of subducting sediment and its consequences for the crust and mantle. Chem. Geol. 145, 325–394.
Pohl, F., Froitzheim, M., et al., 2018. Kinematics and age of syn-intrusive detachment faulting in the Southern Alps: evidence for Early Permian crustal extension and implications for the Pangea A versus B controversy. Tectonics 37, 3668–3689. https://doi.org/10.1029/2018TC004974.

Pomonis, P., Tsikouras, V., Hatzipanagiotou, K., 2004. Comparative geochemical study of the Triassic trachyandesites of Glykomilia and alkali basalts from the Koziakas ophiolite mélange (W. Thessaly): implications for their origin. In: Bull. Geol. Soc. Greece, vol. XXXVI. Proceedings of the 10th International Congress, April 2004, pp. 587–596.

Price, R.C., Johnson, E., Crawford, A.J., 1990. Basalts of the North Fiji Basin: the generation of back arc basin magmas by mixing of depleted and enriched mantle sources. Contrib. Mineral. Petrol. 105, 106–121.

Puga, E., Fanning, M., de Federico, Diaz, Nieto, J.M., Beccaluva, L., Bianchini, G., Diaz Puga, M.A.D., 2011. Petrology, geochemistry and U-Pb geochronology of the Betic Ophiolites: inferences for Pangaea break-up and birth of the westernmost Tethys Ocean. Lithos 124, 255–272.

Puga, E., Dias de Federico, A., Fanning, M., Nieto, J.M., Martinez-Conde, J.A.R., Diaz Puga, M.A., Lozano, J.A., Bianchini, G., Natali, C., Beccaluva, L., 2017. The Betic Ophiolites and the Mesozoic evolution of the Western Tethys. Geosciences 7, 31. https://doi.org/10.3390/geosciences7020031.

Quanru, G., Guitang, P., Zheng, L., Chen, Z., Fisher, R.D., Sun, S., Ou, C., Dong, H., Wang, X., Li, S., Lou, X., Fu, H., 2006. The Eastern Himalayan syntaxis: major tectonic domains, ophiolitic mélanges and geological evolution. J. Asian Earth Sci. 27, 265–285.

Rajabzadeh, M.A., Dehkordi, T.N., Caran, S., 2013. Mineralogy, geochemistry and geotectonic significance of mantle peridotites with high-Cr chromitites in the Neyriz ophiolite from the outer Zagros ophiolite belts. Iran. J. Afr. Earth Sci. 78, 1–5.

Rampone, E., Hofmann, A.W., Reczek, I., 1998. Isotopic contrasts within the Internal Liguride ophiolite (N. Italy): the lack of a genetic mantle-crust link. Earth Planet. Sci. Lett. 163, 175–189.

Rasool, Q.A., Ramanujam, N., Biswas, S.K., 2015. Petrology and geochemistry of gabbros from the Andaman ophiolite: implications for their petrogenesis and tectonic setting. J. Geol. Geophys. 4 (6). https://doi.org/10.4172/2381-8719.1000226.

Rautenschlein, M., Jenner, G.A., Hertogen, J., Hofmann, A.W., Kerrich, R., Schmincke, H.-U., White, W.M., 1985. Isotopic and trace element composition of volcanic glasses from the Akaki Canyon, Cyprus: implications for the origin of the Troodos ophiolite. Earth Planet. Sci. Lett. 75, 369–383.

Regelous, M., Hofmann, A.W., Abouchami, G., Galer, S.J.G., 2003. Geochemistry of the lavas from the Emperor Seamounts, and the geochemical evolution of Hawaiian magmatism from 85 to 42 Ma. J. Petrol. 44 (1), 113–140.

Rizaoğlu, T., 2017. Alkali-silica reaction potential of arc-related volcanic rocks from the Göksun ophiolite (Kahramanmaraş-Turkey). AKU J. Sci. Eng. 17, 247–256.

Robinson, P.T., Malpas, J., Dilek, Y., Zhou, M.-F., 2008. The significance of sheeted dike complexes in ophiolites. GSA Today 18 (11), 4–10. https://doi.org/10.1130/GSATG22A.1.

Ross, P.-S., Bedard, J.H., 2009. Magmatic affinity of modern and ancient subalkaline volcanic rocks determined from trace-element discriminant diagrams. Can. J. Earth Sci. 46, 823–839.

Saccani, E., 2015. A new method of discriminating different types of post-Archean ophiolitic basalts and their tectonic significance using Th-Nb and Ce-Dy-Yb systematics. Geosci. Front. 6, 481–501.

Saccani, E., Principi, G., 2016. Petrological and tectono-magmatic significance of ophiolitic basalts from the Elba Island within the Alpine Corsica – Northern Apennine system. Mineral. Petrol. 110, 713.730.

Saccani, E., Nicolae, I., Tassinari, R., 2001. Tectono-magmatic setting of the Jurassic ophiolites from the South Apuseni Mountains (Romania): petrological and geochemical evidence. Ofioliti 26 (1), 9–22.

Saccani, E., Padoa, E., Photiades, A., 2003. Triassic mid-ocean ridge basalts from the Argolis Peninsula (Greece): new constraints for the early oceanization phases of the Neo-Tethyan Pindos basin. In: Dilek, Y., Robinson, P.T. (Eds.), Ophiolites in Earth History. Geol. Soc. London, Spec. Publ. Vol. 218. pp. 109–127.

Saccani, E., Principi, G., Garfagnoli, F., Menna, F., 2008a. Corsica ophiolites: geochemistry and petrogenesis of basaltic and metabasaltic rocks. Ofioliti 33 (2), 187–207.

Saccani, E., Bortolotti, V., Marroni, M., Pandolfi, L., Photiades, A., Principi, G., 2008b. The Jurassic association of backarc basin ophiolites and calc-alkaline volcanic in the Guevgueli Complex (Northern Greece): implication for the evolution of the Vardar zone. Ofioliti 33 (2), 209–227.

Saccani, E., Photiades, A., Beccaluva, L., 2008c. Petrogenesis and tectonic significance of Jurassic IAT magma types in the Hellenide ophiolites as deduced from the Rhodiani ophiolites (Pelagonian zone, Greece). Lithos 104, 71–84.

Saccani, E., Delavari, M., Beccaluva, L., Amini, S., 2010. Petrological and geochemical constraints on the origin of the Nehbandan ophiolitic complex (eastern Iran): implications for the evolution of the Sistan Ocean. Lithos 117, 209–228.

Saccani, E., Allahyari, K., Beccaluva, L., Bianchini, G., 2013a. Geochemistry and petrology of the Kermanshah ophiolites (Iran): implications for the interaction between passive rifting, oceanic accretion, and OIB-type components in the Southern Neo-Tethys Ocean. Gondwana Res. 24, 392–411.

Saccani, E., Azimzageh, Z., Dilek, Y., Jahangiri, A., 2013b. Geochronology and petrology of the Early Carboniferous Misho Mafic Complex (NW Iran), and implications for the melt evolution of Paleo-Tethyan rifting in Western Cimmeria. Lithos 162-163, 264–278.

Saccani, E., Chiari, M., Bortolotti, V., Photiades, A., Principi, G., 2015. Geochemistry of volcanic rocks and biostratigraphy on radiolarian cherts from the Almopias ophiolites and the Paikon Unit (Western Vardar, Greece). Ofioliti 40 (1), 1.25.

Saccani, E., Dilek, Y., Photiades, A., 2018. Time-progressive mantle-melt evolution and magma production in a Tethyan marginal sea: a case study of the Albanide-Hellenide ophiolites. Lithosphere 10 (1), 35–53.

Safonova, I.Yu., Santosh, M., 2014. Accretionary complexes in the Asia-Pacific region: tracing archives of ocean plate stratigraphy and tracking mantle plumes. Gondwana Res. 25, 126–158.

Safonova, I., Kojima, S., Nakae, S., Romer, R., Seltmann, R., Sano, H., Onoue, T., 2015. Oceanic island basalts in accretionary complexes of SW Japan: tectonic and petrogenetic implications. J. Asian Earth Sci. 113, 508–523.

Safonova, I., Biske, G., Romer, R.L., Seltmann, R., Simonov, V., Maruyama, S., 2016. Middle Paleozoic mafic magmatism and ocean plate stratigraphy of the South Tianshan, Kyrgystan. Gondwana Res. 30, 236–256.

Safonova, I., Kotlyarov, A., Krivonogov, S., Xiao, W., 2017. Intra-oceanic arcs of the Paleo-Asian Ocean. Gondwana Res. 50, 167–194.

Saha, P., Acharyya, S.K., Balaram, V., Roy, P., 2012. Geochemistry and tectonic setting of Tuting metavolcanic rocks of possible ophiolitic affinity from Eastern Himalayan Syntaxis. J. Geol. Soc. India 80, 167–176.

Sahamich, R.Z., Miradpour, A., 2015. Geochemistry and petrology of Harsin-Sahneh ophiolite complex (NE of Kermanshah-west of Iran) an evidence of Southern Neo-Tethys Ocean tectonic. Arab. J. Geosci. 8, 8347–8360.

Saka, S., Uysak, I., Kapsiotis, A., Bağci, U., Ersoy, Y., Su, B.-X., Seitz, H.-M., Hegner, E., 2019. Petrological characteristics and geochemical compositions of the Neotethyan Mersin ophiolite (southern Turkey): processes of melt depletion, refertilization, chromitite formation and ocean crust generation. J. Asian Earth Sci. 176, 281–299.

Santosh, M., 2010. A synopsis of recent conceptual models on supercontinent tectonics in relation to mantle dynamics, life evolution and surface environment. J. Geodyn. 50, 116–133.

Santosh, M., Tsunogae, T., Yang, C.X., Han, Y.S., Hari, K.R., Manu Prasanth, M.P., Uthup, S., 2020. The Bastar craton, central India: a window to Archean – Paleoproterozoic crustal evolution. Gondwana Res. 79, 157–184.

Sarıfakıoğlu, E., Dilek, Y., Sevin, M., 2017. New synthesis of the Izmir-Ankara-Erzincan suture zone and the Ankara mélange in northern Anatolia based on new geochemical and geochronological constraints. In: Sorkhabi, R. (Ed.), Tectonic Evolution, Collision, and Seismicity of Southwest Asia: In Honor of Manuel Berberian's Forty-Five Years of Research Contributions: Geological Society of America Special Paper. Vol. 525. pp. 1–XXX. https://doi.org/10.1130/2017.2525(19).

Sarwar, G., 1992. Tectonic setting of the Bela Ophiolites, southern Pakistan. Tectonophysics 207, 359–381.

Scholl, D.W., van Huene, R., 2007. Crustal recycling at modern subduction zones applied to the past – issues of growth and preservation of continental basement crust, mantle geochemistry, and supercontinent reconstruction. Mem. Geol. Soc. Am. 200, 9–32. https://doi.org/10.1130/2007.1200(02).

Sdrolias, M., Müller, R.D., Mauffret, A., Bernardel, G., 2004. Enigmatic formation of the Norfolk Basin, SW Pacific: a plume influence on back-arc extension. Geochem. Geophys. Geosyst. 5 (6). https://doi.org/10.1029/2003GC000643. Q06005.

Searle, M., Cox, J., 1999. Tectonic setting, origin, and obduction of the Oman ophiolite. Geol. Soc. Am. Bull. 111 (1), 104–122.

Searle, R.C., Escartín, J., 2013. The rheology and morphology of oceanic lithosphere and mid-ocean ridges. In: German, C.R., Lin, J., Parson, L.M. (Eds.), Mid Ocean Ridges. Hydrothermal Interactions Between the Lithosphere and the Oceans. Geophysical Monograph Series Vol. 148. American Geophysical Union, pp. 63–93. 9780875904139. https://doi.org/10.1029/148GM03.

Seck, H.A., Kötz, J., Okrusch, M., Seidel, E., 1996. Geochemistry of a meta-ophiolite suite: an association of metagabbros, eclogites and glaucophanites on the island of Syros, Greece. European J. Mineral. 8, 607–623.

Šegvić, B., Lugović, B., Slovenec, D., Meyer, H.-P., 2016. Mineralogy, petrology and geochemistry of the Kalnik Mt. (Sava Unit, North Croatia): implications for the evolution of North-westernmost part of the Dinaric-Vardar branch of Mesozoic Tethys. Ofioliti 41 (1), 35–58.

Seifert, K.E., Chang, C.-W., Brunotte, D.E., 1997. Evidence from Ocean Drilling Program Leg 149 mafic igneous rocks for oceanic crust in the Iberia Abyssal Plain ocean-continent transition zone. J. Geophys. Res. 102 (B4), 7915–7928.

Seyfried, W.E., Berndt, M.E., Seewald, J.S., 1988. Hydrothermal alteration processes at mid-ocean ridges: constraints from diabase alteration experiments, hot-spring fluids and composition of the oceanic crust. Can. Mineral. 26, 787–804.

Shaw, H.F., Chen, J.H., Saleeby, J.B., Wasserburg, G.J., 1987. Nd-Sr-Pb systematic and age of the Kings River ophiolite, California: implications for depleted mantle evolution. Contrib. Mineral. Petrol. 96, 281–290.

Shervais, J.W., 1982. Ti-V plots and the petrogenesis of modern and ophiolitic lavas. Earth Planet. Sci. Lett. 32, 114–120.

Shi, R., Yang, J., Xu, Z., Qi, X., 2004. Discovery of the boninitic series volcanic rocks in the Bangong Lake ophiolite mélange, western Tibet, and its tectonic implications. Chin. Sci. Bull. 49 (12), 1272–1278.

Shi, R., Yang, J., Xu, Z., Qi, X., 2008. The Bangong Lake ophiolite (NW Tibet) and its bearing on the tectonic evolution of the Bangong-Nujiang suture zone. J. Asian Earth Sci. 32, 438–457.

Shojaat, B., Hassanipak, A.A., Mobasher, K., Ghazi, A.M., 2003. Petrology, geochemistry and tectonics of the Sabzevar ophiolite, North Central Iran. J. Asian Earth Sci. 21, 1053–1067.

Singh, A.K., Singh, N.I., Devi, L.D., Singh, R.K.B., 2012. Geochemistry of Mid-Ocean Ridge Mafic intrusives from the Manipur Ophiolite Complex, Indo-Myanmar Orogenic Belt, NE India. J. Geol. Soc. India 80, 231–240.

Singh, A.K., Chung, S.-L., Bikramaditya, R.K., Lee, H.Y., 2017. New U-Pb zircon ages of plagiogranites from the Nagaland-Manipur Ophiolites, Indo-Myanmar Orogenic Belt, NE India. J. Geol. Soc. Lond. 174, 170–179.

Slovenec, D., Šegvić, B., 2018. Boninite volcanic rocks from the mélange of the NW Dinaric-Vardarophiolite zone (Mt. Medvenica, Croatia) – record of Middle to Late Jurassic arc-forearc system in the Tethyan subduction factory. Mineral. Petrol. https://doi.org/10.1007/s00710-018-0637-0.

Stampfli, G.M., 2000. Tethyan oceans. In: Bozkurt, E., Winchester, J.A., Piper, J.A. (Eds.), Tectonics and Magmatism in Turkey and the Surrounding Area. Geol. Soc. London, Spec. Publ. Vol. 173. pp. 1–23.

Stampfli, G.M., Borel, G.D., 2002. A plate tectonic model for the Paleozoic and Mesozoic constrained by dynamic plate boundaries and restored synthetic oceanic isochrons. Earth Planet. Sci. Lett. 196 (1-2), 17–33.

Stampfli, G.M., Hochard, C., 2009. Plate tectonics of the Alpine realm. In: Murphy, J.B., Keppie, J.D., Hynes, A.J. (Eds.), Ancient Orogens and Modern Analogues. Geol. Soc.

London, Spec. Publ. Vol. 327. pp. 89–111.
Stampfli, G.M., Kozur, H.W., 2006. Europe from the Variscan to the Alpine cycles. In: Gee, D.G., Stephenson, R.A. (Eds.), European Lithosphere Dynamics. Geol. Soc. London, Mem. Vol. 32. pp. 57–82.
Stampfli, G.M., Hochard, C., Vérard, C., Wilhem, C., vonRaumer, F., 2013. The formation of Pangea. Tectonophysics 593, 1–19.
Staudigel, H., Clague, D.A., 2010. The geological history of deep-sea volcanoes: biosphere, hydrosphere, and lithosphere interactions. Oceanography 23, 58–71.
Staudigel, H., Hart, R., 1983. Alteration of basaltic glass: mechanism and significance for the oceanic crust-seawater budget. Geochim. Cosmochim. Acta 47, 37–50.
Staudigel, H., Koppers, A.A.P., 2015. Seamounts and island building. In: Sigurdsson, H., Houghton, B., Rymer, H., Stix, J., McNutt, S. (Eds.), The Encyclopedia of Volcanoes, Second ed. pp. 405–421.
Stern, R.J., Dickinson, W.R., 2010. The Gulf of Mexico is a backarc basin. Geosphere 6 (6), 739–754.
Storck, J.C., Brack, P., Wotzlaw, J.-F., Ulmer, P., 2018. Timing and evolution of Middle Triassic magmatism in the Southern Alps (northern Italy). J. Geol. Soc. Lond. 176, 253–268. https://doi.org/10.1144/jgs2018-123.
Stouraiti, C., 2010. Geochemical characteristics of the amphibolites (ophiolitic metabasites) from the Serifos metamorphic core complex, Attic-Cycladic metamorphic belt, Cyclades, Greece. In: Proceedings of the XIX CBGA Congress, Thessaloniki, Greece. Spec. vol. 99. Scientific Annals, School of Geology, Aristotle University of Thessaloniki, pp. 333–340.
Stouraiti, C., Pantziris, I., Vasilatos, C., Kanellopoulos, C., Mitropoulos, P., Pomonis, P., Moritz, R., Chiaradia, M., 2017. Ophiolitic remnants from the upper and intermediate structural unit of the Attic-Cycladic Crystalline Belt (Aegean, Greece): fingerprinting geochemical affinities and magmatic precursors. Geosciences 7, 14. https://doi.org/10.3390/geosciences7010014.
Tang, Y., Zhai, Q., Hu, P., Xiao, X., Wang, H., 2018. Petrology, geochemistry and geochronology of the Zhongcang ophiolite, northern Tibet: implications for the evolution of the Bangong-Nujiag Ocean. Geosci. Front. 9, 1369–1381.
Tararin, I.A., Lekikov, E.P., Werner, R., 2003. Petrology and geochemistry of the volcanic rocks dredged from Geophysicist Seamount in the Kurile Basin; evidence for the existence of thinned continental crust. Gondwana Res. 6 (4), 757–765.
Tasáryová, Z., Janoušek, V., Frýda, J., 2018. Failed Silurian continental rifting at the NW marging of Gondwana: evidence from basaltic volcanism of the Prague Basin (Teplá-Bassandian Unit, Bohemian Massif). Int. J. Earth Sci. 107, 1231–1266.
Topuz, G., Okay, A.I., Schwarz, W.H., Sunal, G., Altherr, R., Kylander-Clark, A.R.C., 2018. A middle Permian ophiolite fragment in Late Triassic greenschist- to blueschist-facies rocks in NW Turkey: an earlier pulse of suprasubduction-zone ophiolite formation in the Tethyan belt. Lithos 300–301, 121–135.
Torsvik, T.H., Cocks, R.M., 2004. Earth geography from 400 to 250 Ma: a palaeomagnetic, faunal and facies review. J. Geol. Soc. Lond. 161, 555–572.
Tortorici, L., Catalano, S., Monaca, C., 2009. Ophiolite-bearging melanges in southern Italy. Geol. J. 44, 53–166.
Trubelja, F., Marchig, V., Burgath, K.P., Vujović, Ž., 1995. Origin of the Jurassic Tethyan ophiolites in Bosnia: a geochemical approach to tectonic setting. Geologia Croatica 48 (1), 49–66.
Ustaszewski, K., Schmid, S.M., Lugović, B., Schuster, R., Schaltegger, U., Bernoulli, D., Hottinger, L., Kounov, A., Fügenschuh, B., Schefer, S., 2009. Late Cretaceous intra-oceanic magmatism in the internal Dinarides (northern Bosnia and Herzegovina): implications for the collision of the Adriatic and European plates. Lithos 108, 105–125.
Valsami-Jones, E., Ragnarsdottir, K.V., 1997. Controls on uranium and thorium behavior in ocean-floor hydrothermal systems: examples from the Pindos ophiolite. Greece. Chem. Geol. 135, 263–274.
Van Keken, P.E., 2003. The structure and dynamics of the mantle wedge. Earth Planet. Sci. Lett. 215, 323–338.
Vergili, Ö., Parlak, O., 2005. Geochemistry and tectonic setting of metamorphic sole rocks and mafic dikes from the Pinarbaşi (Kayseri) ophiolite, Central Anatolia (Turkey). Ofioliti 30 (1), 37–52.
Verma, S.P., 1992. Seawater alteration effects on REE, K, Rb, Cs, Sr, Th, Pb and Sr-Nd-Pb isotope systematics of Mid-Ocean Ridge Basalt. Geochem. J. 26, 159–177.
Vervoort, J.D., Blichert-Ioft, J., 1999. Evolution of the depleted mantle: Hf isotope evidence from juvenile rocks through time. Geochim. Cosmochim. Acta 63 (3/4), 533–556.
Von Huene, R., Scholl, D.W., 1991. Observations at convergent margins concerning sediment subduction, sediment erosion, and the growth of continental crust. Rev. Geophys. 29, 279–316.
Wakita, K., 2012. Mappable features of melanges derived from Ocean Plate Stratigraphy in the Jurassic accretionary complexes of Mino and Chichibu terranes in southwest Japan. Tectonophysics 568, 74–85.
Wang, W.-L., Aitchison, J.C., Lo, C.-H., Zeng, Q.-G., 2008. Geochemistry and geochronology of the amphibolite blocks in ophiolitic mélanges along Bangong-Nujian suture, central Tibet. J. Asian Earth Sci. 33, 122–138.
Wang, B.-D., Wang, L.-Q., Chung, S.-L., Chen, J.-L., Yin, F.-G., Liu, H., Li, X.-B., Chen, L.-K., 2016. Evolution of the Bangong-Nujiang Tethyan ocean: insights from the geochronology and geochemistry of mafic rocks within ophiolites. Lithos 245, 18–33.
Winchester, J.A., Floyd, P.A., 1977. Geochemical discrimination of different magma series and their differentiation products using immobile elements. Chem. Geol. 20, 323–343.
Windley, B., 1992. Proterozoic collisional and accretionay orogens. Dev. Precambrian Geol. 10, 419–446.
Woelki, D., Regelous, M., Haase, K.M., Beier, C., 2019. Geochemical mapping of a paleo-subduction zone beneath the Troodos Ophiolite. Chem. Geol. 523, 1–8.
Wu, Y-w., Li, C., Xu, M.-J., Xiong, S.-Q., Fan, Z.-Q., Xie, C.-M., Wang, M., 2016. Petrology and geochemistry of metabasalts from the Taoxinghu ophiolite, central Qiangtang, northern Tibet: evidence for a continental back-arc basin system. Austrian J. Earth Sci. 109 (2), 166–176. https://doi.org/10.17738/ajes.2016.0012.
Xia, B., Chen, G.-W., Wang, R., Wang, Q., 2008. Seamount volcanism associated with the Xigaze ophiolite, Southern Tibet. J. Asian Earth Sci. 32, 396–405.
Xiong, F., Yang, J., Dilek, Y., Xu, X., Zhang, Z., 2018. Origin and significance of diamonds and other exotic minerals in the Dingqing ophiolite peridotites, eastern Bangong-Nujiang suture zone, Tibet. Lithosphere 10 (1), 142–155.
Xu, D.-M., Huang, G.-C., Li, Y.-J., 2008. Sm-Nd ages and Nd-Sr-Pb isotope signatures of the Xiugugabu ophiolite, southwestern Tibet. Geol. China 35 (3), 429–435.
Xu, M., Wu, Y., Xie, C., 2014. The petrology, geochemistry, and petrogenesis of E-MORB-type mafic rocks from the Guomangco Ophiolitic Mélange, Tibet. Acta Geol. Sin. 88 (5), 1437–1453.
Xu, Z.-Q., Dilek, Y., Cao, H., Yang, J.S., Robinson, P., Ma, C.Q., Li, H., Jolivet, M., Roger, F., Chen, X.J., 2015a. Paleo-Tethyan evolution of Tibet as recorded in the East Cimmerides and West Cathaysides. J. Asian Earth Sci. 105, 320–337.
Xu, W., Li, C., Xu, M.-J., Wu, Y.-W., Fan, J.-J., Wu, H., 2015b. Petrology, geochemistry, and geochronology of boninitic dikes from the Kangqiong ophiolite: implications for the Early Cretaceous evolution of Bangong-Nujiang Neo-Tethys Ocean in Tibet. Int. Geol. Rev. 57 (16), 2028–2043.
Xu, Y., Liu, C.-Z., Chen, Y., Guo, S., Wang, J.-G., Sein, K., 2017. Petrogenesis and tectonic implications of gabbro and plagiogranite intrusions in mantle peridotites of the Myitkyina ophiolite, Myanmar. Lithos 284–285, 180–193.
Yaliniz, M.K., Floyd, P.A., Göncuoğlu, M.C., 1996. Supra-subduction zone ophiolites of Central Anatolia: geochemical evidence from the Sarikaraman Ophiolite, Aksaray, Turkey. Min. Mag. 60, 697–710.
Yaliniz, K.M., Floyd, P.A., Göncüoğlu, M.C., 2000. Geochemistry of volcanic rocks from the Çiçekdağ Ophiolite, Central Anatolia, Turkey, and their inferred tectonic setting within the northern branch of the Neotethyan Ocean. In: Bozkurt, E., Winchester, J.A., Piper, J.D.A. (Eds.), Tectonics and Magmatism in Turkey and the Surrounding Area. Geol. Soc. London, Spec. Publ. Vol. 173. pp. 203–218.
Yamamoto, S., Senshu, H., Rino, S., Omori, S., Maruyama, S., 2009. Granite subduction: tectonic ersion and sediment subduction. Gondwana Res. 15, 443–453.
Yang, G., Dilek, Y., 2015. OIB- and P-type ophiolites along the Yarlung-Zangbo Suture Zone (YZSZ), Southern Tibet: poly-phase melt history and mantle sources of the Neotethyan oceanic lithosphere. Episodes 38 (4), 250–265.
Yang, J.S., Duan, X.D., Xiong, F.H., Liu, Z., Li, H.Q., 2012. Discovery of Jurassic SSZ ophiolite in the Myitkyina region of Myanmar. Acta Pet. Sin. 28 (6), 1710–1730.
Yildirim, E., 2015. Geochemistry, petrography and tectonic significance of the ophiolitic rocks, felsic intrusions and Eocene volcanic rocks of an imbrication zone (Helete area, Southeast Turkey). J. Afr. Earth Sci. 107, 89–107.
Zachariadis, P.T., 2007. Ophiolites of the Eastern Vardar Zone, N, Greece. Ph.D.. Johannes Gutenberg-Universität, Mainz (131 pp).
Zaigham, N.A., Mallick, K.A., 2000. Bela ophiolite zone of southern Pakistan: tectonic setting and associated mineral deposits. Geol. Soc. Am. Bull. 112 (3), 478–489.
Zarrinkoub, M.H., Pang, K.-N., Chung, S.-L., Khatib, M.M., Mohammadi, S.S., Chio, H.-Y., Lee, H.-Y., 2012. Zircon U-Pb age and geochemical constraints on the origin of the Birjand ophiolite, Sistan suture zone, eastern Iran. Lithos 154, 392–405.
Zeng, X.-W., Wang, M., Fan, J.-J., Li, C., Xie, C.-M., Zhang, T.-Y., 2018a. Geochemistry and geochronology of gabbros from the Asa Ophiolite, Tibet: implications for the early Cretaceous evolution of the Meso-Tethys Ocean. Lithos 320–321, 192–206.
Zeng, Y.-C., Xu, J.-F., Chen, J.-L., Wang, B.-D., Kang, Z.-Q., Huang, F., 2018b. Geochronological and geochemical constraints on the origin of the Yunzhug ophiolite in the Shiquanhe.Yunzhug-Namu Tso ophiolite belt, Lhasa Terrane, Tibetan Plateau. Lithos 300–301, 250–260.
Zhang, L.-L., Liu, C.-Z., Wu, F.-Y., Ji, W.-Q., Wang, J.-G., 2014. Zedong terrane revisited: an intra-oceanic arc within Neo-Tethys or part of the Asian active continental margin? J. Asian Earth Sci. 80, 34–55.
Zhang, C., Liu, C.-Z., Wu, F.-U., Zhang, L.-L., Ji, W.-Q., 2016a. Geochemistry and geochronology of mafic rocks from the Luobusa ophiolite, South Tibet. Lithos 245, 93–108.
Zhang, L.-L., Liu, C.-Z., Wu, F.-Y., Zhang, C., Ji, W.-Q., Wang, J.-G., 2016b. Sr-Nd-Hf isotopes of the intrusive rocks in the Cretaceous Xigaze ophiolite, southern Tibet: constraints on its formation setting. Lithos 258–259.
Zhang, H., Yang, T., Hou, Z., Dai, M., Hou, K., 2017. Permian back-arc basin basalts in the Yushu area: new constrain on the Paleo-Tethyan evolution of the north-Central Tibet. Lithos 286-287, 216–226.
Zhang, P., Wang, G., Polat, A., Shen, T., Chen, Y., Zhu, C., Wu, G., 2018a. Geochemistry of mafic rocks and cherts in the Darbut and Karamay ophiolitic mélanges in West Junggar, northwest China: evidence for a Late Silurian to Devonian back-arc basin system. Tectonophysics 745, 395–411.
Zhang, P., Wang, G., Polat, A., Zhu, C., Shen, T., Chen, Y., Chen, C., Guo, J., Wu, G., Liu, Y., 2018b. Emplacement of the ophiolitic melanges in the west Karamay area: implications for the Late Paleozoic tectonic evolution of West Junggar, northwestern China. Tectonophysics 747-748, 259–280.
Zhao, G., Wang, Y., Huang, B., Dong, Y., Li, S., Zhang, G., Yu, S., 2018. Geological reconstruction of the East Asian blocks: from the breakup of Rodinia to the assembly of Pangea. Earth-Sci. Rev. 186, 262–286.
Zhong, Y., Xia, B., Liu, W.-L., Yin, Z.-X., Hu, X.-C., Huang, W., 2015. Geochronology, petrogenesis and tectonic implications of the Jurassic Namco-Renco ophiolites, Tibet. Int. Geol. Rev. 57 (4), 508–528.
Zhong, Y., Liu, W.-L., Xia, B., Liu, J.-N., Guan, Y., Yin, Z.-X., Huang, Q.-T., 2017. Geochemistry and geochronology of the Mesozoic Lanong ophiolitic mélange, northern Tibet: implications for petrogenesis and tectonic evolution. Lithos 292–293, 111–131.